Universitetet i Stavanger

**FACULTY OF SCIENCE AND TECHNOLOGY**

# MASTER'S THESIS

| | |
|---|---|
| Study programme / specialization:<br>**Risk Management** | Spring semester, 2017<br><br>**Open / ~~Confidential~~** |
| Author:<br>**Albert Hutama** | ……..<br>(signature of the author) |

Faculty Supervisor:
**Jan Roar Bakke**

External Supervisor:
**Kees van Wingerden (Gexcon AS)**

Title of master's thesis:
**Simulation of BLEVEs in Unconfined and Confined Areas Using FLACS**

Credits:
**30 ECTS**

| | |
|---|---|
| Keywords:<br>*BLEVE, flashing liquid, vapour explosion, CFD modelling, FLACS* | Pages: 79 pages<br>+ Appendix: 49 pages<br><br>Stavanger, 9th June 2017 |

# Abstract

BLEVE is a type of explosion that constitutes a major hazard in (but not limited to) the process industries, and which may lead to catastrophic effects. It can happen in storage facility or in transport system (road and train tankers). The subsequent effects of BLEVEs such as blast overpressure, fireball, and so on are the main considerations for safety engineers to achieve an acceptable and required level of safety during operations.

To have a better understanding of the consequences of a possible BLEVE accident, computer simulations may be required because of their ability to perform many calculations in a relatively short time. But, unlike the well-known expanding gas process, the flashing liquid process that occurs in a BLEVE accident involves more complex physics. The complexity necessitates simplification to be able to describe the flashing process. Interactions between the BLEVE itself and confinement and congestion have to be analysed when discussing possible BLEVEs inside a tunnel, such as may be possible during transport by train or truck.

To establish a proper method to simulate a BLEVE, the simulation approach by Hansen and Kjellander (2016) is used as a starting point. To simplify the description of the flashing process Hansen and Kjellander (2016) used a pseudo-source. Several adaptations have been made regarding the pseudo-source region. In addition, some simulations required several trials to achieve a more consistent method.

Regarding the blast overpressures and impulses, the simulation results are mostly above the actual experiment results. These may represent a more conservative value which is good from a safety point of view. This satisfactory level of results does not happen for fireball simulations. Fireball characteristics are below the values of actual experiments. Several changes on the simulation setups are necessary to reproduce fireball properties seen in actual experiments.

A BLEVE inside a semiconfined area will have a lower decay rate of blast overpressure due to the confinement. Relatively high overpressures are observed at far distances from the centre of the explosion. Congestion will introduce turbulences and will disturb the blast wave, thus reducing the overpressures.

*This page intentionally left blank*

# Preface

The development of industries, particularly in the chemical and petroleum sectors, is increasing rapidly due to the increase of product demands from the end users. Some of the commercial products are hydrocarbons (gaseous and liquid), LPG, LNG, ammonia, hydrogen, medical oxygen, refrigerants, etc. Most of them are gaseous at ambient pressure and temperature. The only way to store those gaseous products in efficient manner is by pressurizing the containment or vessel, thus reducing required volume to store. Pressurized vessels have become a “saviour” in the chemical and petroleum sectors.

On the other hand, pressurized vessels introduce an issue related to safety. The pressure inside vessel can be very high compared to atmospheric pressure and higher than the human body can withstand. Accidental event regarding pressurized vessels such as BLEVE can be hazardous. By compressing gaseous product into its liquid state, the final volume can be extremely small. Sudden decompression might alter its state into gaseous state i.e. the liquefied gas boils and expands suddenly.

To achieve an acceptable safety level in a facility, all possible hazards including BLEVE must be assessed. Analysis using CFD (Computational Fluid Dynamics) software is the effective solution since it can simulate the real phenomenon. It can perform many calculations in a relatively shorter time compared to the manual calculation by hands. To accurately represent the real world, all aspects must be defined properly into the simulations.

Modelling a BLEVE with CFD software is not a straight-forward process. There is a flashing process which is influenced by many factors and involves complex physics. The BLEVE model in this thesis will be compared to some past experiments in order to verify and validate the model. The calculation and simulation method will be reported in detail and in a systematic manner.

*This page intentionally left blank*

# Table of Contents

# List of Figures

# List of Tables

# Glossary

| | |
|---|---|
| BLEVE | Boiling Liquid Expanding Vapour Explosion |
| CCPS | Center for Chemical Process Safety |
| CFD | Computational Fluid Dynamics |
| LFL | Lower Flammability Limit |
| PLG | Pressurized Liquefied Gas |
| PVB | Pressure Vessel Burst |
| SEP | Surface Emissive Power |
| UFL | Upper Flammability Limit |
| VCE | Vapour Cloud Explosion |

*This page intentionally left blank*

# 1 Introduction

## 1.1 Background

A BLEVE is a type of explosion that often occurs in storage facilities or during transportation where liquefied gas is stored under high pressure, much higher than atmospheric pressure. Most of steel containments or vessels are designed to withstand high pressure and are adequate to store the substance in liquid state at ambient temperature. When the containment loses its ability to contain due to some factor, the contents will be exposed to a sudden drop of pressure to atmospheric pressure. Then, the contents will undergo a violent and instantaneous process. Vapour inside the vessel will expand, and liquid inside the vessel will vaporize depending on the superheat limit and ambient temperature. The effect will be more severe if there is a fire which increases the temperature.

A BLEVE and the subsequent events depend on the properties of the containment failure. There are some other factors beside the pressure at failure as discussed by Venart (2000). These various properties of failure result in different time delay, fireball characteristics, subsequent processes inside the containment, and so on.

FLACS is a CFD software specialized for predicting the consequences of fire and explosion. Simulation of BLEVEs can be done using FLACS but there are several limitations and assumptions that have to be made. Liquid content inside the vessel or containment must be converted to gas (Gexcon, 2016). The liquid content cannot be modelled straight forward in FLACS. The flashing process is not as well-understood as the expanding gas process (Hansen & Kjellander, 2016). A proper model of BLEVE must be established to simulate the actual BLEVE event for every condition. One way to simulate BLEVE is described briefly by Hansen and Kjellander (2016).

BLEVE may occur inside a tunnel or other confined and congested area. The shock wave from a BLEVE may cover larger distances in highly confined spaces. The decay rate of the pressure is lower in a confined space than the one in open space (van den Berg & Weerheijm, 2006). This simulation has been conducted by Hansen & Kjellander (2016) with qualitative and quantitative results presented. Assessment of blast overpressure decay will be done after a proper method to simulate BLEVEs has been established.

## 1.2 Objectives of Work

The objectives of this work are:

1. to create a proper model to simulate blast from BLEVEs with FLACS, and which can be used to represent the real-world situation.
2. to obtain the decaying trend and assess the effect of blast overpressure in congested and semiconfined scenarios.

## 1.3 Scope of Work

This thesis shall address the following specific aspects.

1. Analyse the blast static overpressure decay in the areas surrounding a BLEVE using an appropriate computational model and an analytical calculation based on existing data or experiments. The analytical calculation method is based on guidelines published by CCPS (1994).
2. A computational model which has been mentioned in paragraph (1) will be created using a software package called FLACS (version 10.5r1). The software was released in May 2016. Several improvements of this software have been developed at the time of writing, therefore it is necessary to mention the software version that was used for thesis work.
3. Detailed suggestions for a BLEVE model using the FLACS software on how to translate the physical parameters in the real world to the input parameter in FLACS software, specifically FLACS version 10.5r1. The physical parameters consist of but are not limited to the containment volume and shape, absolute internal pressure, fluid contents, and time. These include the BLEVE itself and the simulation of subsequent events.
4. Suggestions on future development of CFD software which specializes on BLEVE simulations such as an auto-generated model and additional parameters to be included.

## 1.4 Methodology

To achieve the objectives of this thesis, several elements have been addressed as described below.

- Literature studies. There are several literature sources which have been studied particularly about the chronology of BLEVE from pressure build-up to possible aftermaths. This helped the author to create proper models of BLEVE using necessary assumptions.
- Modelling in FLACS and analyses. The FLACS software will be used extensively throughout this thesis and analyses of the output in comparison to experiments is required to obtain and verify the results.

## 1.5 Structure of Report

The report of this work is organized in a systematic way.

Chapter 1 discusses the introduction and foundation of this thesis work. Brief explanations are presented including some background, the objectives, scope of work, and the main structure of this report.

Chapter 2 discusses the BLEVE event in depth, the FLACS software by Gexcon AS in general, and the applicability of FLACS to simulate BLEVEs. Details about BLEVEs consist of the definitions that had been presented in several papers, the mechanisms of how BLEVEs occur, and the effects of a BLEVE that may occur afterwards. The description of the FLACS

software consists of general information, the applicability of FLACS from an HSE point of view, and the possibility to simulate BLEVEs using FLACS.

Chapter 3 discusses shock waves from BLEVE in depth as shock waves are the main consequences of BLEVE addressed in this thesis. In that chapter, analytical calculations of blast wave overpressures are presented. Later, the calculations will be compared to actual past experiments.

Chapter 4 discusses the computational simulation of a BLEVE using FLACS from setup to results. Chapter 4 focuses on open space BLEVEs. Discussions concerning comparison with actual experiments and simulation time for each simulation will be presented.

Chapter 5 discusses the simulation of BLEVE in confined and congested areas. A planned road tunnel in Rogaland county of Norway as a future part of E39 road was used. Chapter 5 presents the simulation setup and results, a comprehensive discussion about the effect of confinement and congestion, and some additional notes regarding simulation best practice.

Chapter 6 presents the final conclusions and suggestions based on the theoretical approaches and simulations that have been done.

*This page intentionally left blank*

# 2 BLEVEs and FLACS

## 2.1 BLEVE

### 2.1.1 Definitions of BLEVE

BLEVE is the acronym for Boiling Liquid Expanding Vapour Explosion. It is an explosion due to the failure of a vessel containing a liquid that has temperature above its boiling point at normal atmospheric pressure. It was first used to describe steam explosions (CCPS, 1994). Normally, a BLEVE involves flammable fuel which can result in another subsequent phenomenon regarding fire and explosion. There are several definitions, summarized by CCPS (1994), which mention implicitly the main components or aspects necessary to cause BLEVEs.

The term "BLEVE" was introduced by J.B. Smith, W.S. Marsh, and W.L. Walls of Factory Mutual Research Corporation back in 1957. Walls et.al (1979), as cited in CCPS (1994) p.157, defined a BLEVE as follows.

> *"Walls (1979), then with the National Fire Protection Association, defined a BLEVE as the failure of a major container into two or more pieces, occurring at a moment when the contained liquid is at a temperature above its boiling point at normal atmospheric pressure."*

Reid's paper in 1976 and 1980, as cited in CCPS (1994) p.157, defined a BLEVE as follows.

> *"... a BLEVE is the sudden loss of containment of a liquid that is at a superheat temperature for atmospheric conditions."*

More recent publications such as Birk et.al. (2007) mentioned another definition by Reid (1979). Reid suggested that a sudden drop of pressure must bring the liquid into superheat limit spinodal, so that homogeneous nucleation takes place in the bulk liquid. It is mentioned that the real BLEVE based on Reid's definition has never occurred. Later, Birk et.al. (2007) defined a BLEVE as follows.

> *"A BLEVE is the explosive release of expanding vapour and boiling liquid when a container holding a PLG (pressurized liquefied gas) fails catastrophically."*

Birk et.al. (2007) emphasized the phrase "fails catastrophically". The phrase means that the tank is fully opened and releases its content almost instantaneously.

A BLEVE causes instantaneous boiling of the liquid inside the vessel that will produce a shock wave. In practice and most cases, liquid that is stored inside a pressurized vessel has a boiling point lower than ambient temperature. In other cases, it is possible to have a BLEVE caused by heated liquid that has boiling point above ambient temperature. The external heat source varies from natural heat to fire heat.

Figure 2-1. A fireball resulted by a BLEVE experiment conducted by A.M. Birk in 2001 (Birk et.al., 2003, p.101).

Lewis' paper in 1985, as cited in CCPS (1994) p.157, gave a more specific definition of BLEVE as follows.

> *"Consequently, Lewis (1985) suggested that a BLEVE be defined as a rapid failure of a container of flammable material under pressure during fire engulfment."*

Lewis' definition of BLEVE includes the additional condition: fire engulfment and flammable material.

In the present context, BLEVE is defined by CCPS (1994) as a sudden loss of containment of a pressure-liquefied gas existing above its normal atmospheric boiling point at the moment of its failure, which results in rapidly expanding vapour and flashing liquid. Most of cases, a BLEVE is followed by fireball radiation, fragmentation of vessel material, and blast effects. If the involved liquid is flammable, fireball, vapour cloud explosion (VCE), or flash fire can occur afterwards. A VCE or flash fire may arise if containment failure is not due to fire impingement.

### 2.1.2 Mechanism of BLEVE

Some of the BLEVE definitions have been mentioned in the previous section. There are several keywords from the definitions to describe how BLEVEs can occur. The keywords are properties of the fluid and containment failure. In addition, fill level of containment can determine the severity of BLEVE. This will determine the partition of vapour space and liquid space as shown in Figure 2-2. According to CCPS (2011, p.311), a BLEVE requires three key elements:

- a liquid that exists above its normal atmospheric pressure boiling point,
- containment that causes the pressure on the liquid to be sufficiently high to suppress boiling, and
- a sudden loss of containment to rapidly drop the pressure on the liquid.

The fluid inside a containment consists of liquid (PLG) and its saturated vapour. Usually before the containment failure, the liquid is in equilibrium with the saturated vapour (CCPS, 1994). The liquefied gas is stored at high pressure at ambient temperature. It means that the liquid has a temperature higher than its boiling point at atmospheric pressure. The fill level is defined as the ratio of liquid space volume to the total volume of containment.

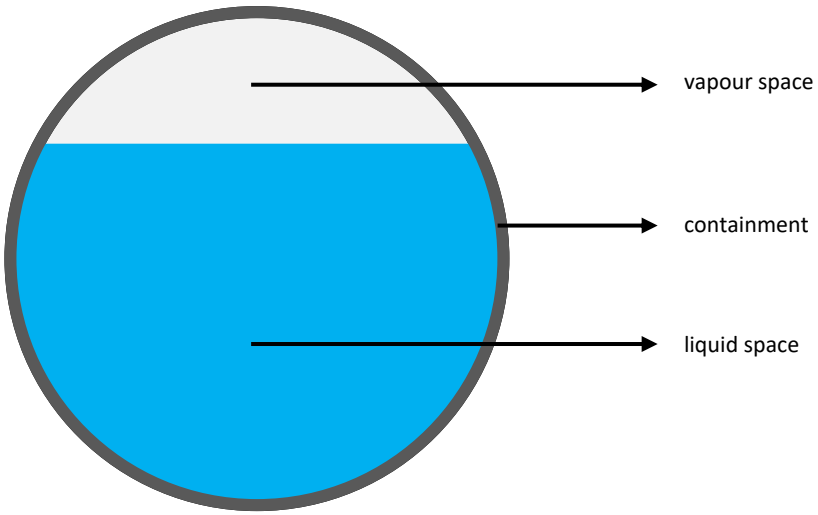


Figure 2-2. Illustration of typical cross section of a containment.

The main feature of a BLEVE is containment failure. The severity of failure will determine the further effects of a BLEVE. Birk et.al. (2007) explained about the severity of containment failure varying from a tiny hole to sudden failure in the order of containment cross-sectional area. Birk et.al. (2007) relates the size of hole to the rate of vaporization.

Causes of containment failure are limited to unintended defects of containment material, mostly metal, such as corrosion, fatigue, manufacturing defects, overheating, etc. (CCPS, 1994, p.158). Metal overheating can occur by introducing external heat such as a flame torch or fire around the vessel. High temperature due to fire can weaken the metal strength and result in plastic deformation of the containment's wall at the hottest location as mentioned by Venart (2000). This plastic deformation leads to the formation of a crack which will cause depressurization in addition to that of the pressure relieving valve, if any. Furthermore, Venart (2000) mentions that the size of initial fissure or crack is a function of the metal temperature, the fill level, and the available energy in the vapour space.

According to CCPS (1994, p.158), the boiling process takes place at submicron nucleation sites such as impurities, crystals, or ions. At those sites, the bubble is created while the rest of liquid will be superheated where its boiling point is exceeded without boiling. However, there is a limit where liquid cannot exist as superheated which is called the critical point. At these conditions, the vapour develops instantaneously in the bulk liquid without nucleation sites.

As mentioned before, the size of the hole will determine the rate of vaporization of liquid. A small hole in a containment wall causes some of the vapour to escape, hence decrease the pressure. The vapour escapes due to the increase of volume of vapour space (expanding).

This pressure reduction sends the liquid to a small-degree of superheat, causes some liquid to flash to vapour. The boiling at nucleation sites takes place in the liquid space near the hole.

On the other hand, a large hole or, more extreme, sudden containment failure causes a large-degree of superheat in the liquid space, i.e. superheat occurs in a large volume of liquid. This creates a stronger flashing of the liquid part in a very short time. The degree of flashing is depending on the superheat limit. In addition, the vapour space expands violently due to sudden pressure reduction to ambient pressure and must occupy a much greater volume (Johnson et.al., 1991). This sudden expansion of vapour creates a shock wave that may propagate at supersonic speed. This is a 2D or 3D equivalence of a shock tube problem which has a well-known analytical solution unlike the flashing liquid process (Hansen and Kjellander, 2016, p.200). Sudden flashing of liquid might create a shock wave with more significant effects in the near-field range. Birk et.al. (2007, p.205) concluded that the process of rapid flashing after containment failure is too slow to produce a shock wave, i.e. low impulse, in a single-step BLEVE. Details about shock wave generation will be discussed in Section 2.1.3.

The superheat limit will determine the effect of a flashing liquid. Reid (1979), as cited in CCPS (1994), suggested a plot of superheat-temperature-limit locus for propane. Superheat limit locus on the graph is the line where a pressure decrease will create sudden flashing. When the lower limit of the locus is reached, all superheated liquid will be vaporized i.e. violent flashing.

Furthermore, Casal et.al. (2002) proposed an expression to calculate the vaporization fraction of flashing liquid, i.e. the fraction of liquid that will vaporize during depressurization. The expression is as follows.

$$f = 1 - \exp\left[-2.63\,\frac{C_p}{H_v}\,(T_c - T_b)\cdot\left(1 - \left(\frac{T_c - T_0}{T_c - T_b}\right)^{0.38}\right)\right] \qquad \text{eq. 2.1}$$

$f$ : Vaporization fraction of flashing liquid [-]
$C_p$ : Specific heat at constant pressure [J kg$^{-1}$ K$^{-1}$]
$H_v$ : Enthalpy of vaporization of the substance [kJ/kg]
$T_c$ : Critical temperature of the substance [K]
$T_b$ : Boiling temperature of the substance at atmospheric pressure [K]
$T_0$ : Temperature of the substance at the moment of explosion [K]

Moreover, Casal et.al. (2002) explained about the uncertainty of using the formula since there is a possibility of a non-homogeneous distribution of temperature of the substance, i.e. a temperature stratification.

Some literature sources mention two-step BLEVE. Venart (2000, p.4) suggests that this two-step BLEVE process may be the cause of BLEVEs. The two-step process is defined as a 'leak before break' (LBB) crack initiator followed by a total loss of containment (LOC). Birk et.al. (2007) also mention this two-step process by describing the frequency characteristics of an explosion. The two-step process is marked by a high frequency crack noise, like that from a whip or a nearby lightning strike. In addition, they suggest that a much stronger shock must

be expected if a two-step process occurs because parts of the liquid evaporate and contribute to a higher pressure of vapour before the containment totally loses its strength.

### 2.1.3 Effects of BLEVE

A BLEVE can lead to several catastrophic consequences such as a fireball, a flash fire, high-pressure shock waves, and propelling fragments of the broken containment. A fireball and a flash fire will produce heat radiation that might lead to fatalities. Also, depending on the size of it the surroundings may be exposed to the radiation causing damage. Shock waves can break or shatter objects located at some distances from the centre of BLEVE. Propelled fragments can cause injuries or can break equipment. The severity of a BLEVE depends on the explosion power and substances inside the containment. Analytical formulas to estimate the effects of BLEVE are given in the next sections.

#### 2.1.3.1 Fireball

A fireball may occur after a BLEVE if the gas cloud produced by the BLEVE is flammable, ignited, and within its flammability limits, i.e. between UFL and LFL. As described by SINTEF (2003), a fraction of liquefied gas inside the containment will evaporate at ambient conditions in case of volatile fuels. Strong buoyancy forces due to the hot burned gases results in high turbulence introducing rapid air entrainment, allowing for better mixing of fuel and air. A hemispherical shape of the burning cloud is maintained during most of the initial expansion until the fireball growth is exceeded by the buoyancy and the spherical shape develops. After the fireball formed completely, the fireball will lift up, entraining further air which results in a cooling of the fireball. This complete process takes 5 to 30 seconds.

The fireball occurs due to delayed ignition of the gas-air cloud. The potential radiation of a fireball to the human can be determined. According to CCPS (2011, p.336), the radiation effects due to a fireball depend on:

- the maximum diameter of the fireball, that is, fuel mass contributing to fireball generation,
- the surface-emissive power of the fireball, and
- the duration of combustion.

A basic assumption is a spherical shape of fireball, although the actual shape of a fireball is not a smooth sphere. There are several formulas to estimate the diameter and combustion duration of fireballs. CCPS (1994) explained four models for BLEVE fireballs to estimate the diameter, some of them with combustion rate calculation.

Empirical formula for fireball diameter and duration

According to CCPS (1994, pp.171 - 176), the equation is derived from the average of three publications by Roberts (1982), Jaggers et.al. (1986), and Pape et.al. (1988). The empirical equations are obtained from experiments and from theoretical considerations. The combined formula is given as follows.

$$D_c = 5.8 m_f^{\frac{1}{3}} \quad \text{eq. 2.2}$$

$$t_c = 0.45 m_f^{\frac{1}{3}} \quad \text{for} \quad m_f < 30000 \text{ kg} \quad \text{eq. 2.3}$$

$$t_c = 2.6 m_f^{\frac{1}{6}} \quad \text{for} \quad m_f > 30000 \text{ kg} \quad \text{eq. 2.4}$$

$D_c$ : Maximum diameter of fireball (at end of combustion phase) [m]
$m_f$ : Mass of fuel [kg]
$t_c$ : Combustion duration [s]

Fireball diameter model

Fireball diameter model in this part assumes that the fuel is premixed with air (in some cases, oxidant) at ambient temperature. According to CCPS (1994), the fireball diameter model is introduced by Lihou and Maund (1982), Roberts (1982), and others. The basic starting point of this model is a constant molar volume of gas at standard condition (0 °C and 1 atm). Therefore, the diameter of sphere can be calculated from the released mass of fuel and air, and the ambient temperature.

$$D_0 = \left[\frac{6}{\pi}\frac{V_M}{M}\frac{T_a}{273}\left(m_f + m_a\right)\right]^{\frac{1}{3}} = 0.539\left[\left(m_f + m_a\right)\frac{T_a}{M}\right]^{\frac{1}{3}} \quad \text{eq. 2.5}$$

$M$ : Average molecular weight of fuel-air mixture [kg/kmol]
$V_M$ : Molar volume at 273 K and atmospheric pressure (i.e. 22.4 $m^3$/kmol)
$T_a$ : Initial (ambient) temperature [K]
$m_f$ : Mass of fuel [kg]
$m_a$ : Mass of air [kg]
$D_0$ : Initial sphere diameter [m]

Isothermal model

Lihou and Maund (1982), as cited by CCPS (1994), also introduced an isothermal model by assuming that a fireball burns at constant temperature. Combustion is controlled by the supply of air and ceases after a certain amount of time. Assuming that $f_c$ is fraction of fuel that burns stoichiometrically, the rate of increase of fireball volume can be written as follows.

$$\frac{\pi D^2}{2}\frac{dD}{dt} = \frac{dV_a}{dt}\frac{T_c}{T_a}\left(1 + \frac{n_j f_c}{\mu}\right) \quad \text{eq. 2.6}$$

$D$ : Diameter [m]
$T_c$ : Temperature of fireball [K]
$T_a$ : Temperature of ambient air [K]
$dD/dt$ : Rate of increase of fireball diameter [m/s]
$dV_a/dt$ : Rate of air entrainment [$m^3$]
$D_0$ : Initial sphere diameter [m]
μ : Stoichiometric molar fuel-air ratio [-]
$n_i$ : Increase in total number of moles per mole of flammable gas [-]

The rate of combustion is equal to the rate of heat applied to warm the entrained air plus the radiative heat losses.

$$\frac{273}{T_a}\frac{dV_a}{dt}\frac{Mh_c f_c}{V_M \mu} = \frac{273}{T_a}\frac{dV_a}{dt}\frac{M_a c_{pa}(T_c - T_a)}{V_M} + \pi D^2 \epsilon \sigma T_c^4 \qquad \text{eq. 2.7}$$

$\sigma$ : Stefan-Boltzmann constant ($5.67 \times 10^{-11}$ kW m$^{-2}$ K$^{-4}$)
$\epsilon$ : Emissivity [-]
$T_a$ : Temperature of ambient air [K]
$V_M$ : Molar volume (i.e. 22.4 m$^3$/kmol)
$M$ : Molecular weight of fuel [kg/kmol]
$M_a$ : Molecular weight of air [kg/kmol]
$h_c$ : Lower heat of combustion of fuel [kJ/kg]
$c_{pa}$ : Specific heat of air at constant pressure [kJ/(kg·K)]

The final diameter of the fireball, $D_c$, is written as:

$$D_c = \left[\frac{6}{\pi}\frac{V_M}{M}\frac{T_c}{273}\{\mu + (n_i + 1)f_c\}m_f\right]^{\frac{1}{3}} \qquad \text{eq. 2.8}$$

The duration of combustion is suggested by Roberts (1982). It can be written by:

$$t_c = 0.45 m_f^{\frac{1}{3}} \qquad \text{eq. 2.9}$$

Therefore, the rate of increase of diameter is given by:

$$\frac{dD}{dt} = \frac{D_c - D_0}{t_c} = \frac{0.425 V_M^{\frac{1}{3}}}{M^{\frac{1}{3}}}\left[\{\mu + (n_i + 1)f_c T_c\}^{\frac{1}{3}} - T_a^{\frac{1}{3}}\right] \qquad \text{eq. 2.10}$$

Roberts' model

Roberts (1982), as cited by CCPS (1994), uses a heat production of fireball to calculate its final diameter. It is assumed that at the time the maximum size of fireball, the total increase in enthalpy can be related to the initial mass ratio of fuel to air. Assuming that $R$ is the mass ratio of fuel-air mixture, i.e. mass of air relative to mass of fuel, the approximation of enthalpy rise can be written by:

$$H = \frac{\eta m_a h_c}{R} \quad \text{for} \quad m_a \le R m_f \qquad \text{eq. 2.11}$$

$$H = \frac{\eta m_f h_c}{R} \quad \text{for} \quad m_a > R m_f \qquad \text{eq. 2.12}$$

$h_c$ : Heat of combustion [kJ/kg]
$\eta$ : Thermal efficiency that recognizes fuel losses and unburned fuel ($\eta < 1$) [-]
$R$ : Mass ratio of fuel-air mixture ($m_a/m_f$) [-]

The maximum diameter of the fireball can be expressed by:

$$D_c = \left[\frac{6}{\pi}\left\{1 + \frac{H}{T_0 c_p (m_f + m_a)}\right\}\frac{\frac{m_a}{m_f} + 1}{\rho_0}\right]^{\frac{1}{3}} m_f^{\frac{1}{3}} \quad \text{eq. 2.13}$$

$\rho_0$ : Density of combustion products at initial temperature $T_0$ [kg/m$^3$]

$c_p$ : Average specific heat of mixture considered to be constant from $T_0$ to maximum fireball temperature [kJ/(kg·K)]

Lift-off time can be determined by using following formula:

$$t_{lo} = 1.1 m_f^{\frac{1}{6}} \quad \text{eq. 2.14}$$

$t_{lo}$ : Lift-off time [s]

$m_f$ : Mass of fuel [kg]

The formula is suggested by Hardee and Lee (1978) as cited by CCPS (1994).

Related to the mass of fuel contributing to a fireball, Mudan, as cited by SINTEF (2003, p.7-50), suggests the rule of thumb for it as follows.

- If the flash fraction, $f$, exceeds 30 percent, it should be assumed that the entire mass of fuel is contained in the vapour cloud.
- If the flash fraction is less than 15 percent, it may be assumed that the remaining liquid will burn in the form of a pool fire.
- If the flash fraction ranges from 15 to 30 percent, a linear interpolation is assumed for the liquid fraction.

#### 2.1.3.2 Radiation

Radiation emitted by heat (thermal radiation) can cause severe burns to people. A fireball that might be produced after a BLEVE can emit high thermal radiation. There are two approaches to calculate the radiation intensity of a fireball: point-source model and flame model. Both formulas are given in Appendix B.

To assess the severity of radiation intensity to human body, Table 2-1 shows the various level of radiation intensity with the respective time to reach pain threshold. In addition, Table 2-2 shows the qualitative observed effects of specific radiation intensity. CCPS (1994) suggested a comparison with the radiation intensity of a hot summer day which approximately is 1 kW/m$^2$.

#### 2.1.3.3 Blast Wave Overpressure

CCPS (1994) suggested that a containment with PLG inside can produce blast waves upon bursting in three ways. First, the highly-pressurized vapour cap (vapour space) above the liquid space produces a blast. Second, blast from liquid space can occur if the liquid boils violently upon depressurization, i.e. the liquid has reached the superheat limit. Third, if the liquid is combustible and the BLEVE is not fire induced, a VCE may occur. Table 2-3 shows some effects on structural elements depending on the incoming side-on overpressure. An example of shock wave time series is shown in Figure 2-3.

CCPS (1994) provided the guidelines to calculate the blast wave overpressure at certain distances from the centre of an explosion. This will be discussed later with a calculation sample.

Table 2-1. Exposure Time to Reach the Pain Threshold Based on API 521 (1982) (CCPS, 1994, p.181)

| **Radiation Intensity** | | **Time to Reach Pain Threshold** |
|---|---|---|
| **[Btu $h^{-1}$ $ft^{-2}$]** | **[$kW/m^2$]** | **[s]** |
| 500 | 1.58 | 60 |
| 740 | 2.33 | 40 |
| 920 | 2.90 | 30 |
| 1500 | 4.73 | 16 |
| 2200 | 6.94 | 9 |
| 3000 | 9.46 | 6 |
| 3700 | 11.67 | 4 |
| 6300 | 19.87 | 2 |

Table 2-2. Effects of Thermal Radiation (CCPS, 1984, p.181)

| **Radiation Intensity [$kW/m^2$]** | **Observed Effect** |
|---|---|
| 37.5 | Sufficient to cause damage to process equipment<br>Minimum energy required to ignite wood at indefinitely long exposures |
| 12.5 | Minimum energy required for piloted ignition of wood, melting of plastic tubing |
| 9.5 | Pain threshold reached after 8 s; second degree burns after 20 s |
| 4.0 | Sufficient to cause pain to personnel if unable to reach cover within 20 s; however, blistering of the skin (second degree burns) is likely; 0 % lethality |
| 1.6 | Will cause no discomfort for long exposure |

Table 2-3. Conditions of Failure of Side-on Overpressure-Sensitive Elements (CCPS, 1994, p.203)

| **Structural Element** | **Failure** | **Approx. Overpressure** | |
|---|---|---|---|
| | | **[bar]** | **[psi]** |
| Glass windows | Usually shattering, occasional frame failure | 0.03-0.07 | 0.5-1 |
| Corrugated asbestos shading | Shattering | 0.07-0.14 | 1-2 |
| Corrugated steel or aluminium | Connection failure followed by buckling | 0.07-0.14 | 1-2 |
| Wood siding panels standard house construction | Failure, usually at main connections, allowing a whole panel to be blown in | 0.07-0.14 | 1-2 |
| Concrete or cinder-block wall panels 8 or 12 inch thick (not reinforced) | Shattering of wall | 0.14-0.20 | 2-3 |
| Self-framing steel panel building | Collapse | 0.20-0.28 | 3-4 |
| Oil storage tank | Rupture | 0.20-0.28 | 3-4 |
| Wooden utility poles | Snapping failure | 0.34 | 5 |
| Loaded rail cars | Overturned | 0.48 | 7 |
| Brick wall panel 8 or 12 inch thick (not reinforced) | Shearing, flexure failure | 0.55 | 7-8 |

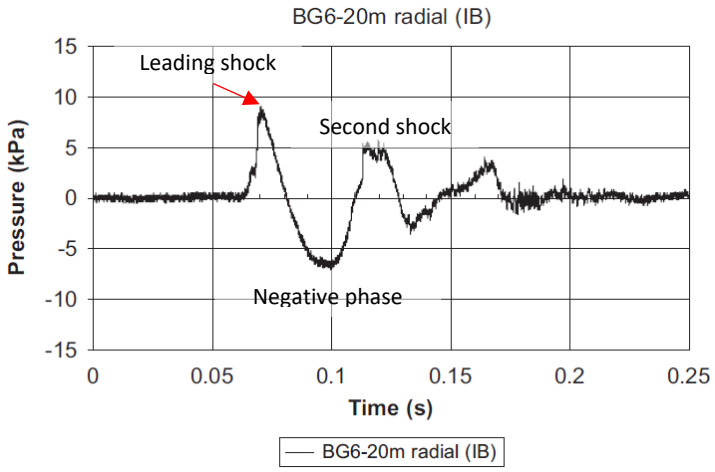


Figure 2-3. Blast wave time series at 20 m from side of a 2000 L propane tank BLEVE (Birk et.al., 2007, p.200).

### 2.1.3.4 Projectile Fragments

A BLEVE can produce projectiles (fragments) which fly away rapidly from the explosion source (CCPS, 1994). These fragments are dangerous and may result in damage to structures and injuries to people even though the number of fragments produced by BLEVEs is less than the one produced by a high explosive detonation. Moreover, the fragments are varying in size, shape, and therefore initial velocity. Also, we have to consider the trajectory of the fragments.

Figure 2-4 shows an example of projected trajectory of the fragments in three BLEVE tests. In the second test, there were nine tracked fragments, some of them were identified up to 400 m from the tank axis (explosion source). Another test conducted by BAM (German Federal Institute for Materials Research and Testing / *Bundesanstalt für Materialforschung und -prüfung*) produced four major fragments which were identified up to 200m away from the explosion source (Balke et.al., 2001). Projectile fragments are not discussed and treated further in this thesis.

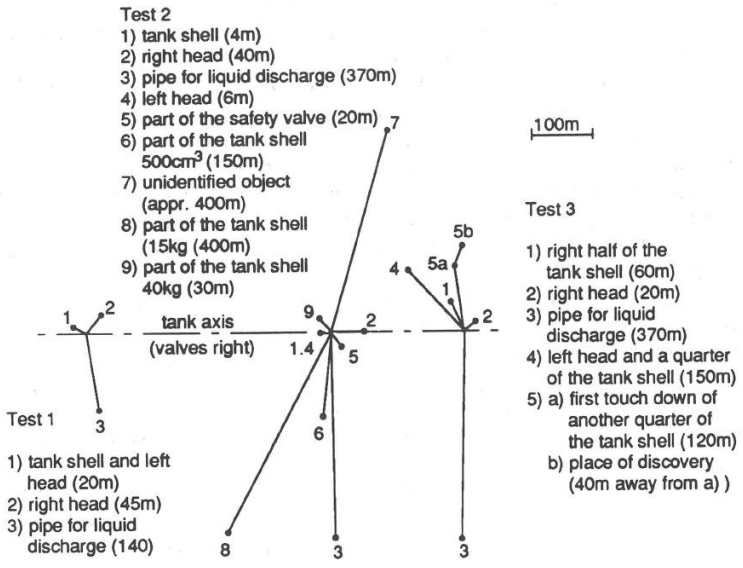


Figure 2-4. Schematic view of vessel fragments' flight after vessel bursts in three BLEVE tests (Schulz-Forberg et.al., 1984). Reference: CCPS (1994, p.224)

## 2.2 FLACS

### 2.2.1 Introduction of FLACS

FLACS is an abbreviation of Flame Acceleration Simulator which was developed by Gexcon AS. The development of the software has been being ongoing at Gexcon (CMR/CMI) since 1980. The first public release was in 1986 and since then the software is the most reliable software for gas explosions. The latest release, at the time of writing, is FLACS v.10.5r1 which consists of several essential modules to handle various gas incidents such as dispersion, explosion, DDT, blast, etc. Gexcon is also developing an integrated package to assist QRA (Quantitative Risk Analysis) activities and help decision makers to understand the meaning of simulation output in an actual safety context (FLACS-Risk).

The FLACS software consists of three main packages which has their own role. The three packages are FLACS Run Manager, CASD (Computer Aided Scenario Design), and Flowvis. The first package has a purpose to execute the scenarios that have been created using CASD package. In CASD, we can create not only the scenarios (physical parameters) but also the geometry approximation of an actual facility. Flowvis has a purpose to visualize the output parameters in 1D, 2D, and 3D.

### 2.2.2 Application Areas of FLACS

FLACS is developed as a tool for safety applications. Major disasters cause huge losses in industry and society in general, and most of these disasters are related to loss of fluid containment. According to Marsh (2012), as cited by the FLACS User's Manual, a majority of the 100 largest property losses in hydrocarbons industries from 1972 to 2011 involved fire and explosions. FLACS is developed to answer several problems related to safety as follows.

- Loss of containment and dispersion of flammable, asphyxiating, malodorous, toxic, and/or radioactive material in gaseous, liquid, and/or solid form.
- Gas explosions, vapour cloud explosions, mist explosions, dust explosions, colliery explosions, hybrid explosions, and vapour explosions.
- Detonation of condensed explosives and propagation of blast waves.
- Jet fires and pool fires.

## 2.3 Applicability of FLACS to Simulate BLEVE

### 2.3.1 BLEVE Model Using FLACS

A BLEVE can cause several negative impacts on the surroundings caused by shock waves and projectiles. Therefore, we need to analyse the effect of BLEVEs during a planning and design phase to investigate the negative impacts to the surroundings.

BLEVE involves a complex phenomenon of flashing liquid. As described in the previous section, Casal et.al. (2002) discussed the fraction of liquid which vaporizes upon depressurization but there is an uncertainty about the true value due to stratification of liquid temperature. Further, the consequences depend on the position of containment or vessel relative to the ground, the characteristics of the substance inside the containment, fire engulfment of the containment, the rupture mode, etc. Hence, there are a lot of possible physical and chemical phenomena, and it is not feasible to investigate all of them. Assumptions and simplifications

are needed in a model; therefore, we also need a process for verification and validation to assess if our model can describe the BLEVE in a proper way.

Hansen and Kjellander (2016) described briefly a way to create a BLEVE model in the FLACS software using so-called two high-pressure regions. The vapour space, i.e. vapour cap, can be modelled directly because the physics are well-known. The liquid space cannot be modelled directly due to the complexity of the flashing phenomenon. A pseudo-source is needed to represent the contribution of the flashing-liquid part to the shock wave. Hansen and Kjellander (2016, p.201) proposed that the pressure and mass of the pseudo-source are determined such that the irreversible expansion energy of the pseudo-source is equal to that of the actual liquid source. The way to determine the mass of flashed gas has been discussed by Casal et.al. (2002). The mass of flashed gas is added as a second high-pressure region next to the vapour space. This method tends to overestimate the overpressure. Genova (2008), as mentioned by Hansen and Kjellander (2016), suggests using only 7 % of the available thermal energy. This will result in pressure reduction of pseudo-source up to 80 %, i.e. the initial pressure of pseudo-source is 20 % of the actual pressure. The illustration of the model described by Hansen and Kjellander (2016) is shown in Figure 2-5. Due to the characteristics of the shock wave which may propagate at supersonic speed, a special setting key is required to allow supersonic propagation in FLACS. By default, FLACS does not allow any supersonic flow during simulation.

The method described by Hansen and Kjellander (2016) somehow raised a question on the use of two high-pressure regions. FLACS only allows the user to put one high-pressure region. There is no further explanation on how to generate two high-pressure regions in FLACS. Different approximations for this challenge will be explained later.

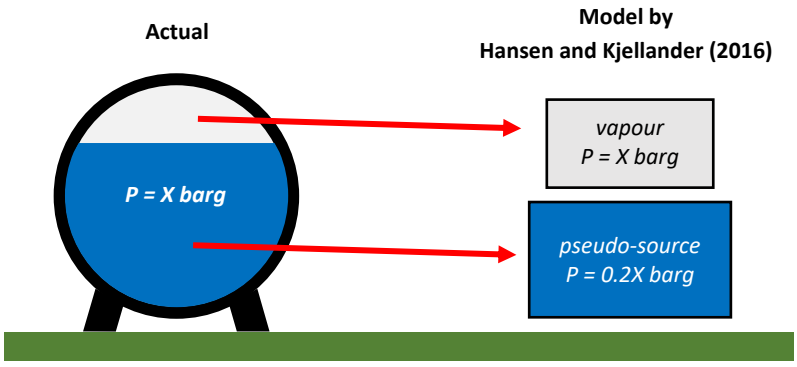


Figure 2-5. Illustration of actual containment and in the model as described by Hansen and Kjellander (2016).

### 2.3.2 Vapour Space

As mentioned by Hansen and Kjellander (2016), the vapour space inside the PLG containment can be modelled straight-forward since the physics are well-known. This can be achieved by the high-pressure region setting in FLACS. The physical parameter of the region is manageable by using the actual values of absolute pressure, absolute temperature, and dimension. The liquid space, on the other hand, must be separated from the vapour space using a different approximation and physical process.

The only difficulty is the shape of the containment. Cylindrical and spherical shapes are available inside the high-pressure region setting, but the actual shape of vapour and liquid shape may be not cylindrical nor spherical. Due to this limitation, simple shapes must be used to represent the vapour and liquid space: a rectangular shape. Since FLACS is using block grids, a rectangular shape can minimize another problem regarding mass residual. Conservative values are expected because the rectangular shape occupies larger space than cylindrical segment or spherical cap. The illustration is shown in Figure 2-6 below.

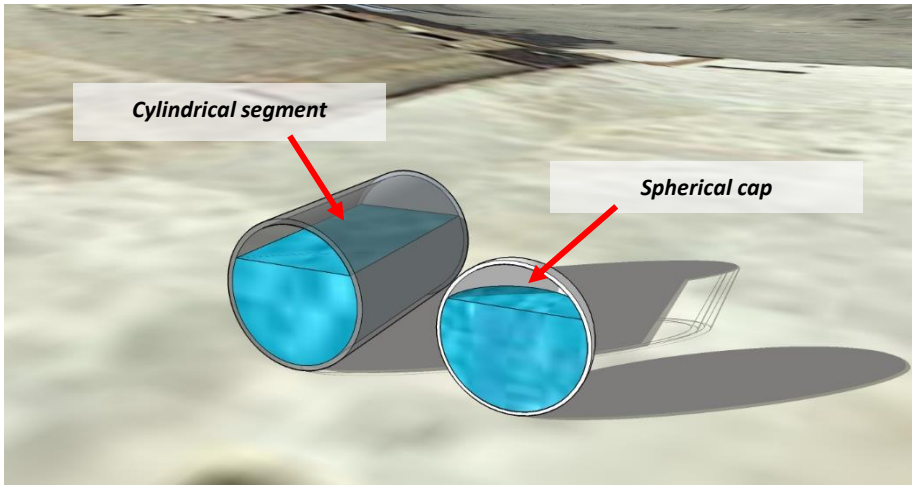


Figure 2-6. Illustration of cylindrical segment and spherical cap.

### 2.3.3 Liquid Space, the Pseudo-Source

Similar with the vapour space, a simple block must be used to represent the high-pressure region in FLACS. Since the flashing process cannot be captured by FLACS, we must convert the flashed liquid into gas as mentioned before. The fraction of excess heat and vaporization factor leads to several adjustments in pressure and volume. The formulas are shown in the previous section. Methods to establish the pseudo-source region will be explained later in Chapter 4.

### 2.3.4 Gas Composition

The gas composition inside the containment should be defined in FLACS. The software allows for the user to specify up to eleven gases of a gas-air mixture. In addition, the properties of several common gases including light- to medium-weight paraffin, hydrogen, carbon dioxide, methanol, and so on have been defined by FLACS. For a complete list of gases, it is referred to the FLACS user's manual.

Most of the BLEVE cases involve large amounts of pressurized gas which are released into the atmosphere at ambient pressure. It can be assumed that at the time of rupture the released gas will contain a large volumetric fraction of gas-air mixture close to 100 %. In other words, the released gas is pure gas with a negligible amount of air (oxygen, nitrogen, and inert gases).

To achieve this pure gas condition, we have to set the equivalent ratio of gas in rich condition to a high number. According to Gexcon (2016), the equivalent ratio is a measure of the concentration of fuel compared to the stoichiometric concentration, i.e. ER equals unity at

stoichiometric concentration. The mole of air can be represented by the mole of oxygen. This can be written as follows:

$$ER = \frac{\left(\frac{V_{\text{fuel}}}{V_{O_2}}\right)_{\text{actual}}}{\left(\frac{V_{\text{fuel}}}{V_{O_2}}\right)_{\text{st}}} \qquad \text{eq. 2.15}$$

By setting the ER to a large value, it suggests that the volumetric fraction of fuel is very large (close to infinity) while the volumetric fraction of oxygen is very small (close to infinitesimal). Therefore, FLACS will create a pure gas inside the containment. The large value itself can be defined as ten to the thirty ($10^{30}$). Smaller power numbers have been tried and still produce 100 % volumetric fraction of gas, such as ten to the ten ($10^{10}$). With the use of smaller numbers, mass residual issues might be minimized.

### 2.3.5 Coarse Validation of The Approach

A coarse validation of the approach has been done using simple and omni-symmetrical shapes. Two coarse simulations have been performed to see the blast wave propagation and fireball shape from spherical and cubical shapes. The objective is to see whether the blast wave propagation and fireball shape for simple source shapes are approaching what is known from experience. Due to its symmetrical shape, both simulations should produce symmetric contours of blast wave and shape of fireball.

The first simulation assumes a spherical shape with a 5 m diameter and 20 barg initial pressure. FLACS aborted the simulation due to mass residual issue when it was simulating the blast wave. This issue did not appear when FLACS was simulating the fireball. Due to the use of a Cartesian grid, it is difficult for FLACS to deal with a spherical shape. Hence, the spherical shape will be simulated as a pixelated sphere instead of a smooth sphere as shown in Figure 2-7. FLACS must calculate the porosity on the surface of the sphere. Therefore, the pixelated edge of spherical volume will have lower pressure than it should.

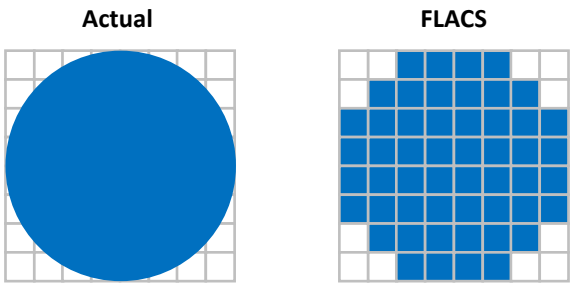


Figure 2-7. Illustration of pixelated spherical shape in FLACS.

The second simulation assumes cubical shape with 1.6 m sides and 7.7 barg initial pressure. Smaller volume and pressure were chosen to minimize the possibility of mass residual issue. In addition, due to its shape the control volumes were fully filled (no porosities) and it is easier for FLACS to deal with it.

Based on the results of the second simulation using a cubical pressure region, we can see that the blast wave propagates symmetrically along horizontal axes (x- and y- axis). The blast wave contour creates a similar pattern which repeated every 90°. From the blast overpressure curves at distance 10 m and 25 m in x- and y- axis, we can only see two curves and the other two curves are hidden because of this symmetric pattern as shown in Figure 2-8 and Figure 2-9.

For the fireball simulation, the shape is, more or less, symmetric and also has a 90°-repetition pattern. But there are some differences with respect to details as shown in Figure 2-10. From the picture, the ignition takes place at the lowest value of x-, y-, and z-position. Therefore, the fireball is slightly larger (well-developed) in negative x- and y-quadrant. A different fireball shape is produced for a spherical pressure region. Its shape creates a 180°-repetition pattern even though the maximum distance is the same for four directions (x- and y- axis). Snapshots of results of an initial spherical region simulation is shown in Figure 2-11.

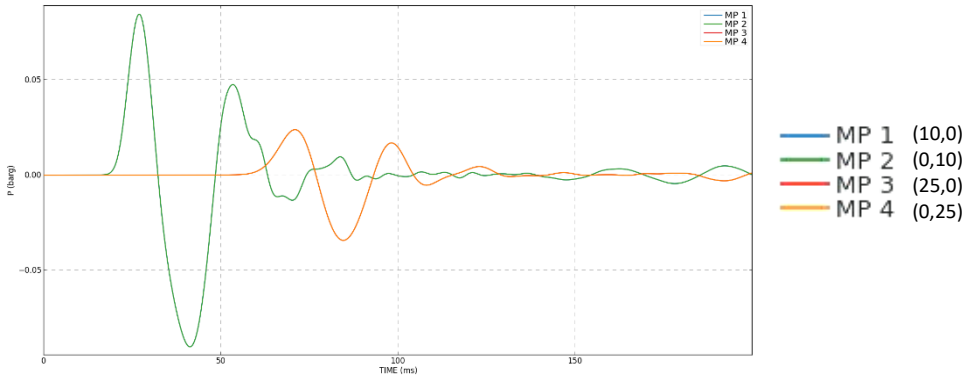


Figure 2-8. Blast overpressure curve for cubical pressure region.

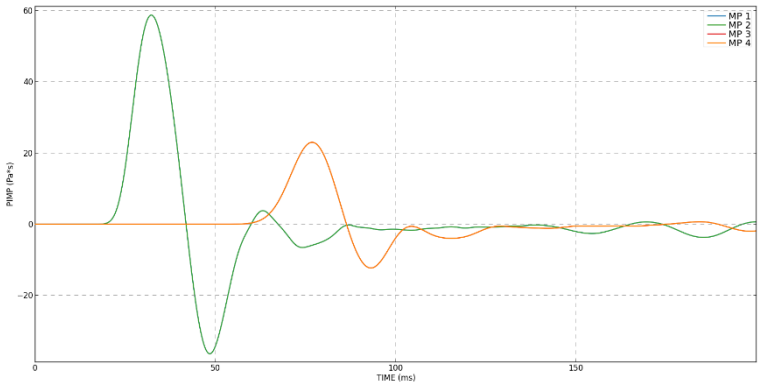


Figure 2-9. Blast impulse curve for cubical pressure region.

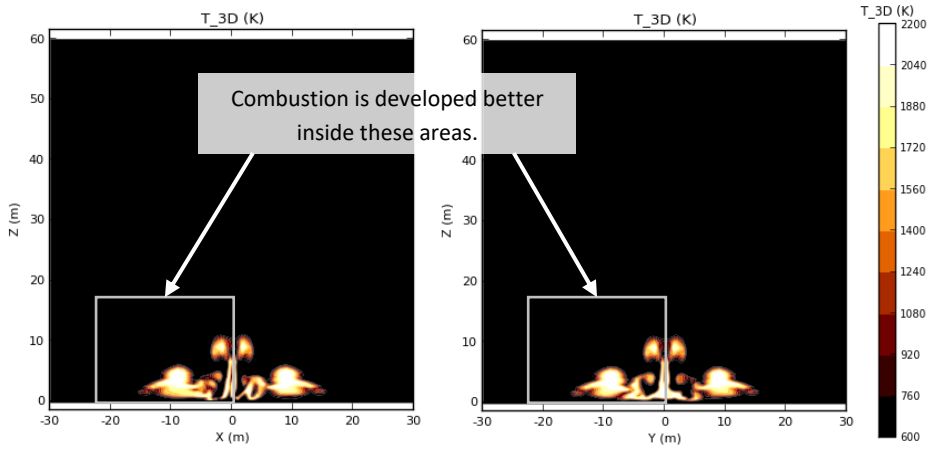


Figure 2-10. Snapshot of fireball using a cubical pressure region.

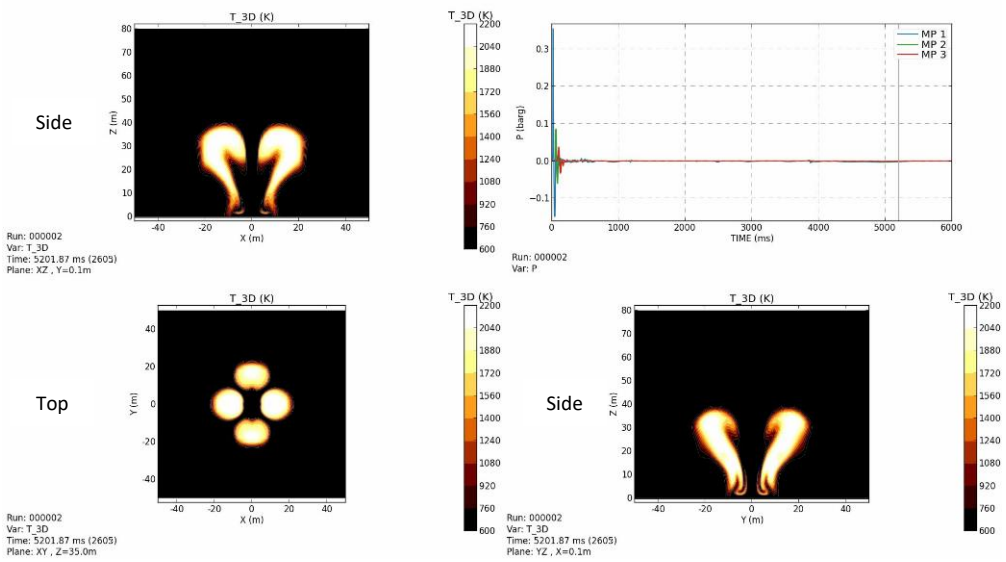


Figure 2-11. Snapshot of fireball using spherical pressure region.

# 3 Shock Waves from BLEVE

## 3.1 Analytical Calculation of Blast Parameters

### 3.1.1 Calculation of Blast Parameters Using CCPS Guidelines

Blast parameters (static overpressure and impulse) of BLEVEs can be calculated using the guidelines issued by the CCPS (1994, pp.202 - 222). The systematic calculation consists of three methods and firstly depends on the content inside the vessel or containment. The guide to select the blast calculation method is shown in Figure 3-1. The three methods mentioned by CCPS (1994) are (1) basic method, (2) refined method, and (3) explosively flashing method. The diagram of calculation steps for the methods are shown in Figure A-5, Figure A-6, and Figure 3-2 respectively. The calculation method described by CCPS (1994) will provide maximum values for horizontal direction.

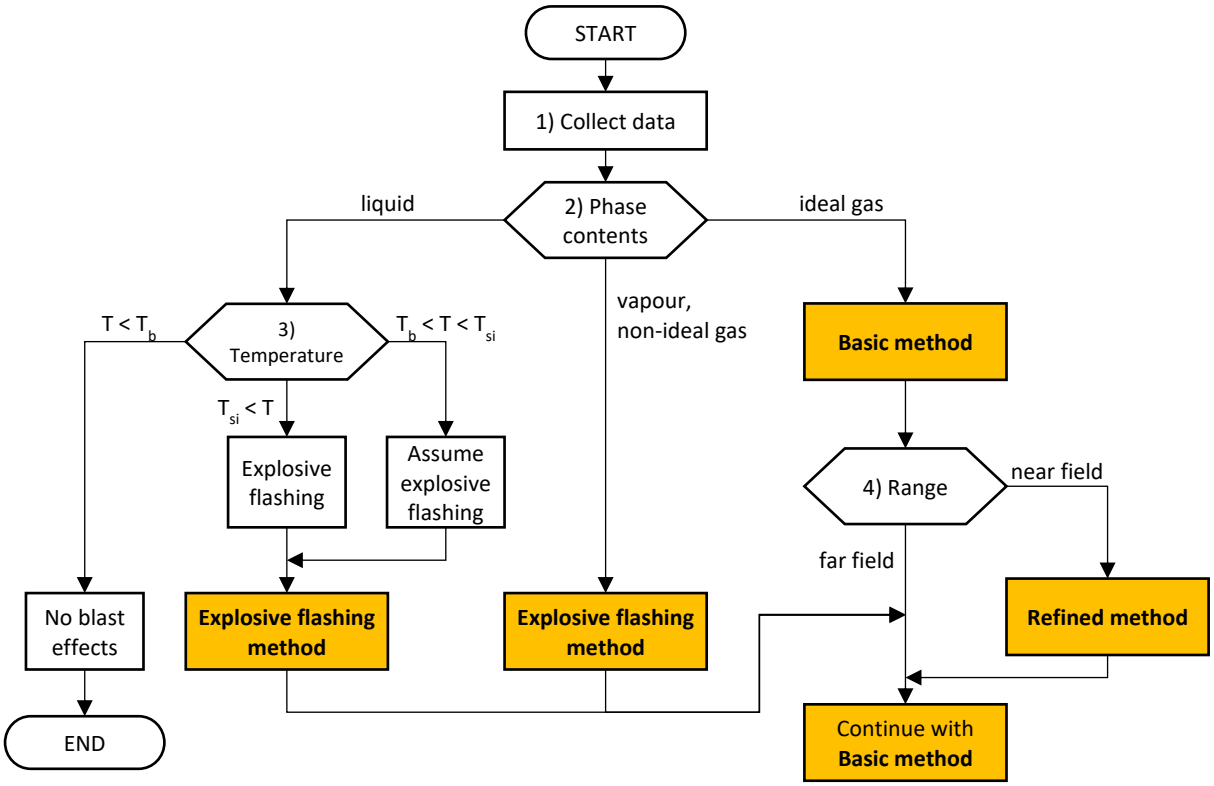


Figure 3-1. Selection of blast parameters calculation method (CCPS, 1994).

#### 3.1.1.1 Basic Method

The basic method is applied when the gas inside the containment is assumed to be an ideal gas. The ideal gas has a compressibility factor equal to or approximately 1 (one) and follows ideal gas law:

$$PV = nRT \quad \text{eq. 3.1}$$

$P$ : Pressure of the gas [Pa]
$V$ : Volume of the gas [$m^3$]
$n$ : Number of moles of the gas [mol]
$R$ : Gas constant [8.314 J/(K·mol)]
$T$ : Absolute temperature of the gas [K]

The calculation steps and flowchart for the basic method are attached in Appendix A.

#### 3.1.1.2 Refined Method

The refined method is applied when the target is relatively close to the blast source ($\bar{R}$<2). There are some calculations in addition to the basic method.

The calculation steps and flowchart for the refined method are attached in Appendix A.

#### 3.1.1.3 Explosively Flashing Method

Explosively flashing method is applied when the gas is considered as non-ideal. Most of the cases, the containment or vessel is filled with fluids whose behaviour cannot be described by the ideal gas law. In addition, some liquids may vaporize violently when suddenly exposed to ambient condition. This violent vaporization is also known as flashing. Furthermore, in most cases both liquid and vapour of the substance exist at the same time. Therefore, we need to consider contribution of both phases to the explosion.

**Step 1: Collect data**

The following data must be collected to perform the calculation using this method.

- Absolute internal pressure $p_1$ at failure.
- Ambient pressure $p_0$.
- Quantity of the fluid (volume $V_1$ or mass).
- Distance from centre of containment to target, $r$.
- Shape of containment: cylindrical or spherical.

Additional data must be collected if the fluid is not listed in Step 2 later.

**Step 2: Check the fluid**

CCPS (1994) provides specific work done for seven common fluids namely ammonia, carbon dioxide, ethane, propane, isobutane, nitrogen, and oxygen. When the fluid is not listed, additional thermodynamic data for the fluid must be collected such as specific enthalpy ($h$), specific entropy ($s$), and specific volume ($v$). Those data can be found in Perry and Green (1984) or Edmister and Lee (1984).

If the fluid is listed, the data provided in Table 6.12, Figure 6.30, and Figure 6.31 of CCPS (1994) can be used and the calculation step can be skipped to Step 5.

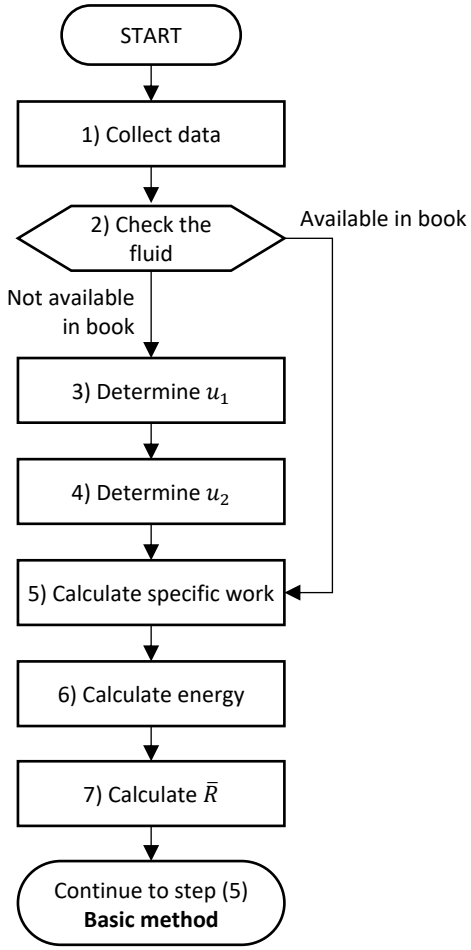


Figure 3-2. Calculation of flashing liquid energy and pressure vessel burst filled with vapour or non-ideal gas (CCPS, 1994).

**Step 3: Determine internal energy in initial state, $u_1$**

The work done by an expanding fluid is defined as the difference in internal energy between the fluid's initial and final states. Most thermodynamic data only provide *h*, *p*, *v*, *T* (absolute temperature), and *s* (specific entropy). Therefore, $u$ must be calculated using the following equation.

$$u_1 = h_1 - p_1 v_1 \qquad \text{eq. 3.2}$$

$h_1$ : Specific enthalpy in initial state [J/kg]
$u_1$ : Specific internal energy in initial state [J/kg]
$p_1$ : Absolute pressure in initial state [Pa]
$v_1$ : Specific volume in initial state [$m^3$/kg]

**Step 4: Determine internal energy in expanded state, $u_2$**

Following equation must be used to calculate the specific internal energy in expanded state, $u_2$.

$$u_2 = (1 - X)h_f + Xh_g - (1 - X)p_0 v_f - Xp_0 v_g \quad \text{eq. 3.3}$$

$X$ : Vapour ratio [-] = $\frac{s_1 - s_f}{s_g - s_f}$

$s$ : Specific entropy [J/(kg·K)]

Subscript 1 refers to initial state.

Subscript f refers to state of saturated liquid at ambient pressure.

Subscript g refers to state of saturated vapour at ambient pressure.

The eq. 3.3 is only valid when the value of *X* is between 0 and 1.

**Step 5: Calculate the specific work**

The specific work done by an expanding fluid is defined as

$$e_{ex} = u_1 - u_2 \quad \text{eq. 3.4}$$

$e_{ex}$ : Specific work [J/kg]

It is also possible to have specific work per unit volume [J/m$^3$]. Graph shown in Figure 6.31 of CCPS (1994) uses work per unit volume instead of unit mass.

**Step 6: Calculate expansion energy**

To obtain the expansion energy, simply multiply the specific work from Step 5 by the mass of fluid released or by the volume if specific work per unit volume is used. There is a multiplication factor of 2 to account for reflection of the shock wave on the ground. Fragment reduction factor is a means of accounting for energy consumed in the production and throw fragments of the vessel.

$$E_{ex} = 2(1 - frag)e_{ex}m_1 \quad \text{eq. 3.5}$$

$m_1$ : Mass of released fluid [kg], or volume of released fluid [m$^3$]

$e_{ex}$ : Specific work per unit mass [J/kg], or specific work per unit volume [J/m$^3$]

$frag$ : Fragment reduction factor [-]

**Step 7: Calculate the non-dimensional range $\bar{R}$ of the target**

The non-dimensional range of the target can be calculated using the following formula.

$$\bar{R} = r\left[\frac{p_0}{E_{ex}}\right]^{\frac{1}{3}} \quad \text{eq. 3.6}$$

$r$ : Distance of target from the centre of containment [m]

The step continues to Step 5 of the basic method (refer to Appendix A) to obtain the value of $\bar{P}_s$ and $\bar{I}$, then the calculated side-on overpressure and impulse of the target.

### 3.1.2 Pseudo-source for Liquid Space

The term "pseudo-source" is derived from two words: pseudo- (Greek: *pseudos*, means false or lying) and source. Basically, pseudo-source means that the source is not the actual source in terms of properties or characteristics. As mentioned before, the physics of the flashing process is very complex and not as well-understood as expanding vapour. Therefore, we need to alter the physics of the liquid in a BLEVE into a source that is well-known, in other words, treat the liquid space as a gas.

Hansen and Kjellander (2016, p.201) uses the term "pseudo-source" to refer to the flashing liquid part. They suggest some key points of this pseudo-source:

- The expansion energy of the pseudo-source corresponds to the energy calculated from the real liquid source.
- The temperature of the pseudo-source is set to the boiling point. The reason is the assumption that the gas cools as it flashes.
- The pressure of the pseudo-source is assumed to be one-fifth of the pressure of vapour space. Genova (2008), as cited by Hansen and Kjellander (2016), suggests using only 7 % of the available thermal energy when applying energy-equivalent method.

Genova et.al (2008, p.113) suggest that the liquid flashing can be regarded as a process thermally driven by the excess heat stored in the liquid itself. Considering a high filling level, they suggest that the expansion work used for blast wave generation can be assumed as a fraction of the excess heat stored in the liquid, which is denoted by $\chi$. Mathematically, it can be written by:

$$W = \chi Q = \chi m C_p \Delta T \qquad \text{eq. 3.7}$$

$W$ : Expansion work for blast wave generation [J]
$\chi$ : Fraction of the excess heat stored in the liquid that converts into expansion work of blast wave [-]
$m$ : Liquid mass [kg]
$C_p$ : Specific heat of the liquid at constant pressure [J/(kg·K)]
$\Delta T$ : Temperature difference between the temperature of the liquid at the moment before bursting and the boiling temperature of the liquid at atmospheric pressure [K]

Later, the value of $\chi$ is set to 7 % which is derived from experimental data. This 7 % value means that only 7 % of the flashed liquid will contribute to blast wave generation. To obtain the equivalent volume of this flashed liquid at a value of 20 % of the initial pressure, thermophysical data of gas are required. One reference of such data is Younglove and Ely (1987). In the thermophysical data they present, there is information about density at particular pressures and temperatures for specific gases (methane, ethane, propane, isobutane, and n-butane). By using the proper information of density at specific conditions, $\rho_{P,T}$, the volume can be obtained. The pressure of the pseudo-source can be obtained using eq. 3.9 as suggested by Hansen and Kjellander (2016). The temperature is assumed to be equal to the temperature of vapour space.

$$V_{PS} = \frac{0.07 f \cdot m_l}{\rho_{P,T}} \qquad \text{eq. 3.8}$$

$V_{PS}$ : Volume of pseudo-source [$m^3$]
$f$ : Vaporization factor of flashing liquid [-]
$m_l$ : Mass of liquid [kg]

$$P_{PS} = \frac{1}{5} p_s \qquad \text{eq. 3.9}$$

$P_{PS}$ : Pressure of pseudo-source [barg]
$p_1$ : Initial shock overpressure [barg]

Since the initial pressure of the shock wave is influenced by the amount of flashing liquid, it is assumed that only a fraction of the liquid will be involved. Casal et.al. (2002, p.15) estimated the vaporization fraction flashing liquid as shown in eq. 2.1. Recalling the equation:

$$f = 1 - \exp\left[-2.63 \frac{C_p}{H_v}(T_c - T_b) \cdot \left(1 - \left(\frac{T_c - T_0}{T_c - T_b}\right)^{0.38}\right)\right]$$

$f$ : Vaporization fraction of flashing liquid [-]
$C_p$ : Specific heat at constant pressure [J/(kg·K)]
$H_v$ : Enthalpy of vaporization of the substance [J/kg]
$T_c$ : Critical temperature of the substance [K]
$T_b$ : Boiling temperature of the substance at atmospheric pressure [K]
$T_0$ : Temperature of the substance in the moment of explosion [K]

Another approximation of the flashing fraction is given by SINTEF (2003) as follows.

$$f = 1 - \exp\left[-\frac{C_{pl}(T_R - T_B)}{h_v}\right] \qquad \text{eq. 3.10}$$

$f$ : Vaporization fraction of flashing liquid [-]
$C_{pl}$ : Heat capacity of liquid [J/(kg·K)]
$T_R$ : Release temperature [K]
$T_B$ : Boiling temperature [K]
$h_v$ : Heat of vaporization [J/kg]

Both equations use a single value of heat capacity or specific heat, meanwhile in reality the value is temperature-dependent. Flashing fractions that approximated by Casal et.al. (2002) tend to have slightly higher values than ones by SINTEF (2003) as shown in Table 3-1. Therefore, the approximation by Casal et.al (2002) will be used throughout this thesis.

Table 3-1. Comparison Between Value of Flashing Fraction by Casal et.al. (2002) and SINTEF (2003)

| Experiment | $H_v$ | $C_p$ | $T_c$ | $T_r$ | $T_b$ | f (Casal) | f (SINTEF) |
|---|---|---|---|---|---|---|---|
| BG-1R | 219500 | 3272 | 408 | 368 | 261.3 | 0.894 | 0.796 |
| BG-2 | 204800 | 3366 | 408 | 374 | 261.3 | 0.933 | 0.843 |
| BG-3 | 298230 | 2733 | 408 | 323 | 261.3 | 0.484 | 0.432 |
| BG-4 | 246600 | 3105 | 408 | 355 | 261.3 | 0.790 | 0.693 |
| BG-5 | 318076 | 2864 | 369.8 | 308 | 230.8 | 0.582 | 0.501 |

Regarding the possible initial shock wave strength due to the flashing process, Hansen and Kjellander (2016) found that complete flashing resulted in overestimation of blast side-on overpressures. Genova et.al. (2008) suggest that the flashing liquid process is governed by the excess heat stored in the liquid which contributes to shock wave generation. Therefore, he suggests 7 % of the energy stored inside the liquid will contribute to shock wave. The calculated explosion energy in CCPS' guidelines should therefore be multiplied by a factor

7 % before both the non-dimensional peak side-on overpressure and side-on impulse are being assessed. In addition, Hansen and Kjellander (2016) conclude that the evaporation may not be fast enough to create pressure waves developing into shock waves.

### 3.1.3 Directional Effects of a BLEVE

The directional effects of a BLEVE (special case of a PVB) were studied by Geng et.al. (2009), as cited by CCPS (2011, p.256), using CFD model. The effects occur due to the non-spherical shapes or non-uniform fractures of the vessel. Both conditions are the most likely occur in PVBs. They used a cylindrical vessel for that study which is placed horizontally relative to the ground. At the time it exploded, the elliptical shock waves were generated, with weaker shock waves along the longitudinal axis (cylindrical axis) and stronger shock waves along the radial axis (normal to cylindrical axis). Both strengths of shock waves also have different propagation speed. Stronger shock waves travel faster than weaker shock waves. Therefore, as the blast waves propagate outward further, the shapes of the blast waves become more spherical and the blast effects become more evenly distributed. Figure 3-3 shows the pressure contours generated from the CFD model. The blast waves have elliptical shapes at the beginning and gradually approach spherical.

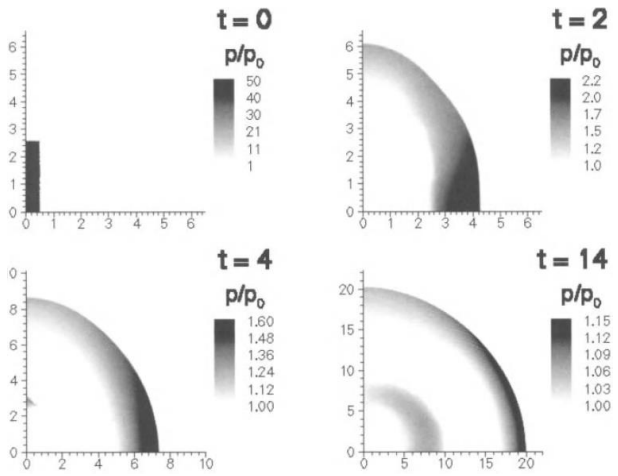


Figure 3-3. Pressure contours of a blast field for a cylindrical burst in X-Y axes (Geng et.al. 2009).
Reference: CCPS (2011)

## 3.2 Comparison with Past Experiments

Several experiments of BLEVE have been conducted by British Gas which are reported by Johnson et.al. (1991), as cited by Hansen and Kjellander (2016). The data of experiments are presented in Table 3-2. British Gas conducted experiments with different parameters to study the effect. In the BG-2 experiment, the mass of gas was reduced to half and in the BG-3 experiment the rupture pressure was reduced to half. In the BG-4, the volume of the tank was almost doubled to see the effect of volume to overpressure. In the BG-5, the gas was changed to propane to see the effect of using a different gas.

The theoretical calculations of those experiments are done based on CCPS (1994). The results are shown in Table 3-3. We can see that some results of overpressure at 25 m radial distance are close to the un-factored calculation, i.e. the calculation without adjustment factors. The guideline states that spherical shapes and close distance above the ground lead to an

amplification of blast wave overpressure. The factored calculation seems to deal with safety factor and introduces a more conservative value.

Based on these results, it can be concluded that calculation procedures provided by CCPS (1994) can be used to predict the blast overpressure of a BLEVE incident. In addition, these results can be used as a reference for computational simulations using FLACS.

Table 3-2. Overview of Experiments by British Gas

| Experiment | Mass [kg] | Volume [$m^3$] | Gas | Pressure [barg] | Fill Level | Liquid Temp [°C] | Vapour Temp [°C] |
|---|---|---|---|---|---|---|---|
| BG-1R | 2000 | 5.7 | Butane | 15.1 | 77 % | 95 | 83 |
| BG-2 | 1000 | 5.7 | Butane | 15.2 | 39 % | 101 | 90 |
| BG-3 | 2000 | 5.7 | Butane | 7.7 | 68 % | 50 | 12 |
| BG-4 | 2000 | 10.8 | Butane | 15.1 | 40 % | 82 | 90 |
| BG-5 | 2000 | 5.7 | Propane | 15.2 | 80 % | 35 | 34 |

Table 3-3. Summary of Blast Wave Pressure at 25m (Radial) from Centre

| Experiment | Actual Pressure [mbarg] | Calculated Pressure (CCPS, 1994) [mbarg] | Calculated Pressure – Factored (CCPS, 1994) [mbarg] |
|---|---|---|---|
| BG-1R | 63 | 55 | 77 |
| BG-2 | 50 | 60 | 96 |
| BG-3 | 10 | 36 | 50.4 |
| BG-4 | 82 | 85 | 136 |
| BG-5 | 23 | 45 | 63 |

# 4 BLEVE Simulation Using FLACS

## 4.1 Preparation

### 4.1.1 Set of Scenario

For this thesis work, experiments by British Gas (reported by Johnson et.al., 1991) and Birk et.al. (2007) will be used for CFD simulations reference. British Gas did six BLEVE experiments, one of them was repeating the first experiment. Birk et.al (2007) conducted two series of tests in 1993/94 and 2001/02. The first series of tests used a 400 L propane tank, and the second series of tests used a 2000 L propane tank.

Experiment BG-2 by British Gas was used to perform a sensitivity analysis. In this analysis, the blast pressure at a distance of 10 m will be used to see how sensitive the pressure to the various volumes of vapour space and pseudo source (liquid space) are. Experiment BG-2 is also used to validate the blast overpressure of the BLEVE model in FLACS.

The simulation consists of three job files:

- BLEVE setup job file. Simulation of this job will produce a file which contains the vapour and liquid regions of the specific scenario. This output file (called dump file) will be used for the next jobs. Further, simulation of this job is called preparation.
- Blast job file. Simulation of this job will produce a dump file to be used in fireball job in addition to the main output result of various monitored variables. It is necessary to have a converted dump file as the main input. Further, simulation of this job is called cold simulation.
- Fireball job file. Simulation of this job will produce some output results from monitored variables regarding the fireball. It is important to have a converted dump file as input. In addition, it is important to specify the location and time of ignition to burn the expanding fuel. Further, simulation of this job is called hot simulation.

Illustration of the flow of simulations is shown in Figure 4-1. The square box indicates the beginning of the job file with all necessary inputs. The circle indicates the generation of a dump file. The small triangle indicates an event. In the hot simulation, the event is ignition which occurs 1ms (simulated time) after the simulation start. Blank ellipses indicate the outputs.

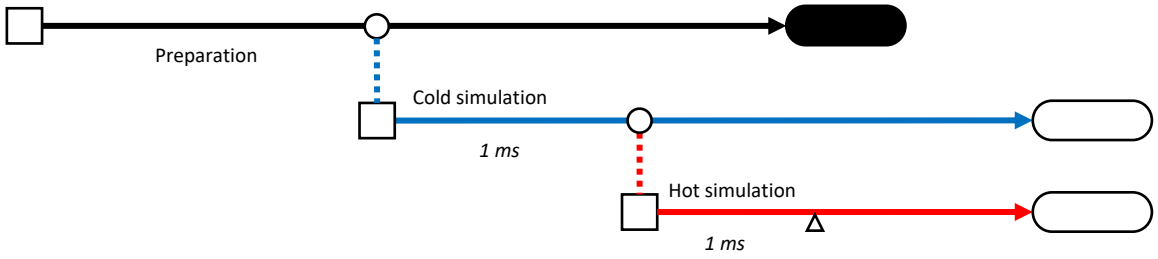


Figure 4-1. Illustration of simulation flow for this thesis work.

Table 4-1 gives an overview of simulation scenarios using FLACS. Some of the experiments were simulated on a coarser grid than they should due to progressive development of the simulation method. The latest five experiments are more consistent in terms of simulation method, grid definition, and so on.

Table 4-1. Overview of Simulation Scenarios

| Experiment | V [$m^3$] | Fuel | Fill Level [ %] | P [barg] | $T_L$ [°C] | $T_V$ [°C] |
|---|---|---|---|---|---|---|
| BG-1R | 5.7 | Butane | 77 | 15.10 | 95 | 83 |
| BG-2 | 5.7 | Butane | 39 | 15.20 | 101 | 90 |
| BG-3 | 5.7 | Butane | 68 | 7.70 | 50 | 12 |
| BG-4 | 10.8 | Butane | 40 | 15.10 | 82 | 90 |
| BG-5 | 5.7 | Propane | 80 | 15.20 | 35 | 34 |
| Birk 01-4 | 2.0 | Propane | 21 | 18.94 | 57 | 101 |
| Birk 02-4 | 2.0 | Propane | 61 | 18.58 | 54 | 57 |

### 4.1.2 Sensitivity Analysis of High-Pressure Volume

Before further and proper simulations start, a sensitivity analysis is necessary to see how the overpressure at a certain distance from the explosion changes when the volume of the high-pressure region changes. In this analysis, sensitivity analyses by changing the volume of the pseudo-source and the volume of vapour are conducted.

Overpressure sensitivity with respect to change in volume of pseudo-source (sensitivity analysis set 1) is shown in Figure 4-2 for 10 m distance and Figure 4-3 for 25 m distance. The curve labelled '000001 (03)' is the reference volume. The reference volume of the pseudo-source is 8.4 $m^3$ (1.2 × 5 × 1.4). The blue line [000001 (01)] is the overpressure curve when the pseudo-source height is 0.4 m less than the reference (6 $m^3$ volume), while the red line [000001 (04)] is the overpressure curve when the pseudo-source height is 0.2 m more than reference (9.6 $m^3$ volume). The list of cases for sensitivity analysis of different volumes of pseudo-sources region is shown in Table 4-2.

The difference of first peak-overpressure at a distance of 10 m is 67 mbar. Therefore, the average sensitivity is 18.6 mbar per $m^3$ difference. At a distance of 25 m, the difference of first peak-overpressure is 17 mbar. Therefore, the average sensitivity is 4.7 mbar per $m^3$ difference.

Table 4-2. List of Cases for Sensitivity Analysis with respect to Pseudo-Source Region

| Job Number | Vapour Region | Pseudo-Source Region |
|---|---|---|
| 000001 (01) | 1.2×5×0.8 | 1.2×5×1.0 |
| 000001 (03) | 1.2×5×0.8 | 1.2×5×1.4 |
| 000001 (04) | 1.2×5×0.8 | 1.2×5×1.6 |

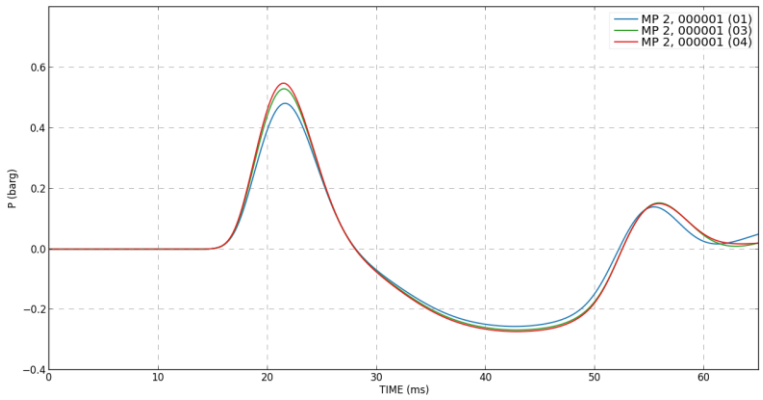


Figure 4-2. Overpressure at 10 m distance for sensitivity analysis set 1.

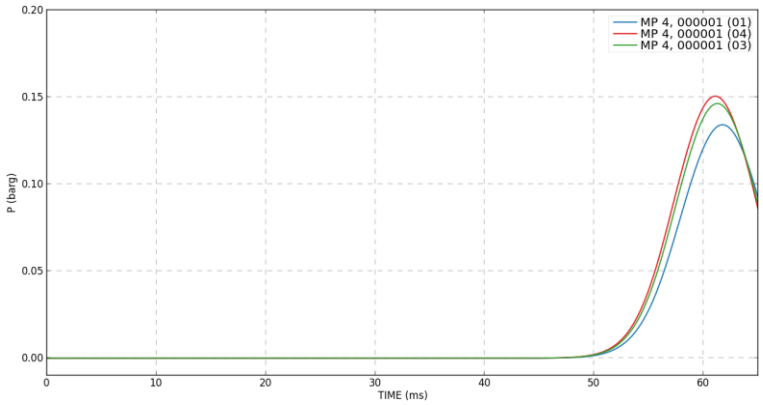


Figure 4-3. Overpressure at 25 m distance for sensitivity analysis set 1.

The overpressure sensitivity with respect to change in volume of vapour space (sensitivity analysis set 2) is shown in Figure 4-4 for 10 m distance and Figure 4-5 for 25 m distance. The curve labelled '000001 (01)' is the reference volume. The reference volume of vapour source is 4.8 $m^3$ (1.2×5×0.8). The green line [000001 (02)], red line, and yellow line are the overpressure curves when the pseudo-source height is 0.2 m, 0.4 m, and 0.6 m respectively more than the reference, giving volumes of 6 $m^3$, 7.2 $m^3$, and 8.4 $m^3$ respectively. A list of cases for the sensitivity analysis of different volumes of vapour region is shown in Table 4-3.

The difference of first peak-overpressure at a distance of 10 m distance is 181 mbar. Therefore, the average sensitivity is 50.3 mbar per $m^3$ difference. At a distance of 25 m, the difference of first peak-overpressure is 45 mbar. Therefore, the average sensitivity is 12.5 mbar per $m^3$ difference.

Table 4-3. List of Cases for Sensitivity Analysis with respect to Vapour Region

| Job Number | Vapour Region | Pseudo-Source Region |
|---|---|---|
| 000001 (01) | 1.2×5×0.8 | 1.2×5×1.4 |
| 000001 (02) | 1.2×5×1.0 | 1.2×5×1.4 |
| 000001 (03) | 1.2×5×1.2 | 1.2×5×1.4 |
| 000001 (04) | 1.2×5×1.4 | 1.2×5×1.4 |

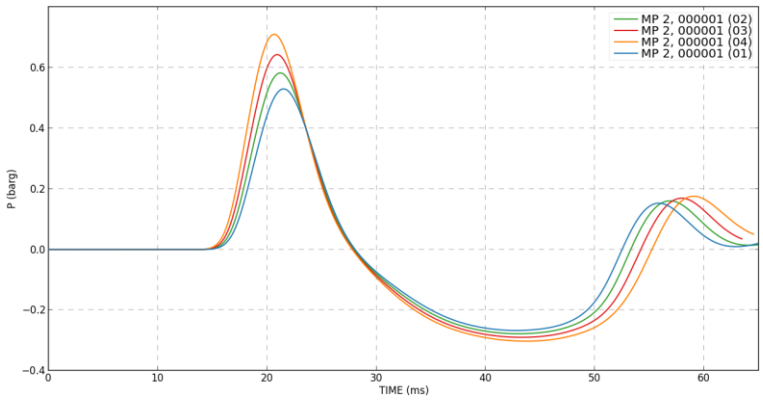


Figure 4-4. Overpressure at 10m distance for sensitivity analysis set 2.

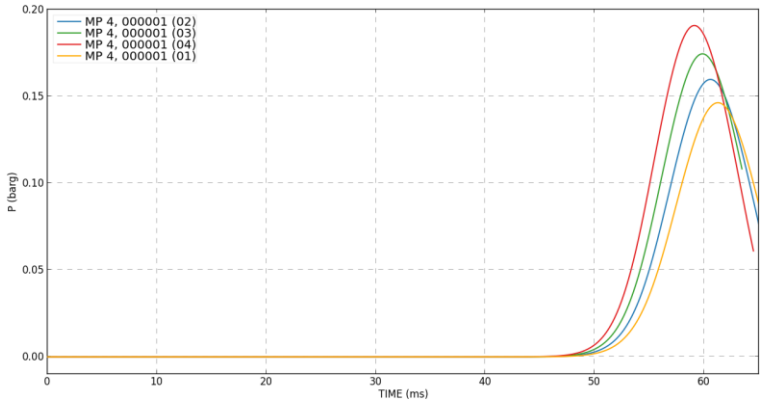


Figure 4-5. Overpressure at 25m distance for sensitivity analysis set 2.

From the figures above, it can be seen that a change in the pseudo-source volume gives smaller contribution to peak overpressures than a change in the vapour space volume. The reason is the explosion energy of the vapour space will be larger when the volume of the vapour space is increased due to higher pressure than the pseudo-source.

In short, the effect of volume deviation in the pseudo-source region will not give a considerable influence on the blast overpressure results compared to volume deviations in vapour region. In addition, if rounding is necessary due to snap-to-grid practices in FLACS, rounding up have to be done, i.e. a control volume must be considered as full region, although it is actually half-full, to be conservative.

### 4.1.3 Simulation Settings

To do a correct and proper simulation, several simulation settings need to be defined. Some important simulation settings are Courant number, duration of simulation, plotting time step, grid definition, and boundary condition.

Courant number, also known as Courant-Friedrichs-Lewy condition, in FLACS is divided into two references: the speed of sound (CLFC) and the speed of convection (CFLV). This number tells that in each time step, the speed of sound or flow is permitted to propagate up to the number of grids. If the CFLC is equal to 2, this means that sound waves can propagate up to 2 grids or control volumes. High number of CFL leads to shorter time to finish the simulation time but an instability or mass residual issue may occur during a simulation and abort the simulation process. On the other hand, a low number of CFL leads to longer times to

finish the simulation but may obtain a good simulation result and minimize mass residual issue. The instability when using high CFL numbers is due to convergence problems, i.e. the number of iterations has reached the limit but the mass residual is still larger than $10^{-4}$ (Gexcon, 2016).

The maximum time of simulation is an important thing to decide to capture the necessary result. A shorter duration leads to improper output because the important part of results might not be captured. The simulation is terminated before the important part comes. Therefore, it is important to do few trial simulations with a coarser grid and a high CFL to obtain the proper duration of simulation.

Also, a proper time step for graph plotting is necessary for the presentation of simulation results. Flowvis, one of the several packages in FLACS, allows users to create time-series plot, distance plots, 2D plots (cross section), and 3D plots. In addition, it allows users to create a movie of the output. Shorter time step results in smooth curves or movies, while bigger time step results in staggered curves or choppy movies.

Grid definition influences the resolution of simulation. Use of a large grid size might sacrifice some small details but it makes the simulation runs faster and has low memory consumption. Small grid size can capture small details but the simulation runs slower and consumes a lot of memory. Here, memory is defined as volatile memory which is known as RAM. In addition, grid characteristics will determine the volume of both vapour and liquid spaces since panels and walls must lie on the grid lines to be impermeable.

Proper type of boundary conditions (BC) is necessary to prevent unwanted results. There are several provided options of BC in FLACS: Euler, plane wave, wind, nozzle, symmetry, Bernoulli, and Eqchar. Plane wave BC is used for far-field blast. It reduces the effect of reflection of pressure waves. It requires large domain volumes, in other words, the domain volume is much larger than the initial cloud size. This boundary condition has been used for most of the simulations.

We also need to define the high-pressure regions based on the scenario data. Due to a limited capability of FLACS, users can only put one high-pressure region with full control of the physical parameters. To put another high-pressure region, several methods can be used with similar limitations: we cannot control the temperature for the region.

- High-pressure region using jet leaks. We can create a high-pressure region by putting jet leaks inside a confinement. The confinement is created using panels and those should be set to withstand extremely high pressure. There are a lot of drawbacks such as long simulation time, not well-distributed pressure, relatively higher probability to crash due to mass residual error, etc.
- High-pressure region using redundant size of pressure. Panels are required in this method to keep both high-pressure regions. The controlled high-pressure region need to be extended beyond the desired volume of, for example, vapour space. We must keep the extension inside another confinement, so the simulation domain is stable. The only drawback of this method is repetition (trial and error) to achieve the desired pressure using a monitor point.

The latter method has been used for all simulations. The illustration of this method is presented in Figure 4-6. The high-pressure region inside the vapour space is kept stable by the panels if the high-pressure region fills the entire vapour space, i.e. the dimension of vapour space is not larger nor smaller than the high-pressure region as shown in Figure 4-7. Larger or smaller dimension will create a pressure instability either inside vapour space or simulation domain. To estimate the initial volume of the redundant volume, the constant P-V equation can be used.

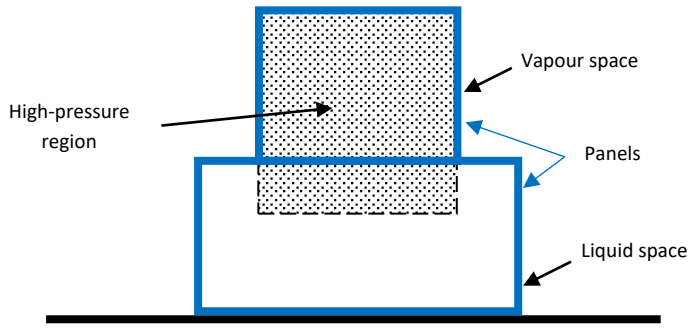


Figure 4-6. Illustration of the selected method to set two high-pressure regions.

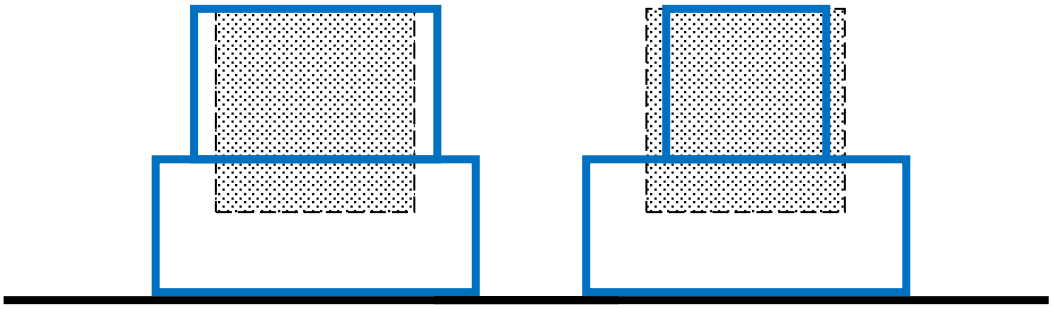

Figure 4-7. Illustration of set up that can create a pressure instability in vapour space (left) and domain (right).

Some important parameters of each simulation are shown in Table 4-4, Table 4-5, and Table 4-6. The first table shows the vaporization fraction of liquid for each simulation. All simulated experiments have vaporization fraction more than half. It means that more than half of the liquid will flash into vapour. The second table shows the information related to volume of pseudo-source and vapour region that were being used in FLACS simulations. The last two columns are the volumes that have been adjusted with the snap-to-grid rule. The calculation sample is shown in Appendix A.3. The latter table shows the grid specification for each simulation. Maximum stretched grid size applies in cold and hot simulations where the accuracy of simulation should be kept high. Stretched control volumes start at a distance of 2 m from the edge of the pressure region.

Table 4-4. Overview of Simulation Scenario with Vaporization Fraction

| Experiment | Fuel | Fill Level [%] | $T_L$ [°C] | $T_V$ [°C] | f [-] |
|---|---|---|---|---|---|
| BG-1R | Butane | 77 | 95 | 83 | 0.8936 |
| BG-2 | Butane | 39 | 101 | 90 | 0.9330 |
| BG-3 | Butane | 68 | 50 | 12 | 0.4843 |
| BG-4 | Butane | 40 | 82 | 90 | 0.7896 |
| BG-5 | Propane | 80 | 35 | 34 | 0.5822 |
| Birk 01-4 | Propane | 21 | 57 | 101 | 0.8155 |
| Birk 02-4 | Propane | 61 | 54 | 57 | 0.7851 |

Table 4-5. Volume Detail of Vapour and Pseudo-Source Regions

| Experiment | Mass [kg] | Flashed Liquid [kg] | $P_{PS}$ [barg] | Vapour Density [kg/m$^3$] | $V_{PS}$ [m$^3$] | $V_{PS}$ grid [m$^3$] | $V_V$ grid [m$^3$] |
|---|---|---|---|---|---|---|---|
| BG-1R | 2000 | 125.1040 | 3.02 | 8.03 | 15.5718 | 15.6 | 2.40 |
| BG-2 | 1000 | 65.3100 | 3.04 | 7.88 | 8.2870 | 8.4 | 4.80 |
| BG-3 | 2000 | 67.8020 | 1.54 | 5.72 | 11.8535 | 12.0 | 3.00 |
| BG-4 | 2000 | 110.5440 | 3.02 | 8.39 | 13.1757 | 13.2 | 9.22 |
| BG-5 | 2000 | 81.5080 | 3.04 | 7.34 | 11.1031 | 11.4 | 1.80 |
| Birk 01-4 | 182.53 | 10.4197 | 3.788 | 8.18 | 1.2735 | 1.5 | 2.40 |
| Birk 02-4 | 537.28 | 29.5273 | 3.716 | 8.11 | 3.6405 | 3.8 | 1.20 |

Table 4-6. Grid Information for Each Experiment

| Experiment | Simulation Domain | Core Grid Size | Stretched Grid Factor | Maximum Stretched Grid Size | Number of CV |
|---|---|---|---|---|---|
| BG-1R | 60×60×50 | 0.2 | 1.2 | 1 | 1304424 |
| BG-2 | 52×52×30 | 0.2 | 1.2 | 1 | 963900 |
| BG-3 | 60×60×60 | 0.1 and 0.2 | 1.2 | 1 | 723330 |
| BG-4 | 60×60×60 | 0.1 and 0.2 | 1.2 | 1 | 908820 |
| BG-5 | 60×60×50 | 0.1 and 0.2 | 1.2 | 1 | 1304424 |
| Birk 01-4 | 60×60×60 | 0.1 and 0.2 | 1.2 | 1 | 1672704 |
| Birk 02-4 | 60×60×60 | 0.1 and 0.2 | 1.2 | 1 | 1672704 |

The following tables describe the parameter of computation time steps. Each simulation has been set for specific CFLC, CFLV, DTPLOT, and TMAX. These four parameters will determine the time step, resolution of plots, and usage of non-volatile memory. The parameters for each experiment are shown in Table 4-7, Table 4-8, and Table 4-9 for preparation, cold, and hot simulation respectively.

Table 4-7. Output Settings for Preparation Simulation

| Experiment | Simulation Domain | Grid Specification | CFLC / CFLV | DTPLOT | TMAX (min, max) |
|---|---|---|---|---|---|
| BG-1R | 60×60×50 | 0.1 core; 1.2× stretched | 2 / 0.4 | 0.002 | 0.4, 0.4 |
| BG-2 | 52×52×30 | 0.1 core; 1.2× stretched | 5 / 1.0 | 0.001 | 0.6, 0.6 |
| BG-3 | 60×60×60 | 0.1 core; 1.2× stretched | 5 / 0.5 | 0.010 | 0.4, 0.4 |
| BG-4 | 60×60×60 | 0.1 core; 1.2× stretched | 5 / 0.5 | 0.002 | 0.4, 0.4 |
| BG-5 | 60×60×50 | 0.1 core; 1.2× stretched | 2 / 0.4 | 0.010 | 0.4, 0.4 |
| Birk 01-4 | 60×60×60 | 0.1 core; 1.2× stretched, max 1.0 | 5 / 0.5 | 0.010 | 0.5, 0.5 |
| Birk 02-4 | 60×60×60 | 0.1 core; 1.2× stretched, max 1.0 | 5 / 0.5 | 0.010 | 0.5, 0.5 |

Table 4-8. Output Settings for Cold Simulation

| Experiment | Simulation Domain | Grid Specification | CFLC / CFLV | DTPLOT | TMAX (min, max) |
|---|---|---|---|---|---|
| BG-1R | 60×60×50 | 0.1 core; 1.2× stretched, max 1.0 | 0.5 / 0.05 | 0.00025 | 0.15, 0.2 |
| BG-2 | 52×52×30 | 0.2 core; 1.2× stretched, max 1.0 | 0.2 / 0.02 | 0.00050 | 0.15, 0.2 |
| BG-3 | 60×60×60 | 0.2 core; 1.2× stretched, max 1.0 | 0.2 / 0.04 | 0.00025 | 0.15, 0.2 |
| BG-4 | 60×60×60 | 0.2 core; 1.2× stretched, max 1.0 | 0.2 / 0.04 | 0.00025 | 0.15, 0.2 |
| BG-5 | 60×60×50 | 0.1 core; 1.2× stretched, max 1.0 | 0.5 / 0.05 | 0.00025 | 0.15, 0.2 |
| Birk 01-4 | 60×60×60 | 0.1 core; 1.2× stretched, max 1.0 | 0.2 / 0.05 | 0.00050 | 0.15, 0.2 |
| Birk 02-4 | 60×60×60 | 0.1 core; 1.2× stretched, max 1.0 | 0.2 / 0.05 | 0.00050 | 0.15, 0.2 |

Table 4-9. Output Settings for Hot Simulation

| Experiment | Simulation Domain | Grid Specification | CFLC / CFLV | DTPLOT | TMAX (min, max) |
|---|---|---|---|---|---|
| BG-1R | 60×60×50 | 0.2 core; 1.2× stretched, max 1.0 | 5 / 0.5 | 0.0020 | 3, 4 |
| BG-2 | 52×52×30 | 0.2 core; 1.2× stretched, max 1.0 | 1 / 0.1 | 0.0010 | 2, 2 |
| BG-3 | 60×60×60 | 0.2 core; 1.2× stretched | 2 / 0.4 | 0.0025 | 5, 5 |
| BG-4 | 60×60×60 | 0.2 core; 1.2× stretched, max 1.0 | 2 / 0.4 | 0.0010 | 3, 5 |
| BG-5 | 60×60×50 | 0.2 core; 1.2× stretched, max 1.0 | 5 / 0.5 | 0.0020 | 3, 4 |
| Birk 01-4 | 60×60×60 | 0.2 core; 1.2× stretched, max 1.0 | 5 / 0.5 | 0.0025 | 5, 6 |
| Birk 02-4 | 60×60×60 | 0.2 core; 1.2× stretched, max 1.0 | 5 / 0.5 | 0.0025 | 5, 6 |

### 4.1.4 Control of Simulations

Control of simulations is important as a part of quality assurance. The purpose is to confirm that all parameters and settings in the simulation are correct regarding input values and simulation purpose. There are three simulations for each experiment which have different purposes.

CASD code lines for panels were generated using an own-made program written in C++. The program has been verified by several visual verification processes using the CASD package. The code lines were copied into a previously-generated scenario file and were checked to see if the scenario file were not corrupted and the panels were placed at the desired position with desired dimensions. The results were satisfying and this program has been used throughout the thesis to optimize the time resources.

Every scenario file generated by the CASD package was checked prior to the simulation against the simulation proposal which contains all required input parameters and simulation settings. Several settings were able to be checked visually in CASD such as grid definition, monitor points, fuel region, ignition region, and so on; others were checked manually by double-checking the values in the scenario file. The high-pressure region setup in the cs-file should be checked before and mainly after the preparation simulation were finished to verify that the values of both vapour and pseudo-source pressure were acceptable.

## 4.2 Simulation Results

Several output variables were computed in every simulation. There are two types of output variables: point output and space output. Point output is stricter than space output in terms of the location. It requires monitor points at several locations which must be defined by users. The variables are selected by the users for both point and spatial output. The results will be saved into two files: r1-file for point output and r3-file for spatial output. The latter uses

huge space of storage because r3-file records all results of the whole simulation domain. It depends on the grid size, the time step of simulation, and the simulation time.

Monitor points in all simulations were set along two main axes: radial (x-axis) and longitudinal (y-axis). The axis of containment coincides with the y-axis of the simulation domain. These two main axes are used to capture the differences in blast propagation for cylindrical containments. It is expected to have larger overpressure in the radial axis than in the longitudinal axis, for the same distance from the centre of explosion as previously discussed in Section 3.1.3. Monitor points are being used to produce a time series of specific variables.

Spatial output can be used to show either 2D plots (cross section) or 3D plots. Both types of plots require spatial data and more hardware resources to work perfectly. Colour scheme is important for both plots to produce better visualization of specific variables. In a 3D plot, the geometry shapes can be shown and help to visualize a specific phenomenon such as fire, explosion, dispersion, smoke, and so on. In this thesis work, there is a problem with 3D visualization due to hardware limitations. Therefore, scalar plots and 2D plots will be used instead. Figure 4-8, Figure 4-9, and Figure 4-10 show examples of simulation results that can be generated using Flowvis.

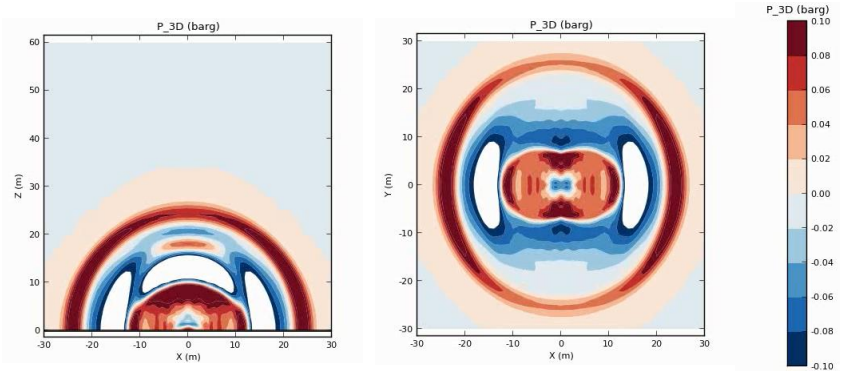


Figure 4-8. Example of 2D (cross section) blast overpressure result at a particular time.

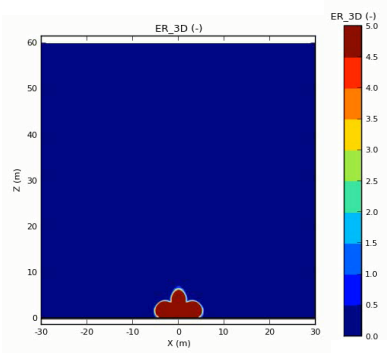


Figure 4-9. Example of 2D fuel equivalent ratio at a particular time.

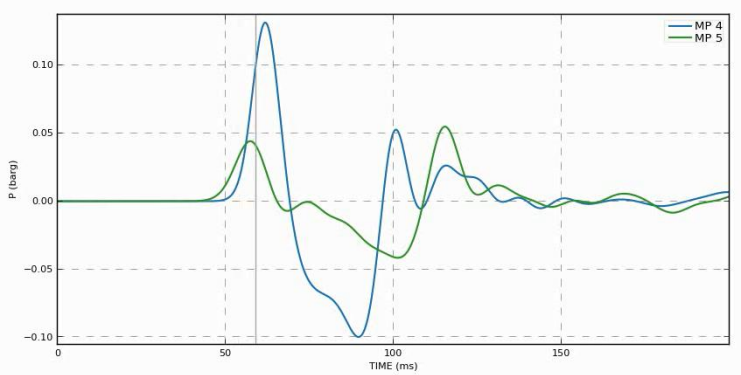


Figure 4-10. Example of blast overpressure result at two monitor points.

During the simulations, several trials for the same experiments have been performed but only the final trial is reported. The trials produce a set of optimum visualization settings for specific types of simulations. Optimum visualization means the domain and resolution of simulation are good enough to visualize the key phenomena. Optimum visualization is necessary due to limited resources. The settings of output parameters are depending on several factors which have been mentioned before for the r3-file brief explanation.

The results for Birk 01-4 simulation are shown in Appendix C. The results are given for selected simulation timepoint with 10 ms step for cold simulation and 100 – 400 ms step for hot simulation. While in Appendix D, plots of blast overpressure and impulse for all simulation are given, including the later Rogfast simulations.

In preparation, the pressure of pseudo-source region was recorded by one monitor point located inside the pseudo-source region. The pressure value must lie around the intended pressure (later called stable pressure) before FLACS generates a dump file that is being used for cold and hot simulations later. This simulation might require more than one trial. The simulation must be repeated if the final stable pressure deviates far from the calculated pressure. The limit of deviation is still unclear but during this work, the deviation is kept below 0.2 bar for lower stable pressure, or below 0.5 bar for higher stable pressure from the calculated or targeted pressure. The upper tolerance is defined larger for conservatism reasons.

In cold simulations, the main output variables are overpressure and impulse. Both variables were recorded by four monitor points. The monitor points are located 10 m and 25 m from the centre of the explosion for both the x- and y-axis. The outcomes of this simulation are pressure contour maps at specific times, blast overpressure time series, and blast impulse time series. Figure 4-11 shows the location of the four monitor points that recorded the relevant output variables with the graphical illustration. It should be noted that the centre of the explosion is located at (0, 0, *z*), with *z* varying with experimental conditions.

The magnitude of peak overpressure and impulse, and time to reach the peak value are shown in Table 4-10 and Table 4-11 respectively. Throughout this work, peak overpressure values are reported in gauge mbar ($10^{-3}$ bar) unit, and peak impulse values are reported in Pa·s.

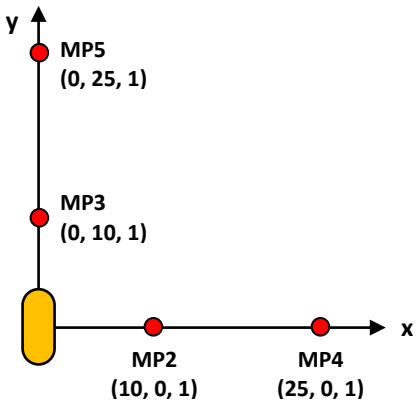


Figure 4-11. Graphical illustration of the location of the monitor points.

Table 4-10. Peak Overpressure and Impulse for Open Space Simulations

| Experiment | Peak Overpressure [mbarg] | | | | Peak Impulse [Pa·s] | | | |
|---|---|---|---|---|---|---|---|---|
| | MP2 | MP3 | MP4 | MP5 | MP2 | MP3 | MP4 | MP5 |
| BG-1R | 186 | 104 | 52 | 28 | 122.42 | 66.92 | 49.22 | 28.27 |
| BG-2 | 211 | 99 | 63 | 29 | 129.67 | 58.12 | 55.08 | 51.16 |
| BG-3 | 141 | 69 | 37 | 20 | 97.84 | 51.34 | 36.72 | 21.96 |
| BG-4 | 478 | 202 | 131 | 44 | 299.50 | 119.33 | 118.60 | 45.42 |
| BG-5 | 187 | 92 | 49 | 26 | 121.22 | 62.45 | 46.41 | 27.47 |
| Birk 01-4 | 191 | 110 | 48 | 33 | 116.35 | 73.13 | 44.80 | 32.64 |
| Birk 02-4 | 130 | 78 | 32 | 22 | 80.80 | 53.32 | 30.27 | 22.64 |

Table 4-11. Time to Reach Peak Overpressure and Impulse for Open Space Simulations

| Experiment | Time to Reach Peak Overpressure [ms] | | | | Time to Reach Peak Impulse [ms] | | | |
|---|---|---|---|---|---|---|---|---|
| | MP2 | MP3 | MP4 | MP5 | MP2 | MP3 | MP4 | MP5 |
| BG-1R | 24.86 | 21.36 | 67.63 | 65.68 | 30.06 | 26.41 | 73.88 | 72.84 |
| BG-2 | 26.77 | 23.96 | 69.17 | 68.37 | 31.82 | 28.73 | 74.91 | 74.49 |
| BG-3 | 24.84 | 21.35 | 67.75 | 65.96 | 30.04 | 27.32 | 73.98 | 93.70 |
| BG-4 | 21.68 | 13.66 | 61.74 | 57.28 | 27.97 | 18.67 | 68.91 | 65.07 |
| BG-5 | 23.50 | 20.44 | 66.29 | 65.08 | 28.62 | 26.16 | 72.56 | 72.69 |
| Birk 01-4 | 22.25 | 21.98 | 65.25 | 66.17 | 27.02 | 27.25 | 71.24 | 72.62 |
| Birk 02-4 | 23.89 | 23.09 | 67.25 | 67.48 | 28.42 | 28.30 | 73.02 | 73.77 |

In hot simulations, the main output variables are temperature and/or combustion product mass fractions. These variables help us to visualize the fireball. The usual practices in Gexcon to visualize fire are as follows (by private communication):

- Using temperature: set the lower limit to 600 K and upper limit to 2200 K.
- Using combustion product mass fraction (PROD): set the lower limit to first tercile and upper limit to second tercile. In other words, the lower limit is one-third of the maximum recorded PROD and the upper limit is two-third of maximum recorded PROD.

The product of hot simulations is fireball visualization using, at least, two horizontal cross-sections to obtain the size of the fireball. Since the ignition source was put in the middle of the source, the cross sections should cross the origin. Another output variable that can be included is equivalent ratio or fuel mole fraction. Height and duration of fireball can be obtained as well

by looking at the cross-section images and the respective time stamp. Figure 4-12 illustrates the result of a hot simulation and how to obtain the important parameters of a fireball.

Several hot simulations have been done with the typical ellipsoid fireball instead of a spherical fireball. Moreover, fireballs that looks like a wheel of cheese appeared just above the ground. This introduces a difficulty to obtain the proper diameter of the fireball. In this thesis work, the fireball is defined as the lifted part of combustion products which looks like a nuclear-explosion mushroom cloud. There are several methods that might be applied to obtain the diameter of fireball assuming a spherical fireball.

- Applying a statistical approach. In other words, maximum or average diameter of all three axes might be used to have one number of diameter.
- Applying an equivalent sphere diameter approach by setting the spherical volume equal to the volume of the ellipsoid. Volume of an ellipsoid and a sphere are given as follows.

$$V_{\text{ellipsoid}} = \frac{1}{6}\pi \cdot D_x D_y D_z \qquad \text{eq. 4.1}$$

$$V_{\text{sphere}} = \frac{1}{6}\pi \cdot D_{eq}^3 \qquad \text{eq. 4.2}$$

$D_{[\text{axis}]}$ : Diameter of simulated fireball at specific axis [m]
$D_{eq}$ : Equivalent diameter of spherical fireball [m]

- Keeping all diameter information of all three axes.

An equivalent sphere diameter approach seems reasonable. The reason is that the volume of fireball region is kept constant when "converting" the different values of diameter into an equivalent diameter. Using the maximum diameter might be fruitful for reason of conservatism especially when talking about safe distances from an explosion. Using a statistical average seems not a good approach but the value is always slightly higher than the equivalent sphere diameter for all simulations.

The duration of fireball is rather difficult to obtain. According to Johnson et.al. (1991) there are several interpretations of this parameter including combustion duration, lift-off time, and duration to reach the maximum diameter as shown in Table 4-13. In addition, one of them is difficult to see qualitatively and quantitatively, the combustion duration of fireball.

Height of fireball is defined in CCPS (1994) as ten times of its duration. It is based on average velocity of rise observed by Lihou and Maund (1982), as cited by CCPS (1994), equal to 10 m/s. Therefore, the height of fireball when it reaches its maximum diameter is ten times the duration to reach maximum diameter. Heights of fireball for all simulations are given in Table 4-14. Some of the values are relatively close to the calculated.

There is a main difficulty when obtaining diameter and height of fireball: the shape of fireball is far from spherical shape. The author would say they are close to ellipsoids, even some of them are completely irregular. The simulation domain is not large enough in several simulations, thus the flame can reach the boundaries.

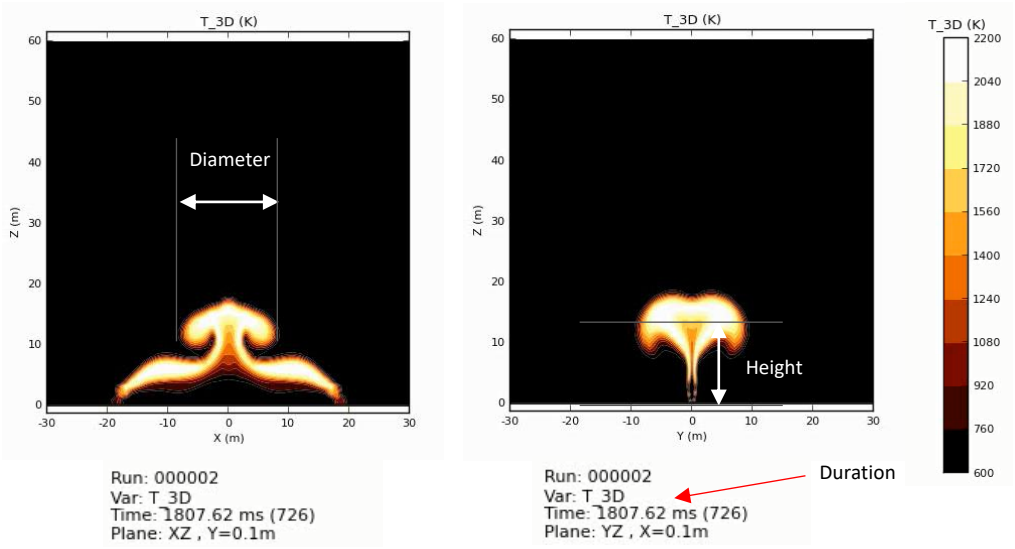


Figure 4-12. Example of cross-section results of fireball using Flowvis.

Table 4-12. Comparison of Different Approaches of Diameter of Fireball

| Experiment | Diameter [m] | | | | Statistical Diameter [m] | |
|---|---|---|---|---|---|---|
| | X | Y | Z | Equivalent D | Max | Average |
| BG-1R | 32.88 | 26.30 | 18.63 | 25.26 | 32.88 | 25.94 |
| BG-2 | 21.62 | 12.58 | 17.42 | 16.80 | 21.62 | 17.21 |
| BG-3 | 20.00 | 11.62 | 22.58 | 17.38 | 22.58 | 18.07 |
| BG-4 | 56.13 | 25.16 | 19.36 | 30.13 | 56.13 | 33.55 |
| BG-5 | 46.49 | 19.46 | 19.46 | 26.01 | 46.49 | 28.47 |
| Birk 01-4 | 21.94 | 23.23 | 11.94 | 18.26 | 23.23 | 19.04 |
| Birk 02-4 | 22.58 | 21.94 | 14.20 | 19.16 | 22.58 | 19.57 |

Table 4-13. Duration of Fireball Based on Several Approaches

| Experiment | Duration [ms] | | |
|---|---|---|---|
| | Max D | Lift-off | Combustion |
| BG-1R | 3584.03 | 2368.39 | - |
| BG-2 | 917.91 | 368.94 | - |
| BG-3 | 4222.59 | 1597.37 | - |
| BG-4 | 4422.97 | 1980.17 | - |
| BG-5 | 3519.46 | 727.99 | - |
| Birk 01-4 | 1990.32 | 1153.04 | - |
| Birk 02-4 | 3620.22 | 1240.39 | - |

Table 4-14. Height of Fireball: Simulated and Calculated

| Experiment | Height [m] | Height – CCPS (1994) [m] |
|---|---|---|
| BG-1R | 29.26 | 35.84 |
| BG-2 | 19.59 | 9.18 |
| BG-3 | 38.62 | 42.23 |
| BG-4 | 29.94 | 44.23 |
| BG-5 | 21.96 | 35.19 |
| Birk 01-4 | 16.88 | 19.90 |
| Birk 02-4 | 28.36 | 36.20 |

## 4.3 Comparison with Existing Experimental Data

All computational simulations are based on actual experiments by British Gas reported by Johnson et.al. (1991) and Birk et.al (2007). Table 4-15 shows the actual and simulated blast overpressure for each experiment. It can be seen from the table that most of the simulated overpressure are above the actual experiment data except blast overpressure of BG-1R simulation. Other comparisons are shown in Table 4-16, Table 4-17, and Table 4-18 for the blast wave overpressure and impulse respectively at distance 25 m from the centre of the explosion except for Birk's experiments. Most of the overpressure values lie between calculated value and factored value. With six out of seven experiments, the current BLEVE simulations using FLACS seem to slightly overpredict the overpressure value which can be considered as conservative value. In the other hand, most of the simulated blast impulse values are more than twice of the calculated values. There is no experimental data regarding the blast impulses.

Table 4-15. Comparison of Blast Peak Overpressure between Experiment and Simulation

| Experiment | 25 m Radial | | 25 m Axial | |
|---|---|---|---|---|
| | Actual [mbarg] | Simulated [mbarg] | Actual [mbarg] | Simulated [mbarg] |
| BG-1R | 63 | 52 | 18 | 28 |
| BG-2 | 50 | 63 | 16 | 29 |
| BG-3 | 10 | 37 | 4.5 | 20 |
| BG-4 | 82 | 131 | 9 | 44 |
| BG-5 | 23 | 49 | 11 | 26 |
| Birk 01-4* | 50 | 191 | - | - |
| Birk 02-4* | 54 | 130 | - | - |
| *) The overpressure value for distance 10 m radial from the centre of the explosion | | | | |

Table 4-16. Comparison of Blast Peak Overpressure Value at 25 m (Radial)

| Experiment | Actual [mbarg] | Calculated [mbarg] | Calculated – Factored [mbarg] | Simulated [mbarg] |
|---|---|---|---|---|
| BG-1R | 63 | 55 | 77 | 52 |
| BG-2 | 50 | 60 | 96 | 63 |
| BG-3 | 10 | 36 | 50.4 | 37 |
| BG-4 | 82 | 85 | 136 | 131 |
| BG-5 | 23 | 45 | 63 | 49 |
| Birk 01-4* | 50 | 150 | 240 | 191 |
| Birk 02-4* | 54 | 120 | 192 | 130 |
| *) The overpressure value for distance 10 m radial from the centre of the explosion | | | | |

Table 4-17. Comparison of Blast Peak Overpressure Value at 25 m (Longitudinal)

| Experiment | Actual [mbarg] | Simulated [mbarg] |
|---|---|---|
| BG-1R | 18 | 28 |
| BG-2 | 16 | 29 |
| BG-3 | 4.5 | 20 |
| BG-4 | 9 | 44 |
| BG-5 | 11 | 26 |
| Birk 01-4 | - | 33 |
| Birk 02-4 | - | 22 |

Table 4-18. Comparison of Blast Impulse Value at 25 m (Radial)

| Experiments | Simulated [Pa·s] | Calculated [Pa·s] | Calculated - Factored [Pa·s] |
|---|---|---|---|
| BG-1R | 49.22 | 26.51 | 26.51 |
| BG-2 | 55.08 | 31.03 | 31.03 |
| BG-3 | 36.72 | 14.26 | 14.26 |
| BG-4 | 118.60 | 48.76 | 48.76 |
| BG-5 | 46.41 | 22.19 | 22.19 |
| Birk 01-4* | 116.35 | 49.25 | 49.25 |
| Birk 02-4* | 80.80 | 36.60 | 36.60 |
| *) The impulse value for distance 10 m radial from the centre of the explosion | | | |

Experimental data of fireball diameters are available for both British Gas and Birk's experiments. In the information by Johnson et.al. (1991), there are complete set of experimental data regarding fireball such as time to each stage of fireball, maximum diameter, and height. While according to Birk et.al. (2003), the selected experiments did not ignite at the time of actual experiment. Table 4-19 and Table 4-20 show the comparison of diameter and duration of the fireball between simulation and experiment, while Table 4-23 shows the comparison of height of fireball between simulation and experiment. The height of fireball is previously defined as the height when the fireball reached its maximum diameter. Table 4-22 shows the comparison between various values of fireball diameter. Calculation using simulated fuel means that the fuel amount for the calculation is based on FLACS simulation. Calculation using initial fuel means that the fuel amount for the calculation is based on the experimental data. Based on the comparisons, most of the simulation results fall quite far from the experimental results for diameter, duration, and height. Simulation results for duration of combustion are not available due to insufficient simulation time, hence the final stage of fireball is not captured. All experimental results are tabulated with yellow background.

Table 4-19. Comparison of Diameter of Fireball Between Simulation and Experimental Data

| Experiment | Equiv. Diameter (sim) [m] | Statistical Diameter (sim) [m] | | Diameter (exp) [m] | |
|---|---|---|---|---|---|
| | | Max. | Average | Max. X | Max. Y |
| BG-1R | 25.26 | 32.88 | 25.94 | 68 | 84 |
| BG-2 | 16.80 | 21.62 | 17.21 | 56 | 64 |
| BG-3 | 17.38 | 22.58 | 18.07 | 64 | 74 |
| BG-4 | 30.13 | 56.13 | 33.55 | 60 | 88 |
| BG-5 | 26.01 | 46.49 | 28.47 | 64 | 66 |
| Birk 01-4 | 18.26 | 23.23 | 19.04 | Did not ignite (Birk et.al., 2003) | |
| Birk 02-4 | 19.16 | 22.58 | 19.57 | Did not ignite (Birk et.al., 2003) | |

Table 4-20. Comparison of Duration of Fireball Between Simulation and Experimental Data

| Experiment | Duration (sim) [s] | | | Duration (exp) [s] | | |
|---|---|---|---|---|---|---|
| | Max. D | Lift-off | Combustion | Max. D | Lift-off | Combustion |
| BG-1R | 3.58 | 2.37 | N/A | 2.00 | 3.20 | 6.30 |
| BG-2 | 0.92 | 0.37 | N/A | 1.20 | 2.70 | 4.50 |
| BG-3 | 4.22 | 1.86 | N/A | 2.20 | 3.90 | 8.40 |
| BG-4 | 1.80 | 1.51 | N/A | 1.50 | 3.60 | 6.50 |
| BG-5 | 1.91 | 1.40 | N/A | 1.90 | 4.00 | 9.20 |
| Birk 01-4 | 1.99 | 1.15 | N/A | Did not ignite | | |
| Birk 02-4 | 3.62 | 1.24 | N/A | Did not ignite | | |

Table 4-21. Comparison of Diameter of Fireball between Simulation and CCPS Calculation Based on Simulated Fuel

| Experiment | Diameter (sim) [m] | | | | Stat. Diameter (sim) [m] | | Fuel Simulated [kg] | Calc. Diameter - CCPS (1994) [m] |
|---|---|---|---|---|---|---|---|---|
| | X | Y | Z | Equivalent | Max. | Average | | |
| BG-1R | 32.88 | 26.30 | 18.63 | 25.26 | 32.88 | 25.94 | 209.47 | 34.45 |
| BG-2 | 21.62 | 12.58 | 17.42 | 16.80 | 21.62 | 17.21 | 104.27 | 27.30 |
| BG-3 | 20.00 | 11.62 | 22.58 | 17.38 | 22.58 | 18.07 | 149.31 | 30.77 |
| BG-4 | 56.13 | 25.16 | 19.36 | 30.13 | 56.13 | 33.55 | 417.47 | 43.35 |
| BG-5 | 46.49 | 19.46 | 19.46 | 26.01 | 46.49 | 28.47 | 141.85 | 30.25 |
| Birk 01-4 | 21.94 | 23.23 | 11.94 | 18.26 | 23.23 | 19.04 | 86.43 | 25.64 |
| Birk 02-4 | 22.58 | 21.94 | 14.20 | 19.16 | 22.58 | 19.57 | 69.84 | 23.89 |

Table 4-22. Comparison of Diameter of Fireball Between Experiment, Calculation, and Simulation

| Experiment | Diameter [m] | | Average of Experiment [m] | CCPS, Using Actual Fuel [m] | CCPS, Using Simulated Fuel [m] | FLACS Simulation [m] |
|---|---|---|---|---|---|---|
| | E-W | N-S | | | | |
| BG-1R | 68 | 84 | 76 | 73.08 | 34.45 | 25.26 |
| BG-2 | 56 | 64 | 60 | 58.00 | 27.30 | 16.80 |
| BG-3 | 64 | 74 | 69 | 73.08 | 30.77 | 17.38 |
| BG-4 | 60 | 88 | 74 | 73.08 | 43.35 | 30.13 |
| BG-5 | 64 | 66 | 65 | 73.08 | 30.25 | 26.01 |
| Birk 01-4 | Did not ignite | | | 32.90 | 25.64 | 18.26 |
| Birk 02-4 | Did not ignite | | | 47.15 | 23.89 | 19.16 |

Table 4-23. Comparison of Height of Fireball Obtained from Simulation and Experiment

| Experiment | Height [m] | Height - Experiment [m] |
|---|---|---|
| BG-1R | 29.26 | 90.00 |
| BG-2 | 19.59 | 45.00 |
| BG-3 | 38.62 | 70.00 |
| BG-4 | 29.94 | 85.00 |
| BG-5 | 21.96 | 90.00 |
| Birk 01-4 | 16.88 | Did not ignite |
| Birk 02-4 | 28.36 | Did not ignite |

The fireball simulations using FLACS do not seem reliable enough if we compare the results with experimental data. There are several reasons that can explain this unreliability.

- Ignition source type. British Gas used three burners as the ignition source according to Johnson et.al. (1991, p.6). The ignition sources were located at one side next to the vessel. Two of them were located 5 m from the vessel and the other one was located 10 m from the vessel. FLACS uses spark-like ignition (ignition with duration close to zero) within one user-defined region. FLACS tries all points inside the region which may result in more than three ignition points. Burners type of ignition source cannot be modelled using FLACS and we cannot specify more than one separated ignition region.
- Fuel quantity cannot be set to desired mass. Using all defined simulation parameters, the initial mass of fuel for all simulations did not meet the desired mass. For example, experiment BG-1R had 2000 kg fuel while the simulation had 216 kg. Further analysis shows that the desired amount of fuel will not be reached with current simulation parameters even though the ER value is set to

a very high number ($10^{30}$ or more). One way to approach the actual fuel amount is either by increasing the high-pressure region volume or by increasing the pressure. Both options will deviate the actual condition, hence, the blast overpressure and impulse results may be deviated even further above the actual values (too high overprediction). The values of vapour space volume or pressure to reach the targeted fuel amount for each simulation are shown in Table 4-24. In addition, two simulations were selected randomly to be rerun using increased amount of pressure and the results are shown in Table 4-25. The results show that FLACS is doing the fireball simulation well by simulating a slightly larger fireball which involves, more or less, actual amount of fuel. The snapshots of the fireball simulations at the maximum diameter are shown in Figure 4-13.

- The flashing process could not be simulated by FLACS. Flashing is considered as a complex process; therefore, Gexcon (2016) recommends converting the liquid part into vapour. By converting the liquid part into lower pressure, it leads to lower fuel amount inside the liquid part than it should. Simulations with FLACS may be reliable for assessing blast wave overpressure but not for fireball or fuel-related assessment. This conversion influences the fuel amount as explained before.
- Shape approximation of the pressurized vessel. Cubical pressure shapes have a different fireball shape with spherical pressure region as shown in Figure 4-14. This may lead to different fuel dispersions hence different fireball shapes. Spherical shape seems better to approach the fireball phenomenon than cubical shape, but as previously discussed, there are some limitations and potential problems when using a spherical shape for the pressure region. Also, it should be noted that the actual shape of vapour and liquid spaces are neither cubical nor spherical shapes.

According to Table 4-22, the calculation based on CCPS (1994) acts as the bridge between experimental result and simulation result. It can be seen that:

- By using the initial fuel amount (1000 and 2000 kg), fireball diameters from calculations using CCPS (1994) are relatively close to the experimental results.
- By using the simulated fuel amount, fireball diameter from calculations using CCPS (1994) are relatively close to the simulated results.

Implicitly, the calculation step of fireball diameter provided by CCPS (1994) is good enough to predict the size of fireball if a BLEVE occurs and the fuel inside is ignited. This is confirmed by experiments and simulations. The value depends on the amount of fuel which is the main difference between experiment and simulation. Increasing the vapour pressure inside the simulation can increase the amount of fuel and the fireball simulation gives a better approach to the actual condition.

Table 4-24. Manipulation of Vapour Volume and Pressure to Reach Targeted Fuel Amount, $M_f$ Target

| Experiment | $M_f$ Target [kg] | $M_f$ Simulated [kg] | $V_{vap}$ [$m^3$] | P [barg] |
|---|---|---|---|---|
| BG-1R | 2000 | 216 | 63.07 | 152.84 |
| BG-2 | 2000 | 114 | 119.03 | 291.17 |
| BG-3 | 2000 | 149 | 93.37 | 122.08 |
| BG-4 | 2000 | 417 | 63.74 | 79.98 |
| BG-5 | 2000 | 142 | 71.22 | 239.37 |
| Birk 01-4 | 182.53 | 86.4 | 6.40 | 41.54 |
| Birk 02-4 | 537.28 | 69.8 | 16.96 | 157.13 |

Table 4-25. Rerun Results of The Selected Simulations Using the Modified Pressure Values

| Experiment | Experiment [m] | Simulated Fuel [kg] | CCPS Using Simulated Fuel [m] | FLACS Simulation [m] |
|---|---|---|---|---|
| BG-4 | 74 | 1687 | 69.05 | 86.54* |
| Birk 01-4 | Did not ignite | 168.50 | 32.04 | 40.70 |
| *) Calculated using the dimensions of the simulation domain. The final diameter might be larger. | | | | |

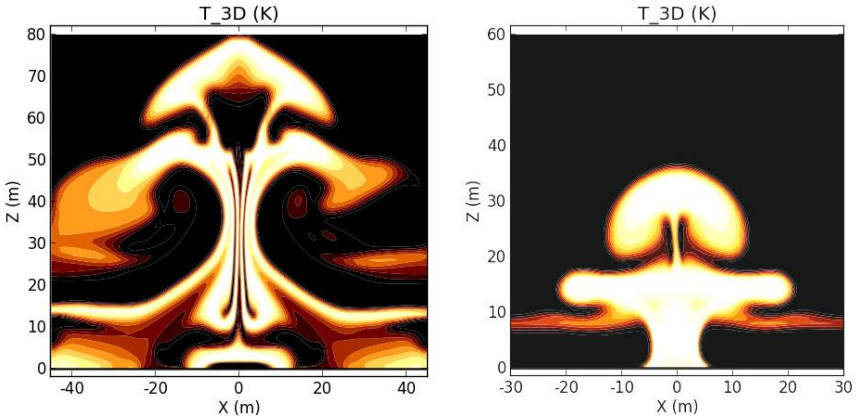


Figure 4-13. Cross section of the fireball for the rerun of BG-4 (left) and Birk 01-4 (right) simulation.

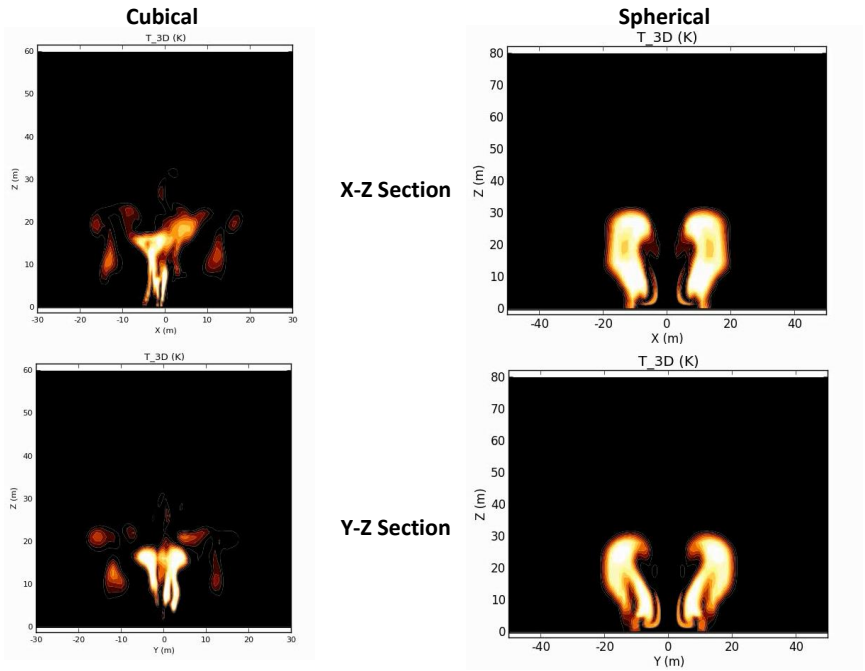


Figure 4-14. Comparison of fireball shape between cubical and spherical pressure region at 4500 ms.

# 5 Simulation of BLEVE in Confined Space

## 5.1 Preparation

### 5.1.1 Scenario

As we may know, BLEVEs might not only occur in open space but also in confined and congested spaces such as tunnels. A tunnel is an important piece of infrastructure to connect two separated points which have complex terrain in order to shorten the travel time. According to vegvesen.no at the time of writing, there are 1174 road tunnels across mainland Norway, 35 of them are underwater. With this high number of tunnels in Norway, cheaper and more efficient distribution of bulk goods such as liquefied gases are expected. One of the worst events in a tunnel is an explosion. Confined spaces such as tunnels will slow down the decay of explosion overpressure, i.e. higher overpressure for relatively long distances.

For this work, one of the future tunnels in Norway will be used to assess the effect of confinement on BLEVEs. The tunnel is called E39 Rogfast and it is still in the planning phase at the time of writing of this thesis. This underwater tunnel will cross Boknafjorden and connect three neighbouring municipalities in Rogaland: Bokn, Kvitsøy, and Randaberg, just north of Stavanger. For better orientation, Figure 5-1 shows the surrounding map and the Norway map.

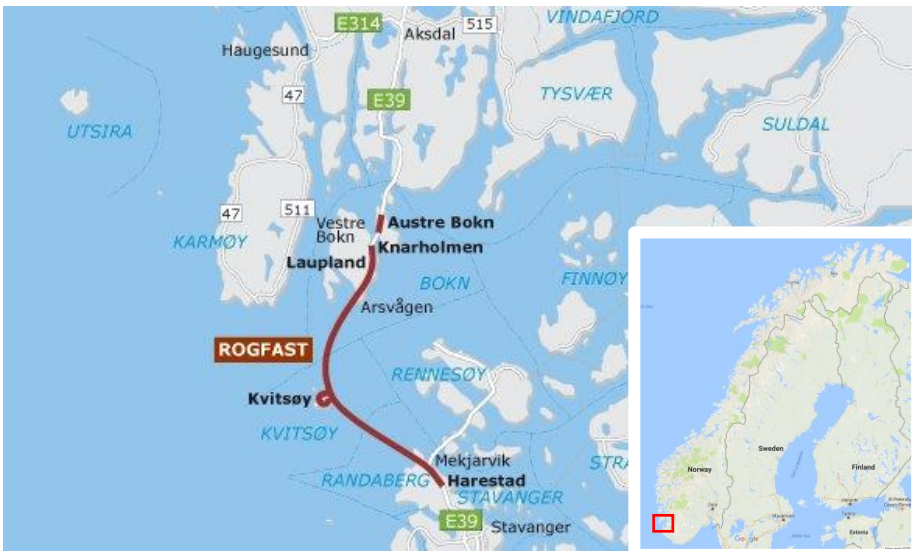


Figure 5-1. Location of future Rogfast tunnel in Rogaland County.
References: vegvesen.no and Google Maps.

This tunnel, which has a 68.5 $m^2$ cross-sectional area, will be assessed using Birk's experiment which involving 2 $m^3$ of propane and typical 10000 US gallons (approximately 37.85 $m^3$) of LPG (95 % propane and 5 % isobutane). According to Norsk Petroleuminstitutt (1997, p.4), in Norway, LPG is mainly transported by tank cars of between 5 and 25 tonnes (12 to 60 $m^3$) and railway tanks of between 13 and 43 tonnes (31 to 103 $m^3$). The objective of why Birk's experiment is discussed first instead of actual conditions is to have a good comparison between BLEVE in open space and confined space. After that, a practical LPG tank volume will be used to see the effect of volume. A summary of the cases for this simulation is shown in Table 5-1.

Table 5-1. Overview of Simulation Scenarios in Confined Space

| Experiment | V [$m^3$] | Fuel | Fill Level [ %] | P [barg] | $T_L$ [°C] | $T_V$ [°C] |
|---|---|---|---|---|---|---|
| Rogfast 1 | 2 | Propane | 21 | 18.94 | 57 | 101 |
| Rogfast 2 and 2R | 37.85 | LPG | 60 | 17.30 | 55 | 55 |

### 5.1.2 Simulation Settings

The main concept and explanation of simulation settings have been discussed earlier. In a confined space, there is not much difference with an open space. The significant differences will be the grid definition, monitor points, and maximum simulated time.

Due to the nature of the tunnel's shape, we cannot use a cubical simulation domain as we do for open space simulations. In tunnel, we are interested in the longitudinal axis of the tunnel rather than radial axis that is limited to the tunnel's wall and tunnel's road pavement. In this thesis work the axis of interest is x-axis, hence the shape of simulation domain will be elongated along the x-axis. Illustration of this elongated domain is shown as Figure 5-2. The yellow box indicates the simulation domain. Red, green, and blue axes indicate the x-, y-, and z- axis of the simulation.

In addition, we have to follow the best practice of FLACS demanding a larger domain volume for plane wave BC to work properly. This affects the length of tunnel that we should consider. A coarse simulation had been conducted before the actual simulations started. Based on the coarse simulation, the basic aspects of BLEVE simulations in tunnels need to be considered:

- We may assume that the characteristics of blast wave act in a similar way for both directions of propagation along the longitudinal axis, i.e. we can assess this in one direction only. In this simulation, one end should be extended far enough from the centre of explosion to reduce the effect of reflection noise.
- The decay rate of blast overpressure in the tunnel is significantly lower than one in open space. This is due to the highly-confined space which create lack of possibilities for spatial expansion (van den Berg and Weerheijm, 2006, p.598). Therefore, the end of the domain should be extended long enough to see the better decay process.
- The velocity of blast wave propagation inside the tunnel is roughly the same as in open space. Increasing the length of domain will increase the maximum time of simulation needed so the blast wave can reach the end of the domain.

The domain used in each simulation together with the overview and volume details are presented in Table 5-4, Table 5-2, and Table 5-3 respectively which are based on those considerations. Since the simulation domain is elongated, monitor points will be located only along the tunnel axis. Therefore, the vessel will be aligned perpendicular and not parallel with the tunnel axis since it will produce blast overpressure effects. In Rogfast 2, the standard LPG tanker length is larger than the width of the tunnel. Therefore, it is not completely perpendicular with respect to the tunnel axis and assumptions have to be made.

In addition, the Rogfast 2 simulation has a line of congestions (vehicles) inside the tunnel. Those are applied in one direction of the axis, so we will have a clear comparison between congested space and uncongested space. The number of vehicles is based on predicted ÅDT (*Årsdøgntrafikk* / Annual Average Daily Traffic or AADT) by the Rogfast's project team. The AADT for the Rogfast Tunnel is predicted to be 13000 vehicles per day (Statens Vegvesen, 2012, p.11). Assuming that:

- the accident occurs in the middle span of tunnel,
- the tunnel is closed immediately at the time of accident,
- the duration to drive through the whole tunnel is 40 minutes, and
- all vehicles beyond the accident point can drive out of tunnel safely,

there are 136 vehicles that would be trapped inside the tunnel. The tunnel will have 2 lanes, therefore, 68 vehicles for each lane. It is assumed that there are 3 types of vehicles for simplicity reasons: compact cars, SUV cars, and buses. The queue starts 100 m in front of the centre of the explosion. Figure 5-3 and Figure 5-4 illustrate the congestion layout for the Rogfast 2 simulation. For Rogfast 2R (repetition of Rogfast 2) simulation, the queue starts 32 m in front of the centre of the explosion. The reason is that the position of congestion was too far away and one could not capture the effect of congestion on the fireball.

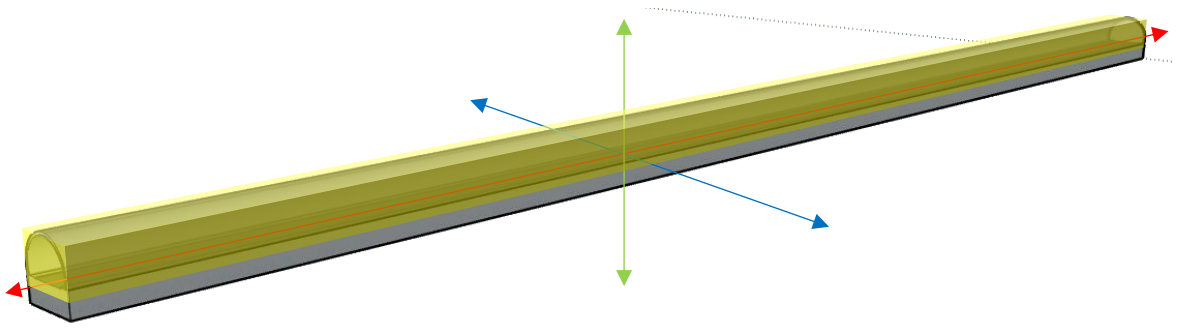

Figure 5-2. Illustration of elongated simulation domain (yellow shades) due to shape of tunnel.

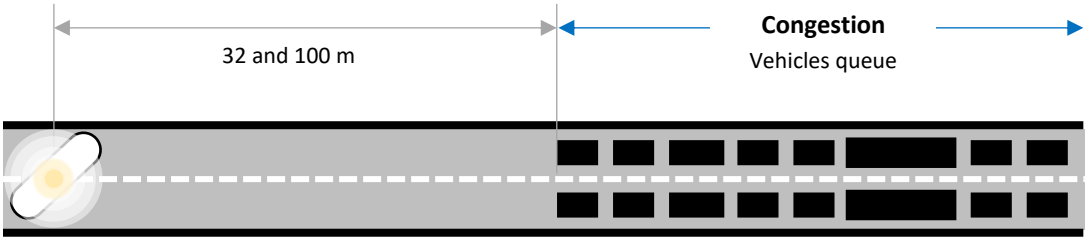


Figure 5-3. Illustration of vessel and congestion inside Rogfast Tunnel.


Figure 5-4. Illustration of global setup for Rogfast 2 simulation.

Table 5-2. Overview of Simulation Scenario with Vaporization Fraction

| Experiment | Fuel | Fill Level [%] | $T_L$ [°C] | $T_V$ [°C] | f [-] |
|---|---|---|---|---|---|
| Rogfast 1 | Propane | 21 | 57 | 101 | 0.8155 |
| Rogfast 2 and 2R | LPG | 60 | 55 | 55 | 0.7804 |

Table 5-3. Volume Detail of Vapour and Pseudo-Source Regions

| Experiment | Mass [kg] | Flashed Liquid [kg] | $P_{PS}$ [barg] | Vapour Density [kg/m$^3$] | $V_{PS}$ [m$^3$] | $V_{PS}$ grid [m$^3$] | $V_V$ grid [m$^3$] |
|---|---|---|---|---|---|---|---|
| Rogfast 1 | 182.53 | 10.4197 | 3.79 | 8.1820 | 1.2735 | 1.50 | 2.40 |
| Rogfast 2 and 2R | 10046.90 | 548.8421 | 3.46 | 8.7096 | 63.0161 | 64.32 | 21.44 |

Table 5-4. Grid Information for Each Experiment

| Experiment | Simulation Domain | Core Grid Size | Stretched Grid Factor | Maximum Stretched Grid Size | Number of CV |
|---|---|---|---|---|---|
| Rogfast 1 | 602×12×8 | 0.1 and 0.2 | 1.05 | 4 | 628836 |
| Rogfast 2 | 1000×12×8 | 0.1 and 0.2 | 1.05 | 4 | 897600 |
| Rogfast 2R | 1000×12×8 | 0.2 | 1.20 | 4 | 771894 |

The following tables describe the parameters relevant for the computational time. Each simulation has been set for specific CFLC, CFLV, DTPLOT, and TMAX. These four parameters will determine the time step, resolution of plot, and usage of non-volatile memory. All parameters for each experiment are shown in Table 5-5, Table 5-6, and Table 5-7 for the preparation, cold, and hot simulations respectively.

Table 5-5. Output Settings for Preparation Simulation

| Experiment | Simulation Domain | Grid Specification | CFLC / CFLV | DTPLOT | TMAX (min, max) |
|---|---|---|---|---|---|
| Rogfast 1 | 602×12×8 | 0.1 core; 1.2× stretched | 2 / 0.2 | 0.005 | 0.3, 0.5 |
| Rogfast 2 | 1000×12×8 | 0.1 core; 1.2× stretched | 5 / 0.5 | 0.001 | 0.5, 0.5 |
| Rogfast 2R | 1000×12×8 | 0.1 core; 1.2× stretched, max 4 | 5 / 0.5 | 0.001 | 0.5, 0.5 |

Table 5-6. Output Settings for Cold Simulation

| Experiment | Simulation Domain | Grid Specification | CFLC / CFLV | DTPLOT | TMAX (min, max) |
|---|---|---|---|---|---|
| Rogfast 1 | 602×12×8 | 0.2 core; 1.05× stretched, max 4 | 0.2 / 0.04 | 0.00025 | 2.5, 3.0 |
| Rogfast 2 | 1000×12×8 | 0.2 core; 1.05× stretched, max 4 | 0.2 / 0.04 | 0.00100 | 2, 2.5 |
| Rogfast 2R | 1000×12×8 | 0.2 core; 1.20× stretched, max 4 | 0.2 / 0.04 | 0.00100 | 2, 2.5 |

Table 5-7. Output Settings for Hot Simulation

| Experiment | Simulation Domain | Grid Specification | CFLC / CFLV | DTPLOT | TMAX (min, max) |
|---|---|---|---|---|---|
| Rogfast 1 | 602×12×8 | 0.2 core; 1.05× stretched, max 4 | 5 / 0.5 | 0.0025 | 5, 6 |
| Rogfast 2 | 1000×12×8 | 0.2 core; 1.10× stretched, max 4 | 5 / 0.5 | 0.0025 | 9, 10 |
| Rogfast 2R | 1000×12×8 | 0.2 core; 1.20× stretched, max 4 | 5 / 0.5 | 0.0025 | 10,11 |

## 5.2 Simulation Results

The outcomes of each simulation are similar to those for open space scenarios. For cold simulations, the blast static overpressure and impulse are the variables of interest. The difference with an open space simulation is that the monitor points are located at 10 m and every 100 m distance from the centre of explosion. All monitor points are located along the axis tunnel at an elevation around 1.5 m above the pavement surface. The outcomes of this simulation are pressure contour maps at specific time, blast overpressure time series, and blast impulse time series. Figure 5-5, Figure 5-6, and Figure 5-7 show an example of results of cold simulations. Table 5-8 shows the location of the monitor points for cold simulation. The elevation of all monitor points is 6 m because the tunnel's pavement is located at 4.5 m of elevation. Therefore, this 1.5 m height above pavement represents the height of the vital part of a human body and the most of vehicles windscreens. Table 5-9 and Table 5-10 show the magnitude of peak overpressure and impulse, and time to reach the peak value, respectively. An asterisk mark (*) in Rogfast 2 and 2R means that the monitor points are in the positive x-direction (MP1 and MP7-11) while Rogfast 2 without asterisk mark means that the monitor points are in the negative x-direction (MP1 and MP12-16).

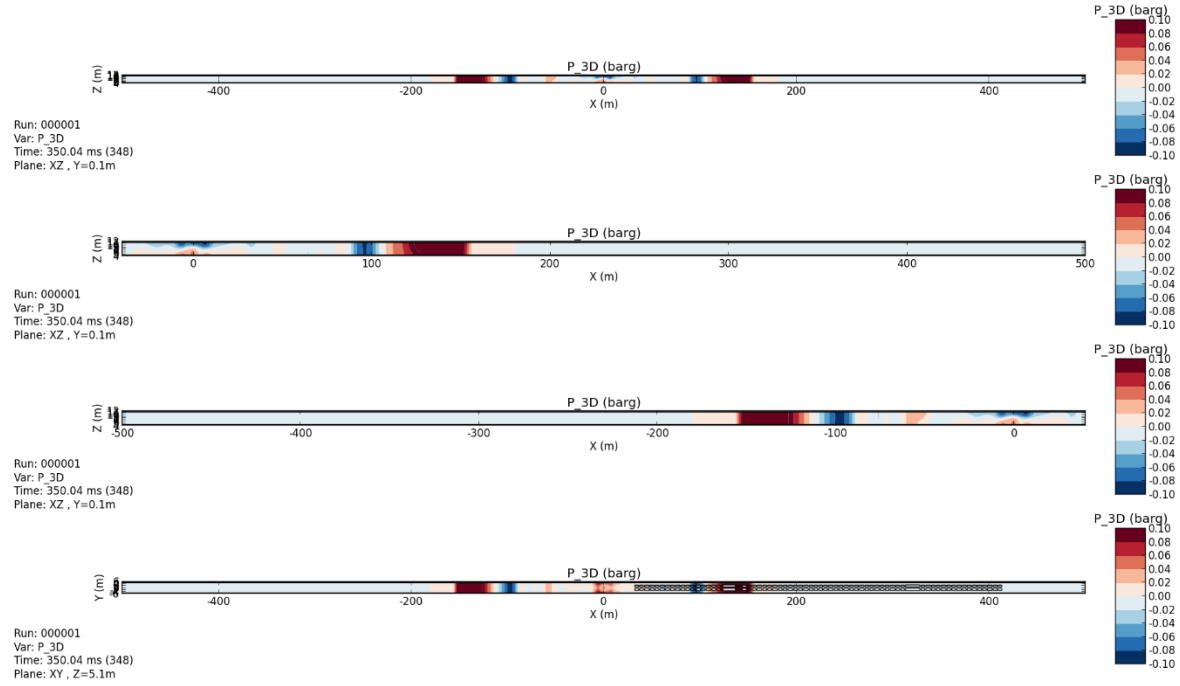


Figure 5-5. Example of 2D (cross section) blast overpressure result inside the tunnel (Rogfast 2R) at a particular moment.

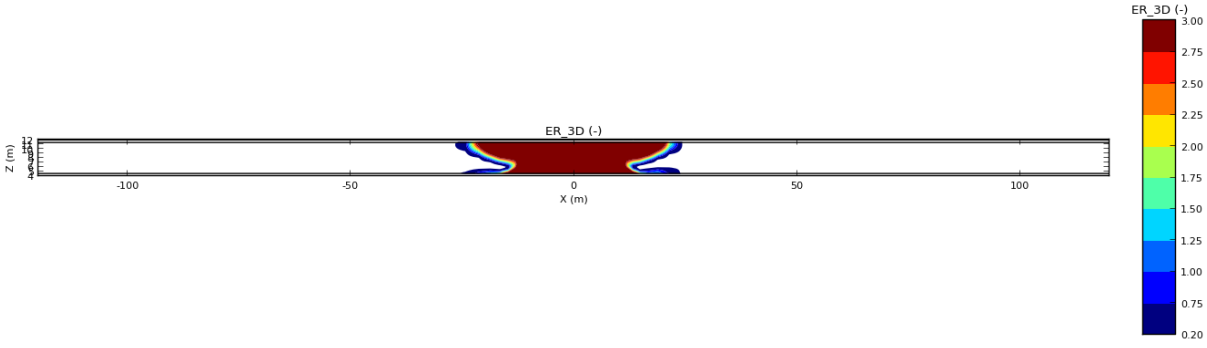


Figure 5-6. Example of 2D fuel equivalent ratio contours inside the tunnel at a particular moment.

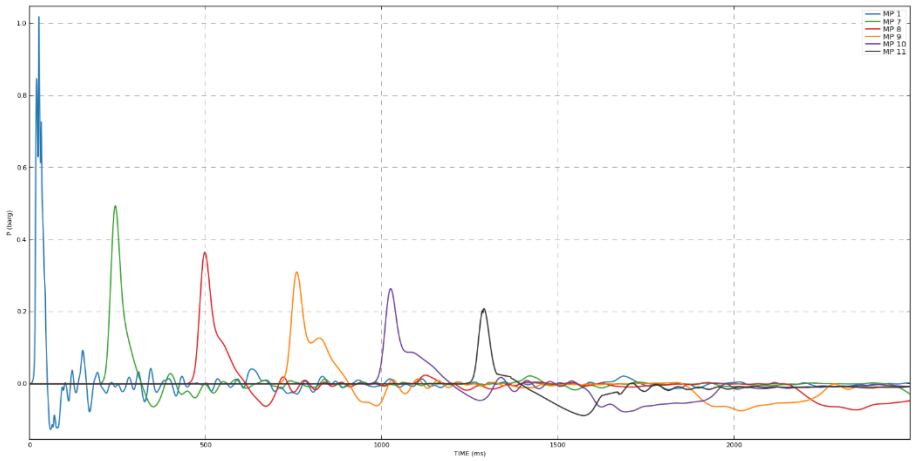


Figure 5-7. Example of blast overpressure result at 6 monitor points along the tunnel (Rogfast 2R).

Table 5-8. Location of Monitor Points for Cold Simulation (Confined Space)

| MP # | Location (x, y, z) [m] |
|---|---|
| 1 | (10, 0, 6) |
| 7 | (100, 0, 6) |
| 8 | (200, 0, 6) |
| 9 | (300, 0, 6) |
| 10 | (400, 0, 6) |
| 11 | (500, 0, 6) |
| 12 | (-100, 0, 6) |
| 13 | (-200, 0, 6) |
| 14 | (-300, 0, 6) |
| 15 | (-400, 0, 6) |
| 16 | (-500, 0, 6) |

Table 5-9. Peak Overpressure and Impulse for Confined Space Simulations

| Experiment | Peak Overpressure [mbarg] | | | | | | Peak Impulse [Pa·s] | | | | | |
|---|---|---|---|---|---|---|---|---|---|---|---|---|
| | 10 | 100 | 200 | 300 | 400 | 500 | 10 | 100 | 200 | 300 | 400 | 500 |
| Rogfast 1 | 451 | 73 | 53 | 38 | - | - | 261.92 | 229.64 | 237.34 | 180.95 | - | - |
| Rogfast 2 | 1131 | 434 | 350 | 302 | 268 | 226 | 1693.72 | 1831.20 | 1885.57 | 1910.22 | 1925.19 | 990.36 |
| Rogfast 2* | 1131 | 463 | 371 | 295 | 257 | 193 | 1693.72 | 1943.85 | 1940.86 | 1936.62 | 1886.23 | 874.25 |
| Rogfast 2R | 1019 | 495 | 394 | 334 | 292 | 244 | 1831.08 | 1967.17 | 2027.90 | 2060.87 | 2080.96 | 1053.43 |
| Rogfast 2R* | 1019 | 495 | 381 | 312 | 264 | 208 | 1831.08 | 2047.00 | 2026.82 | 2166.91 | 1896.81 | 914.44 |

Table 5-10. Time to Reach Peak Overpressure and Impulse for Confined Space Simulations

| Experiment | Time to Reach Peak Overpressure [ms] | | | | | | Time to Reach Peak Impulse [ms] | | | | | |
|---|---|---|---|---|---|---|---|---|---|---|---|---|
| | 10 | 100 | 200 | 300 | 400 | 500 | 10 | 100 | 200 | 300 | 400 | 500 |
| Rogfast 1 | 35.51 | 284.52 | 573.64 | 853.76 | - | - | 43.16 | 305.62 | 604.12 | 886.60 | - | - |
| Rogfast 2 | 25.26 | 242.79 | 498.54 | 758.77 | 1022.19 | 1284.92 | 49.26 | 310.29 | 602.63 | 893.96 | 1182.65 | 1391.63 |
| Rogfast 2* | 25.26 | 242.24 | 499.43 | 764.23 | 1031.36 | 1298.67 | 49.26 | 310.73 | 601.19 | 901.32 | 1197.78 | 1400.40 |
| Rogfast 2R | 25.99 | 241.84 | 492.37 | 749.99 | 1011.20 | 1271.86 | 49.87 | 313.87 | 604.82 | 894.93 | 1184.72 | 1374.85 |
| Rogfast 2R* | 25.99 | 243.26 | 497.02 | 758.30 | 1024.14 | 1288.95 | 49.87 | 316.69 | 612.44 | 905.83 | 1195.12 | 1389.74 |

For hot simulations, the main output variables are temperature and mass fraction of combustion product. These variables help us to visualize the fireball. Here, the term “fireball” has to be used throughout the discussion although the actual shape of ignited fuel is cylindrical or hemicylindrical due to the boundary limitation (tunnel walls and pavement). As with open space simulations, the outcomes of hot simulation are fireball visualization at longitudinal and radial cross sections to obtain the size of fireball. Radial cross section is set at a certain distance inside the tunnel. Another output variable that can be included is equivalent ratio or fuel mole fraction. Figure 5-8 and Figure 5-9 show examples of output of hot simulations. The simulation results are shown in Appendix C for the blast overpressure and fireball timestep, while the plots of blast overpressure and impulse are shown in Appendix D.

It is interesting to discuss the physics of fireballs inside a tunnel which depend on many factors. The shape of the fireball is not a sphere; thus, it is not relevant to use the terms diameter and height to centre of fireball. Based on the three simulations, it is more fruitful to discuss the length and vertical position of the fireball as shown in Figure 5-8. The length of the fireball is defined as the maximum reach of fire along the tunnel axis. It should be noted that the fireball is not always symmetric. It depends on the conditions prevailing in the tunnel on both sides of the initial location of the source of the BLEVE. Congestion and ventilation system (both natural ventilation and blowers) might influence the fireball behaviour.

In these three simulations, unfortunately the maximum simulated time is not sufficient to reveal the whole fireball life-cycle until the end. The length and height of the fireball presented in Table 5-11 is the length of the fireball at the moment the simulation stops.

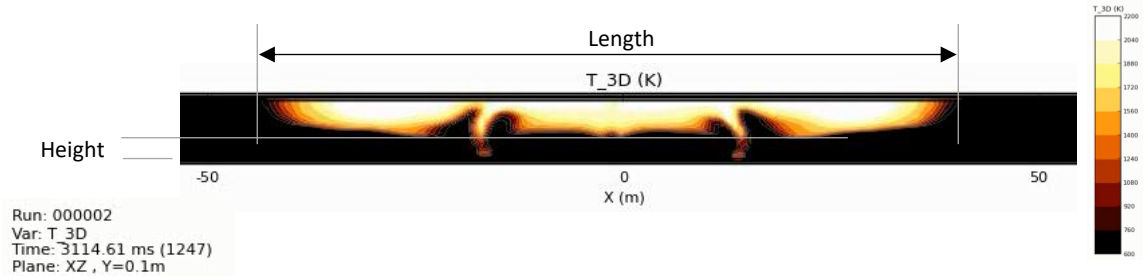


Figure 5-8. Example of the longitudinal cross-section result of fireball inside a tunnel using Flowvis.

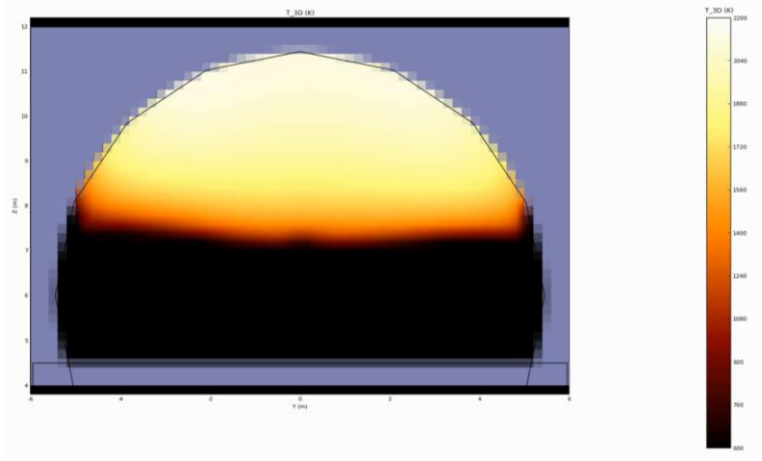

Figure 5-9. Example of axial cross-section of fireball inside a tunnel.

Table 5-11. Length and Height of Fireball Based on BLEVE Simulation Inside Rogfast Tunnel

| Experiment | Length [m] | Height [m] | Time [ms] |
|---|---|---|---|
| Rogfast 1 | 179.72 | 0 | 5985.11 |
| Rogfast 2 | 168.82 | 1.3 | 9985.52 |
| Rogfast 2R | 177.52 | 0.9 | 10999.80 |

In addition, the fireball inside a tunnel tends to develop slowly compared to the one in open space. In both simulations, the fireball did not propagate rapidly. It develops slowly due to the concentrated fuel (far above UFL). Rapid propagation of deflagration or detonation inside a confined space occurs when the whole space is filled with gas within its flammability limits. In addition, congestions such as cars, buses, and so on, have less influence on better mixing of gas-air because the fireball tends to fill the upper part of the tunnel. This part will be discussed further in the next section. The ventilation fan may introduce turbulence hence better mixing. The Rogfast tunnel will be equipped with direct ventilation to open-air as shown in Figure 5-10.

It should be noted that the Rogfast simulations were done using the simulation procedure for blast overpressure. This implies smaller amounts of fuel for the fireball than in reality as discussed before in Chapter 4. When using the fuel available for the fireball, the results will be different from those shown previously.

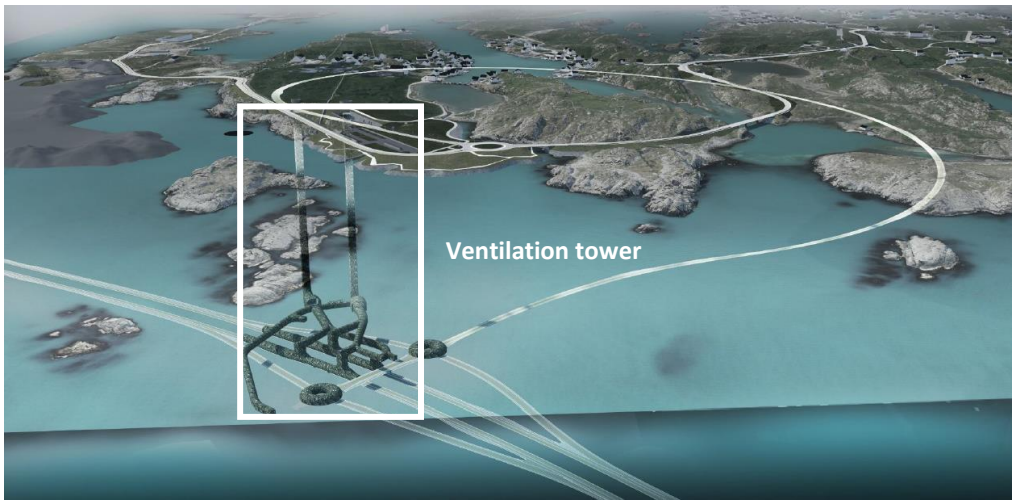


Figure 5-10. Illustration of direct ventilation in Rogfast tunnel. (Espedal, 2016, p.22)

## 5.3 Comparison with Open Space BLEVE

For this purpose, the containment setups (volume, pressure, temperature, and gas composition) of Birk 01-4 was intentionally applied in the Rogfast 1 simulation. Blast wave contours at 50 ms after ignition for both simulations are shown in Figure 5-11 where the Rogfast 1 simulation results are shown below the open-space simulation results. We can see that the blast overpressure in Rogfast 1 is still larger than 100 mbarg, compared to the open-space simulation which has decreased to between 60 and 80 mbarg at the same moment in time. Based on the overpressure curves, the maximum value of overpressure after 50 ms in Rogfast 1 is more than 200 mbarg. To decay to an overpressure of 80 mbarg in Rogfast 1, the

blast wave should travel to a distance approximately 86 m from the centre of explosion, while in open space case the blast wave travels only 17 m to decay to a similar pressure. This demonstrates that the decay rate of overpressure inside a tunnel is much lower than the decay rate of overpressure in open space, which has been stated in Section 5.1.1 before. This is due to limited expansion for the blast wave, i.e. the blast wave is forced to propagate along the relatively slender and confined space.

Does the confinement contribute to an increase of blast wave's propagation speed? Figure 5-12 and Figure 5-13 show the illustrations on how to obtain the blast waves propagation speed. Based on ten-millisecond-step propagation of the blast wave front in Birk 01-4 simulation (Figure 5-12), the propagation speed of blast wave is 400.16 m/s (339.33 m/s peak-to-peak). For the confined space simulation (Rogfast 1), there is a slight increase of the propagation speed to 418.15 m/s (343.68 m/s peak-to-peak) for the congested area and 420.35 m/s (342.47 m/s peak-to-peak) for the uncongested area. There are two numbers of blast wave propagation speed which depend on the pressure contour reference. The first reference for speed calculation is using the front face of tan contour (0-0.02 barg), and the second is using the middle span of dark red contour (>0.08 barg). The first reference gives much higher values. This might be caused by the blast wave front which could disturb the surrounding atmosphere. Therefore, it is more reliable to use the dark red contour as the reference to obtain the propagation speed, i.e. using peak-to-peak speed.

Refer to the standard 1 Mach (343 m/s), the maximum deviation between both simulations is around 0.0589 Mach (0.0127 Mach peak-to-peak). Note that the calculation of propagation speed is based on a detailed visual analysis of FLACS results. Unlike the overpressure decay, there is a slight increase of the propagation speed even if it is a small deviation from the one Mach reference.

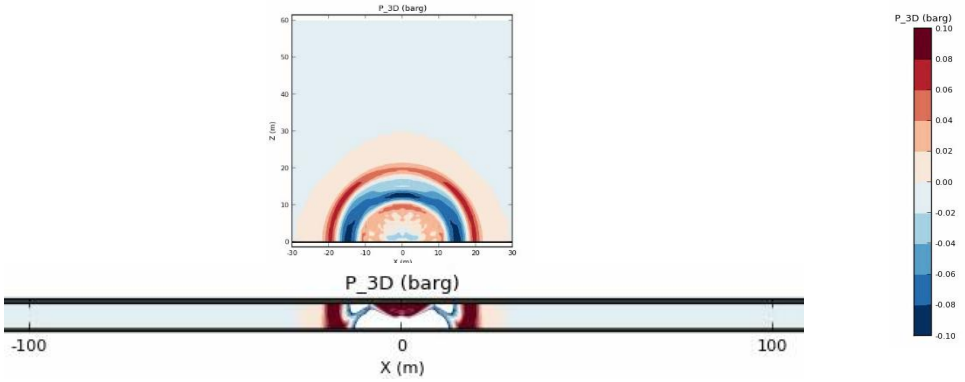


Figure 5-11. Comparison of blast wave between experiment Birk 01-4 and Rogfast 1 at 50 ms.

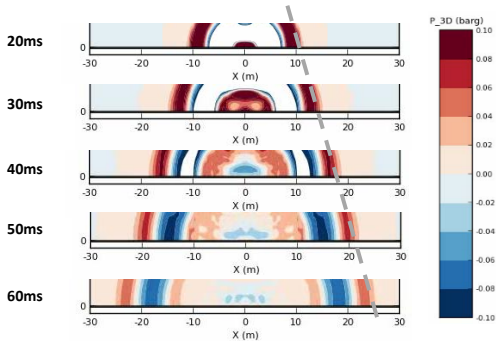


Figure 5-12. Ten-millisecond step of blast wave propagation in open-space (Birk 01-4).

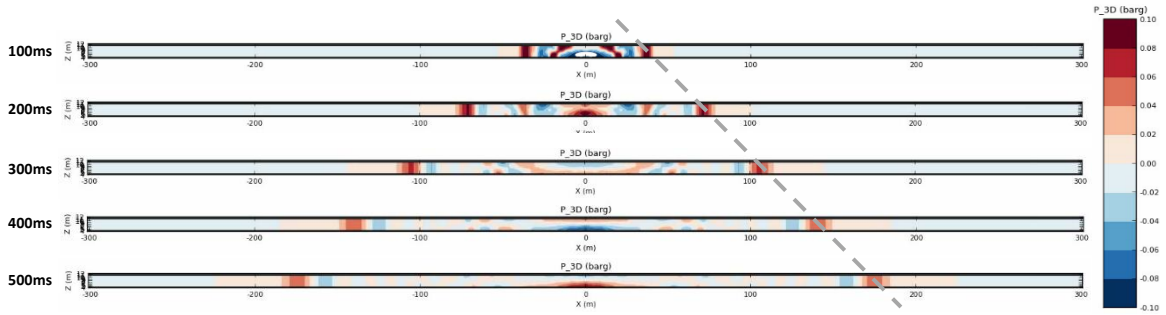


Figure 5-13. Hundred-millisecond step of blast wave propagation in tunnel (Rogfast 1).

To compare the overpressure between the Rogfast 1 and the Birk 01-4 simulations, the dimensionless overpressure amplification factor, $\phi$, of the specific explosion was used. It can be defined as the ratio of blast overpressure values at the same distance. Qualitatively, this can be obtained using the blast overpressure curves of all monitor points.

Based on the results, the regression equation for predicting the blast overpressure $P$ (in mbarg) with respect to the distance from the centre of the explosion $x$ (in metre) can be obtained for both simulations, Birk 01-4 and Rogfast 1, as follows.

- Birk 01-4: $P(x) = 6074.1x^{-1.505}$
- Rogfast 1: $P(x) = 2324.3x^{-0.726}$

By looking at the equations, we can predict the blast overpressure at a specific distance. The results are shown in Table 5-12. In the table, the overpressure amplification factor is defined as the blast overpressure in the Rogfast 1 simulation divided by the blast overpressure at the same distance from the explosion in Birk 01-4 simulation. Mathematically, it can be written as:

$$\phi = \frac{P_{\text{Rogfast}}(x)}{P_{\text{Birk}}(x)} \qquad \text{eq. 5.1}$$

$P_{\text{Rogfast}}(x)$ : Blast overpressure in Rogfast 1 at distance $x$ [mbarg]
$P_{\text{Birk}}(x)$ : Blast overpressure in Birk 01-4 at distance $x$ [mbarg]

Therefore, we have the overpressure amplification factor function with respect to the distance in metre: $\phi(x) = 0.3827x^{0.779}$. Figure 5-14 shows the relation between the overpressure amplification factor and the distance. The overpressure amplification factor is a

power function with form $f(x) = ax^b$ and has two parameters: scaling parameter ($a$) and shape parameter ($b$). In the equation, the involving parameters might be related to cross-sectional properties: area and smallest distance from the centre of explosion. The tunnel characteristics such as shape and dimension proportion will determine the parameters of the power function. As far as the blast wave has not reached the wall or the ceiling, the undisturbed blast wave inside a tunnel can be treated as a blast wave in an open space. Circular walls may introduce a focusing effect and will potentially cause an increase of blast overpressure locally if the monitor point is located at the focal point of the wall.

Table 5-12. Blast Overpressure of Both Simulations at Specific Distance and the OAF

| Distance [m] | Blast Overpressure [mbarg] | | OAF [-] |
|---|---|---|---|
| | Birk 01-4 | Rogfast 1 | |
| 10 | 189.88 | 436.81 | 2.30 |
| 20 | 66.90 | 264.09 | 3.95 |
| 30 | 36.34 | 196.74 | 5.41 |
| 40 | 23.57 | 159.66 | 6.77 |
| 50 | 16.85 | 135.78 | 8.06 |
| 100 | 5.94 | 82.09 | 13.83 |
| 150 | 3.22 | 61.16 | 18.97 |
| 200 | 2.09 | 49.63 | 23.73 |
| 250 | 1.49 | 42.21 | 28.24 |
| 300 | 1.14 | 36.97 | 32.55 |
| 350 | 0.90 | 33.06 | 36.70 |
| 400 | 0.74 | 30.01 | 40.72 |
| 450 | 0.62 | 27.55 | 44.63 |
| 500 | 0.53 | 25.52 | 48.45 |

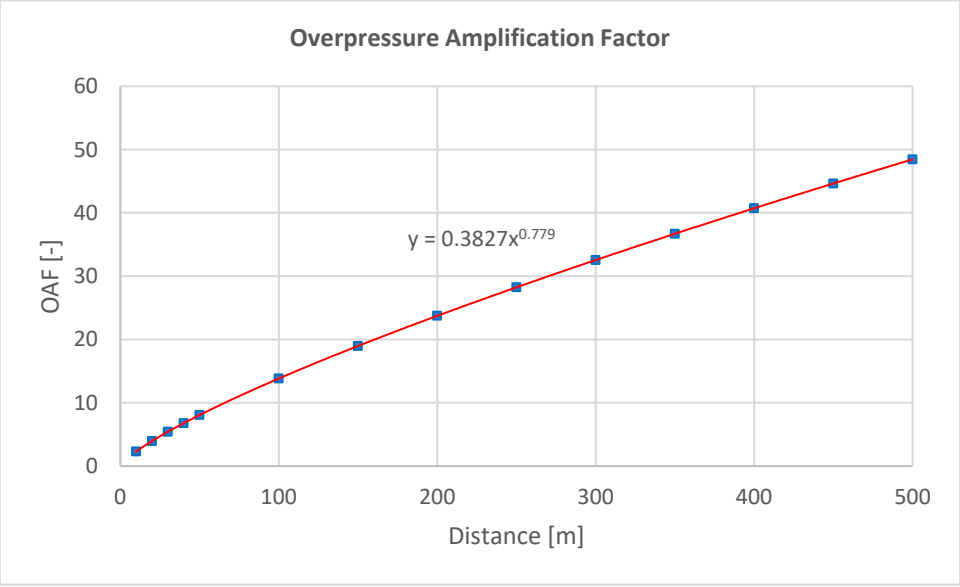


Figure 5-14. Plot of propagation factor vs open space distance.

For hot simulations, the shapes of the fireball between both simulations are different due to the effect of confinement. As mentioned before, the shape of the fireball inside the tunnel will be determined by the shapes of the tunnel. In addition, there is a difference in the burning rate and the time to reach the peak of burning rate. Figure 5-15 shows the time series of burning

rate for both simulations. We can see that the burning process for Rogfast 1 initially slower than in open space, i.e. the Birk 01-4 simulation. The burning rate maximum occurs later. The burning process in the tunnel takes also longer.

In the Rogfast 1 simulation more fuel than in the Birk 01-4 simulation is consumed. Based on the result at 5 s after ignition, there is 0.432 kg of fuel left for Rogfast 1 and 1.74 kg of fuel left for Birk 01-4. This is caused by longer and more effective burning process during the Rogfast 1 simulation. We can obtain from the graph that the burning process of the Birk 01-4 simulation lasts 2.76 s, while in the Rogfast 1 simulation it lasts 5.08 s. In the Rogfast 1 simulation, the fuel could not escape easily compared to the Birk 01-4 simulation where the gas could escape vertically.

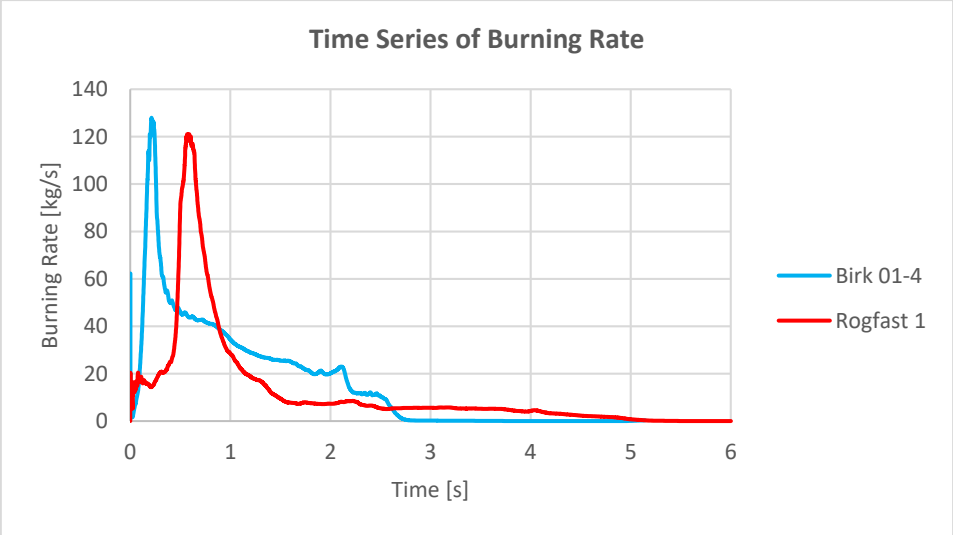


Figure 5-15. Time series of burning rate for Birk 01-4 and Rogfast 1 simulation.

In conclusion, a confinement such as a tunnel will influence the decay rate of the blast overpressure by slowing it down. Limited expansion direction forces the blast to propagate in along the tunnel. The overpressure amplification factor can be used to assess the behaviour of the blast wave overpressure with distance. On the other hand, the propagation speed of the blast wave inside a tunnel is roughly the same as the speed of the blast wave in open-space. The confinement has little effects on the propagation speed.

## 5.4 Effects of Congestion

Two simulations have been performed to study the effect of congestion on the behaviour of a BLEVE: Rogfast 2R (the Rogfast 2 simulation is disregarded due to the problem of congestion location). In this simulation, congestion was introduced on one side of the tunnel and open space on the other side as shown in Figure 5-4.

For the cold simulation, based on the overpressure curves for both sides which are shown in Figure 5-16 and Figure 5-17, the overpressure values in the congested area are slightly lower than in the uncongested area. The maximum values of overpressures are presented in Table 5-13. At distance of 200 m, the overpressure in the uncongested area starts to have a larger value than in the congested area. It means that the congestion reduces the blast overpressure. Note that the queue of congestions starts at 32 m from the centre of the explosion.

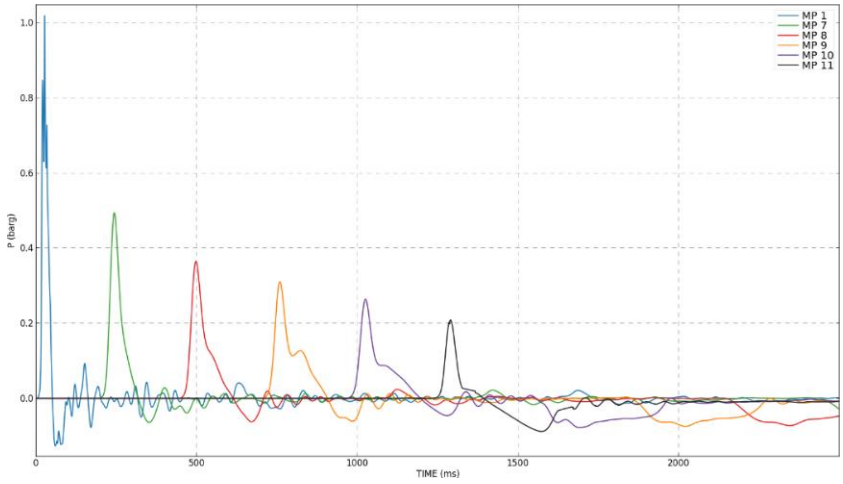


Figure 5-16. Overpressure curve recorded by monitor points that located in congested area.

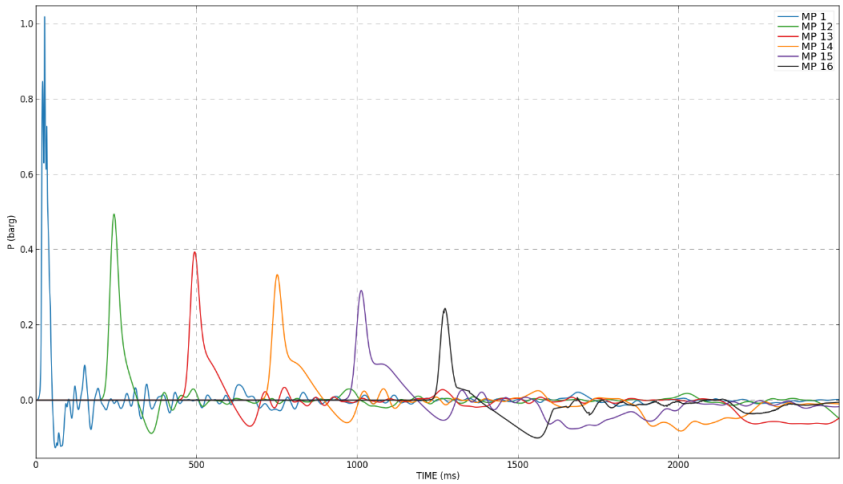


Figure 5-17. Overpressure curve recorded by monitor points that located in uncongested area.

Table 5-13. Overview of Overpressure Recordings in Rogfast 2R Simulation

| **Congested Area** | | **Uncongested Area** | |
|---|---|---|---|
| **Monitor Point** | **Maximum Overpressure (mbarg)** | **Monitor Point** | **Maximum Overpressure (mbarg)** |
| MP1 (+10 m) | 1019 | MP1 (+10 m) * | 1019 |
| MP7 (+100 m) | 495 | MP12 (-100 m) | 495 |
| MP8 (+200 m) | 381 | MP13 (-200 m) | 394 |
| MP9 (+300 m) | 312 | MP14 (-300 m) | 334 |
| MP10 (+400 m) | 264 | MP15 (-400 m) | 292 |
| MP11 (+500 m) | 208 | MP16 (-500 m) | 244 |
| *) No congestion around distance 10 m, therefore it is expected to have same value with + 10m. | | | |

Squeezing effects which occur due to the narrowing spaces might be expected. According to Figure 5-18 which shows plot of blast overpressure with respect to distance from the centre of explosion, this squeezing effect is barely seen. As the blast wave propagates in the congested area, the blast overpressure tends to decay slightly faster than that in the uncongested part.

Slight changes on the simulation setup were established. The monitor points had been lifted to 5.5 m above the road pavement to assure that the lower overpressure values are not caused by the location of monitor points behind the congestion. The results are almost similar

with the previous simulation, i.e. it still shows that the overpressure is slightly lower in the congested area. The main reason for lower overpressure along the congestion must be reflection at the obstructions introducing a loss of energy in that direction. In a real condition, energy of the blast wave is also absorbed by congestion and being converted into kinetic and mechanical energies. It is assumed that the congestions are stayed in place while in the real world the congestions can be moved and deformed at a certain amount of forces or energies.

Berger et.al. (2009) conducted experiments on shock wave attenuation by varying shape and size of obstacles inside a tube. This experiment was compared to this simulation because it can be used to describe congestions inside a tunnel. They use the term ROF (relative opening fraction) to quantify the unblocked cross section to total cross section. An experiment where one 90°-obstacle (rectangular) was used shows a linear relation between overpressure and ROF. Lower ROF causes overpressure to decrease, in other words, existence of congestion causes the overpressure to drop. Figure 5-19 shows the result of the experiment. Another similar experiment conducted by Sha et.al. (2014) shows the effects of multiple obstacles inside a tube. The multiple obstacles decrease the overpressure of wave front almost in a linear manner. Figure 5-20 shows the average overpressure at the blast wave front for rectangular and obtuse triangular obstacles.

For the hot simulation, the Rogfast 2 simulation was not adequate regarding chosen simulation time, thus it was disregarded. The Rogfast 2 simulation used 10 seconds of simulation time and at that moment the fireball had not reached the congestion yet. At the end of the simulation, 989 kg of fuel was left. Initially, there was 1160 kg of fuel. It means that only 14.74 % of the fuel had been consumed during the simulation. It is estimated that it will take an additional 416 thousand CPU-seconds or around 116 CPU-hours to burn all fuel left, assuming that the average rate of combustion is constant.

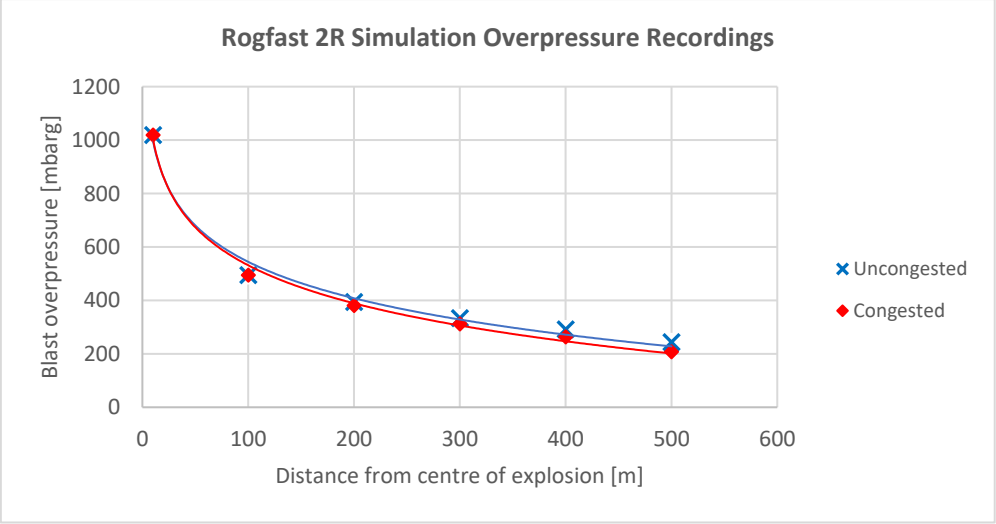


Figure 5-18. Plot of blast overpressure vs distance from centre of explosion for Rogfast 2R.

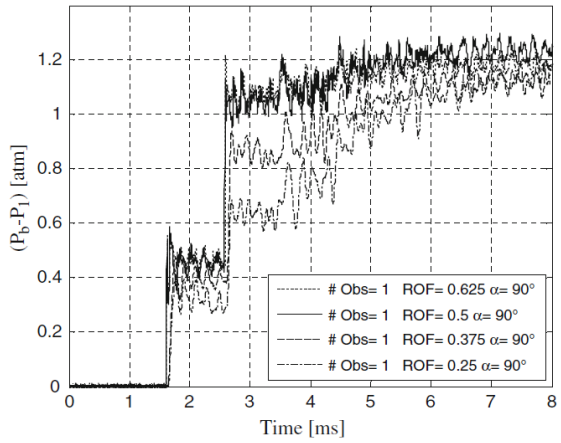


Figure 5-19. Pressure time series for the case of a 90°-obstacle with different ROF (Berger et.al., 2009, p.34).

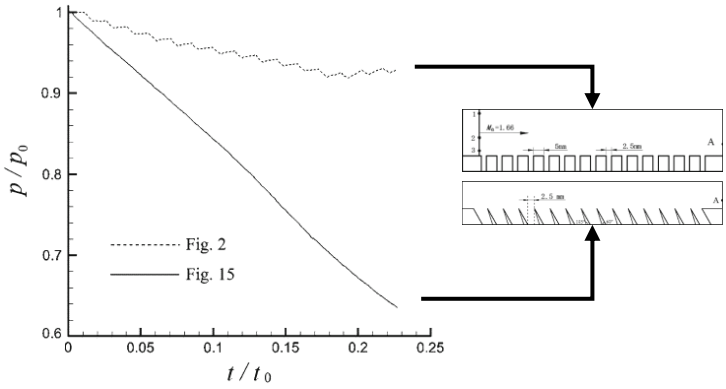


Figure 5-20. Time series of mean overpressure at blast wave front (Sha et.al., 2014, p.9).

At the end of the Rogfast 2 hot simulation, the maximum extent of fireball is 75 m while the congestion queue starts at 100 m. Based on the result, the fireball seems to be growing and expanding. Figure 5-21, Figure 5-22, and Figure 5-23 show the expansion of the fireball which has a significant rate of expansion for the Rogfast 2 simulation. Figure 5-23 shows the shape of fireball at the end of simulation time. Based on Figure 5-23, the expansion process had not stopped yet and is expected to expand more beyond 10000 ms.

Using the results of the Rogfast 2 simulation, the effect of congestion in the behaviour of the fireball cannot be studied directly but at a glance the fireball tends to shift out of the origin axis (x = 0). The dotted line in those three figures indicate the origin axis. The symmetric axis of the fireball in the Rogfast 2 simulation tends to shift to uncongested area. It did not occur in Rogfast 1 simulation, i.e. the shape of fireball in Rogfast 1 simulation is symmetric. It means that there is not any problem with the simulation setting. Based on several simulation trials inside a tunnel, it is discovered that the blast overpressure was still significantly large (in order of 100 mbarg) and reflected back to the domain. This reflection is symmetric for the Rogfast 1 simulation but not for the Rogfast 2 simulation. Therefore, congestion is the main cause of this shifting effect.

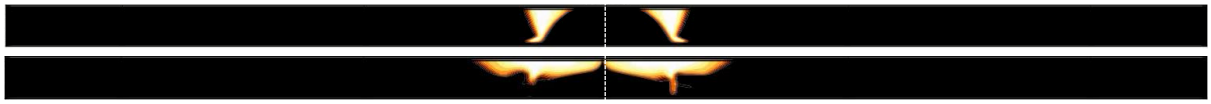

Figure 5-21. Ignition and first expansion of fireball (405 ms and 1780 ms).

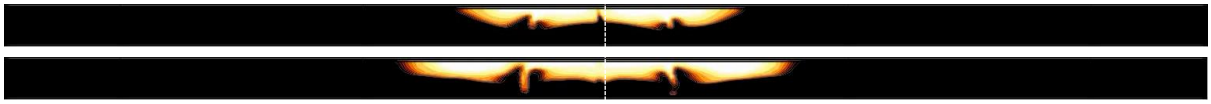

Figure 5-22. Second expansion of fireball (2175 ms and 2990 ms).

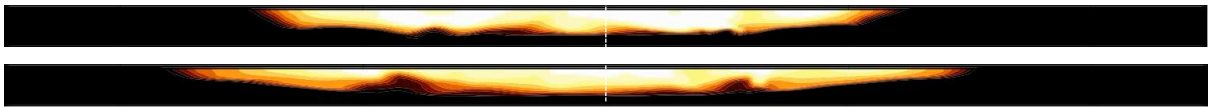

Figure 5-23. Further expansion of fireball (7125 ms and 10000 ms).

To see the effect of congestions, Rogfast 2R simulation was done for that purpose. The queue of congestions starts at x = 32 m. The front of the fireball reached the first congestion at 1044 ms as shown in Figure 5-24. At that moment, the central axis of the fireball has shifted to the uncongested space. Few hundred milliseconds later, a long flame started to grow in the congested part of the tunnel as shown in Figure 5-25 which propagates more into the central parts of the tunnel again due to the congestion. At time 6900 ms, the fireball propagates faster on the congested side than the other side for a while. At the end of simulation (21000 ms), the fireball has a total length of 290.91 m with 156.2 m to uncongested area and 133.9 m to congested area. For comparison, Rogfast 2R has longer fireball size at time 10000 ms (171.65 m) than Rogfast 2 at the same time (168.82 m). Similar with Rogfast 2, the fireball is still expanding at the end of simulation.

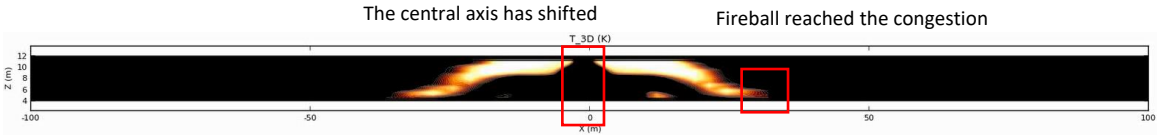


Figure 5-24. Expansion of fireball in Rogfast 2R (1044 ms).

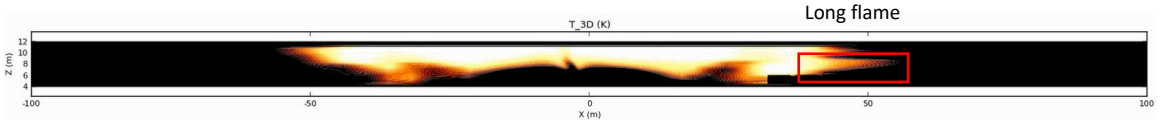


Figure 5-25. A long flame appeared in congested side (2850 ms).

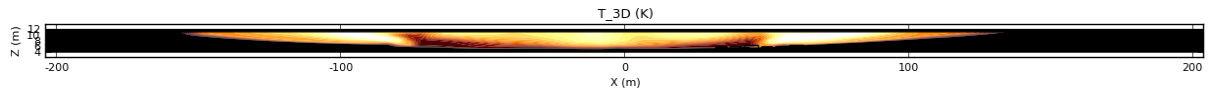


Figure 5-26. Final form of fireball at the end of Rogfast 2R simulation (21000 ms).

The Rogfast 2R simulation is still not adequate to capture the entire process of the fireball. At the end of the simulation, there is 1000 kg of fuel left. There was 1300 kg of fuel initially. It means that the simulation only burned 23.08 % of the fuel. It is estimated that it will take additional 252 thousand CPU-seconds or around 70 CPU-hours to burn all the fuel left, assuming that the average rate of combustion is constant.

In conclusion, congestions have some effects to the fireball development. It will squeeze the sectional area, hence faster flame propagation at some points. We can see this from the development of long flame tongues in the congestion being pulled in the wake of large obstacles and merging with the main flame. Congestions also give a damping effect on blast overpressure. The blast overpressure values in congested area are lower than the values in uncongested area. This decreasing overpressure had been proved by Berger et.al. (2009) and Sha et.al. (2014). It should be noted that the congestions in simulation are represented by immovable blocks. In the real world, the congestions are movable and have a complex shape unlike a simple block probably increasing the blast decay. According to the Table 2-3, with 200 mbarg overpressure (the value at 500 m of distance), the blast wave can break oil storage tanks. This is an indication of what can happen to vehicles in the real world.

## 5.5 Additional Notes About Congested Tunnel Simulation

Table 5-4 to Table 5-7 show some differences regarding grid setting between Rogfast 2 and Rogfast 2R. There was a mass residual issue when the congestions in Rogfast 2 were moved to 32 m. It is caused by a high number of porous control volumes which could not be handled properly by FLACS.

In the Rogfast 2 simulation, constant control volume length begins at x = ±84 m. Therefore, at x = 32 m the control volume length is still varying due to stretching of the grid. It causes many congestions to fall in the middle of the grids and creates porous control volume. By setting the stretching factor to a higher value, for example 1.20, it would be faster to reach a constant control volume length. In the Rogfast 2R simulation, a constant 4 m of control volume length begins at x = ±28 m while the congestion queue starts at x = 32 m. This, at least, minimizes the number of porous control volumes and results in a more stable computation.

In conclusion, to get more stable simulation using FLACS, most of the congestion blocks must coincide with grid lines. This means more control volumes that are fully filled with congestion (zero porosity) than partially filled. This is illustrated in Figure 5-27.

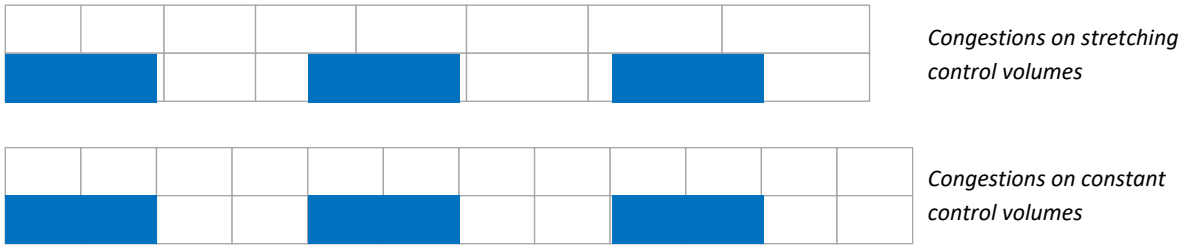


Figure 5-27. Illustration of congestions on stretching (top) and constant (bottom) control volumes.

*This page intentionally left blank*

# 6 Conclusions

## 6.1 Conclusions

A proper model to simulate the blast wave overpressure using FLACS has been established. From the simulations done, the blast wave overpressures and impulses are mostly above the experiment. The simulations seem to overestimate the explosion blast waves effects which are good from a safety perspective but may not be good in economic perspectives. The factored calculations deal with geometrical effects of the explosion such as the location above the ground and the shape of the containment; and have a larger value than the simulations have.

The current method to simulate a BLEVE is not good enough to predict the consequences related to combustion such as the fireball. The amount of fuel participating in fireball generation in FLACS needs to be increased considerably by increasing the volume of high-pressure or increasing the pressure, resulting in over-exaggerating the blast overpressure. The empirical formulas introduced by CCPS (1994 and 2011) can be used to predict the diameter and the height of the fireball in combination with the calculation of flashing liquids and its participation to the fireball. Section 2.1.3.1 presents the equations and the flash fraction rule of thumb described by Mudan, as cited by SINTEF (2003).

Inside a confined space such as a tunnel, the blast wave overpressure will decay slowly due to the limited expansion possibilities of the blast wave propagation. Therefore, the blast waves in a confined space can propagate further than in an open space (unconfined), i.e. a relatively high blast overpressure can be observed at a longer distance from the centre of explosion. The decay rate of the blast overpressure can be described using an overpressure amplification factor (OAF) which depends on the tunnel cross-sectional characteristics. The overpressure amplification factor can be represented using a power equation which is a function of distance. Further research must be done to find the relation between the tunnel cross-sectional characteristics and the parameters for the equation of overpressure amplification factor.

In contrast, the congestions inside a tunnel give several absorbing effects to the blast waves. The blast waves will suffer some disturbances such as reflection and dispersion. For the same distance, the blast overpressure inside a confined-congested area will be slightly smaller than the blast overpressure inside a confined-uncongested area. This indicates energy losses due to the disturbances caused by the congestions.

## 6.2 Suggestions

Several suggestions have been made to do a better BLEVE simulation using FLACS and a better BLEVE assessment.

- Ability to create multiple high-pressure regions for future development of FLACS with full control of parameters. With this additional feature, simulation of BLEVEs using the discussed method will be much easier and controllable, therefore we can have more representative result, close to the what happens in the real world. Auto-generation of a BLEVE model may be possible but the

author realized that it might not be possible at present due to the lack of scientific formulation for flashing processes.

- Several small-scale experiments may be conducted in the future and the results can be used as the benchmark for Gexcon to perform validation and verification (V&V) of FLACS. The small-scale experiments are suggested due to the limited space available at the Gexcon testing site at Sotra, just outside Bergen. Considering the available state-of-the-art technologies, the BLEVE phenomenon can be understood better and more comprehensive for example using high-speed high-resolution cameras.
- Further research about the influence of the tunnel cross-sectional characteristics to the open space explosion. By this research, the relation between the shape and the dimension of a tunnel can be described better by mathematical equations, hence, better and faster predictions of the blast overpressure in the future.
- Further works on the CFD simulation of BLEVE should be focused more on the fireball simulation including thermal radiation emitted by fireball surface. The report of British Gas experiments compiled by Johnson et.al. (1991, p.14) contains the average values and the time series of the surface emissive power (SEP) of the fireball during the experiments. Other literatures can be used such as Roberts et.al. (2000), Prugh (1994), and Baker et.al. (1983). Some settings inside FLACS have to be changed. The solver must be set to simulate a fire. Therefore, the CFLC and CFLV numbers will be changed to higher number by default (which is considered as the FLACS-Fire best practice) and the mass residual issue may appear during simulation. Output variables in FLACS related to fire such as Q, QDOSE, CO2, H2O, SOOT, and so on must be activated. In addition, it should be noted that the fire-related variables in open space are not recorded. There should be a defined geometry and FLACS will record the magnitude of the variables at the surface of the geometry. Using monitor points are also possible and if directionality is one of the considerations, it is necessary to specify the viewing direction of each monitor point, otherwise the maximum value will be recorded instead. Details about the recommended practice for simulation of thermal radiation due to fire can be referred to Gexcon (2016).

# List of References


Baker, W., Cox, P., Kulesz, J., Strehlow, R., & Westine, P. (1983). *Explosion hazards and evaluation* (1st ed.). Amsterdam: Elsevier Scientific Pub. Co.

Balke, C., Heller, W., Konersmann, R., & Ludwig, J. (2001). Fire Test for the Safety in Transport and Storage of Dangerous Goods. *Loss Prevention and Safety Promotion in The Process Industries*, 1005-1015. http://dx.doi.org/10.1016/b978-044450699-3/50019-7

Berger, S., Sadot, O., & Ben-Dor, G. (2009). Experimental investigation on the shock-wave load attenuation by geometrical means. *Shock Waves*, *20*(1), 29-40.

BIPM. (2006). The International System of Units (SI). France: Bureau International des Poids et Mesures.

Birk, A., van der Steen, J., Davison, C., Cunningham, M., & Mirzazadech, I. (2003). *PRV Field Trials – The Effects of Fire Conditions and PRV Blowdown on Propane Tank Survivability in a Fire*. Ontario, Canada: Department of Mechanical Engineering, Queen's University.

Birk, A., Davison, C., & Cunningham, M. (2007). Blast overpressures from medium scale BLEVE tests. *Journal of Loss Prevention in The Process Industries*, *20*(3), 194-206. http://dx.doi.org/10.1016/j.jlp.2007.03.001

CCPS. (1994). Guidelines for Evaluating the Characteristics of Vapor Cloud Explosions, Flash Fires, and BLEVEs 1st ed. New York: American Institute of Chemical Engineers.

CCPS. (2011). Guidelines for Evaluating the Characteristics of Vapor Cloud Explosions, Flash Fires, and BLEVEs 2nd ed. New York: American Institute of Chemical Engineers.

Casal J., Arnaldos J., Montiel H., Planas-Cuchi E., Ichez J.A.V. (2002). *The Handbook of Hazardous Materials Spills Technology, Chapter 22 Modeling and Understanding BLEVEs*. New York: McGraw-Hill.

Espedal, T. (2016). *Infomøte entreprenørbransjen 23. juni 2016 - E39 Rogfast*. Presentation.

Genova, B., Silvestrini, M., & Leon Trujillo, F. (2008). Evaluation of the blast-wave overpressure and fragments initial velocity for a BLEVE event via empirical correlations derived by a simplified model of released energy. *Journal of Loss Prevention in The Process Industries*, *21*(1), 110-117. http://dx.doi.org/10.1016/j.jlp.2007.11.004

Gexcon. 2016. FLACS v10.5 User's Manual.

Hansen, O., & Kjellander, M. (2016). CFD Modelling of Blast Waves from BLEVEs. *Chemical Engineering Transactions*, *48*, 199-204. http://dx.doi.org/10.3303/CET1648034

Johnson, D., Pritchard, M., & Wickens, M. (1991). *A Large Scale Experimental Study of BLEVEs: Contract Report on CEC Co-Founded Research Project*. British Gas plc.

Kjellander, M. (2016). *Modelling shock waves from BLEVEs*. Presentation, Bergen.

Norsk Petroleuminstitutt [Norwegian Petroleum Institute]. (1997). *Beredskapsplan for propantransport jernbane og tankbil* [Preparedness Plan for Propane Transportation using Rail and Car Tanker]. Oslo, from http://www.np.no/getfile.php/Filer/Tema/HMS/Beredskapsplan%20for%20propantransport.pdf

Prugh, R. (1994). Quantitative evaluation of fireball hazards. *Process Safety Progress*, *13*(2), 83-91. http://dx.doi.org/10.1002/prs.680130211

Roberts, T., Gosse, A., & Hawksworth, S. (2000). Thermal Radiation from Fireballs on Failure of Liquefied Petroleum Gas Storage Vessels. *Process Safety and Environmental Protection*, *78*(3), 184-192. http://dx.doi.org/10.1205/095758200530628

Sha, S., Chen, Z., Jiang, X., & Han, J. (2012). Numerical Investigations on Blast Wave Attenuation by Obstacles. *Procedia Engineering*, *45*, 453-457. http://dx.doi.org/10.1016/j.proeng.2012.08.185

SINTEF. (2003). *Handbook for Fire Calculations and Fire Risk Assessment in the Process Industry*. Norway.

Statens vegvesen [Norwegian Public Roads Administration]. (2012). *E39 Rogfast – Reguleringsplaner: Planbeskrivelse* [E39 Rogfast – Zoning Plan: Plan Description]. Retrieved from http://www.vegvesen.no/_attachment/378589/binary/649907?fast_title=E39+Rogfast+felles+planbeskrivelse+(NB!+18+MB).pdf

Statens vegvesen. (2017). E39 Rogfast. Retrieved 19 April 2017, from www.vegvesen.no/Europaveg/e39rogfast

Statens vegvesen. (2017). -. Retrieved 16 March 2017, from www.vegvesen.no/vegkart/vegkart/

van den Berg, A., & Weerheijm, J. (2006). Blast phenomena in urban tunnel systems. *Journal of Loss Prevention in The Process Industries*, *19*(6), 598-603. http://dx.doi.org/10.1016/j.jlp.2006.03.001

Venart, J.E.S. (2000). Boiling Liquid Expanding Vapour Explosions (BLEVE); Possible failure mechanisms and their consequences. *Symposium Series No. 147*. IChemE.

Younglove, B., & Ely, J. (1987). Thermophysical Properties of Fluids II. Methane, Ethane, Propane, Isobutane, and Normal Butane. *Journal of Physical and Chemical Reference Data*, *16*(4), 577-798.

# Appendix A

## A.1 Basic Method

**Step 1: Collect data**

The following data must be collected:

- Absolute internal pressure of the containment, $p$
- Ambient pressure, $p_0$
- Volume of gas-filled space, $V_1$
- Ratio of specific heat of the gas, $\gamma_1$
- Distance from the centre of the containment to the target, $r$
- Shape of the containment: cylindrical or spherical.

**Step 2: Calculate compressed-gas energy**

The energy of a compressed gas is calculated as follows:

$$E_{ex} = \frac{(p_1 - p_0)2V_1}{\gamma_1 - 1} \qquad \text{eq. A.1}$$

$E_{ex}$ : Energy of compressed gas [J]
$p_1$ : Absolute pressure of gas [Pa]
$p_0$ : Absolute pressure of ambient air [Pa]
$V_1$ : Volume of gas-filled space of vessel [$m^3$]
$\gamma_1$ : Ratio of specific heats of gas in system [-]

**Step 3: Calculate $\bar{R}$ of the target**

The energy of a compressed gas is calculated as follows:

$$\bar{R} = r\left[\frac{p_0}{E_{ex}}\right]^{\frac{1}{3}} \qquad \text{eq. A.2}$$

$r$ : Distance of target from the centre of containment [m]

**Step 4: Check $\bar{R}$**

For $\bar{R}$<2, the basic method gives too high value for blast overpressure. In such cases, refined method must be used in addition of basic method. Refined method will give more accurate approximation for near-field blast overpressure.

**Step 5: Determine $\bar{P}_s$**

Non-dimensional side-on overpressure, $\bar{P}_s$, is determined using Figure A-1 or Figure A-2 for the appropriate $\bar{R}$. The curve labelled "high explosive" must be used if Figure A-1 is used.

**Step 6: Determine $\bar{I}$**

Non-dimensional side-on impulse, $\bar{I}$, is determined using Figure A-3 or Figure A-4 for the appropriate $\bar{R}$. The curve labelled "vessel burst" must be used. For $\bar{R}$ in the range of 0.1 to 1.0, curve in Figure A-4 is more convenient.

**Step 7: Adjust $\bar{P}_s$ and $\bar{I}$ for geometry effects**

To account for geometry effects such as shape of containment and location of containment relative to the ground, some adjustments are required which derived from experiments. The adjustment factors for cylindrical and spherical containment are shown in Table A-1 and Table A-2 respectively.

Table A-1. Adjustment Factors for $\bar{P}_s$ and $\bar{I}$ for Cylindrical Containment (CCPS, 1994)

| $\bar{R}$ | Multiplier for | |
|---|---|---|
| | $\bar{P}_s$ | $\bar{I}$ |
| < 0.3 | 4 | 2 |
| $0.3 \leq \bar{R} \leq 1.6$ | 1.6 | 1.1 |
| $1.6 < \bar{R} \leq 3.5$ | 1.6 | 1 |
| > 3.5 | 1.4 | 1 |

Table A-2. Adjustment Factors for Spherical Containment Slightly Elevated Above Ground (CCPS, 1994)

| $\bar{R}$ | Multiplier for | |
|---|---|---|
| | $\bar{P}_s$ | $\bar{I}$ |
| < 1.0 | 2 | 1.6 |
| > 1.0 | 1.1 | 1 |

**Step 8: Calculate $p_s$ and $i_s$**

Following equations are being used to calculate side-on peak overpressure $p_s$ and side-on impulse $i_s$ from non-dimensional side-on peak overpressure and non-dimensional side-on impulse.

$$p_s - p_0 = \bar{P}_s p_0 \qquad \text{eq. A.3}$$

$$i_s = \frac{\bar{I} p_0^{\frac{2}{3}} E_{ex}^{\frac{1}{3}}}{a_0} \qquad \text{eq. A.4}$$

$\bar{P}_s$ : Non-dimensional side-on peak overpressure [-]

$p_0$ : Absolute pressure of ambient air [Pa]

$\bar{I}$ : Non-dimensional side-on peak impulse [-]

$a_0$ : Speed of sound in ambient air [m/s]

**Step 9: Check $p_s$**

CCPS (1994) states that this method has limited accuracy especially in the near field. If the calculated side-on peak overpressure is larger than initial pressure in the vessel $p_1$, the initial pressure $p_1$ should be taken as side-on peak overpressure.

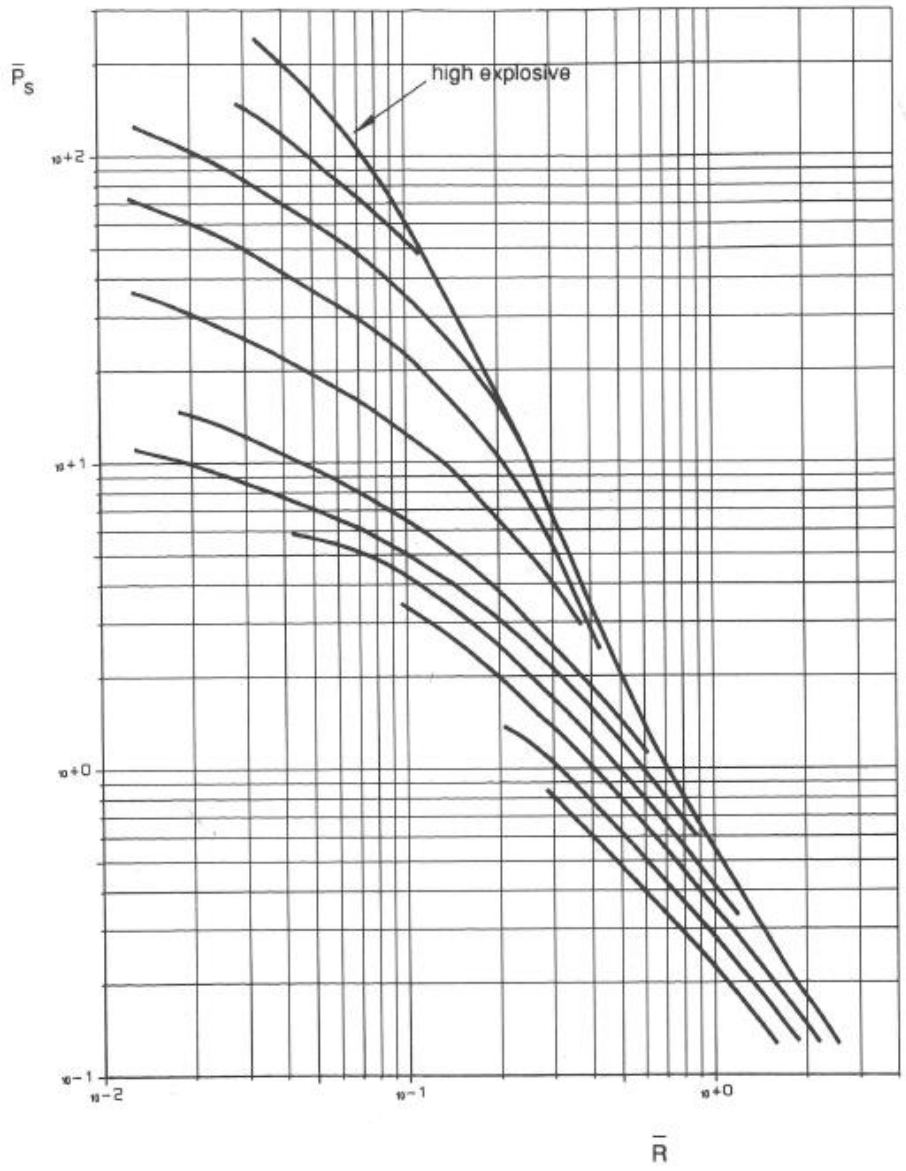


Figure A-1. Non-dimensional overpressure versus non-dimensional distance for overpressure calculation. (CCPS, 1994, p.207)

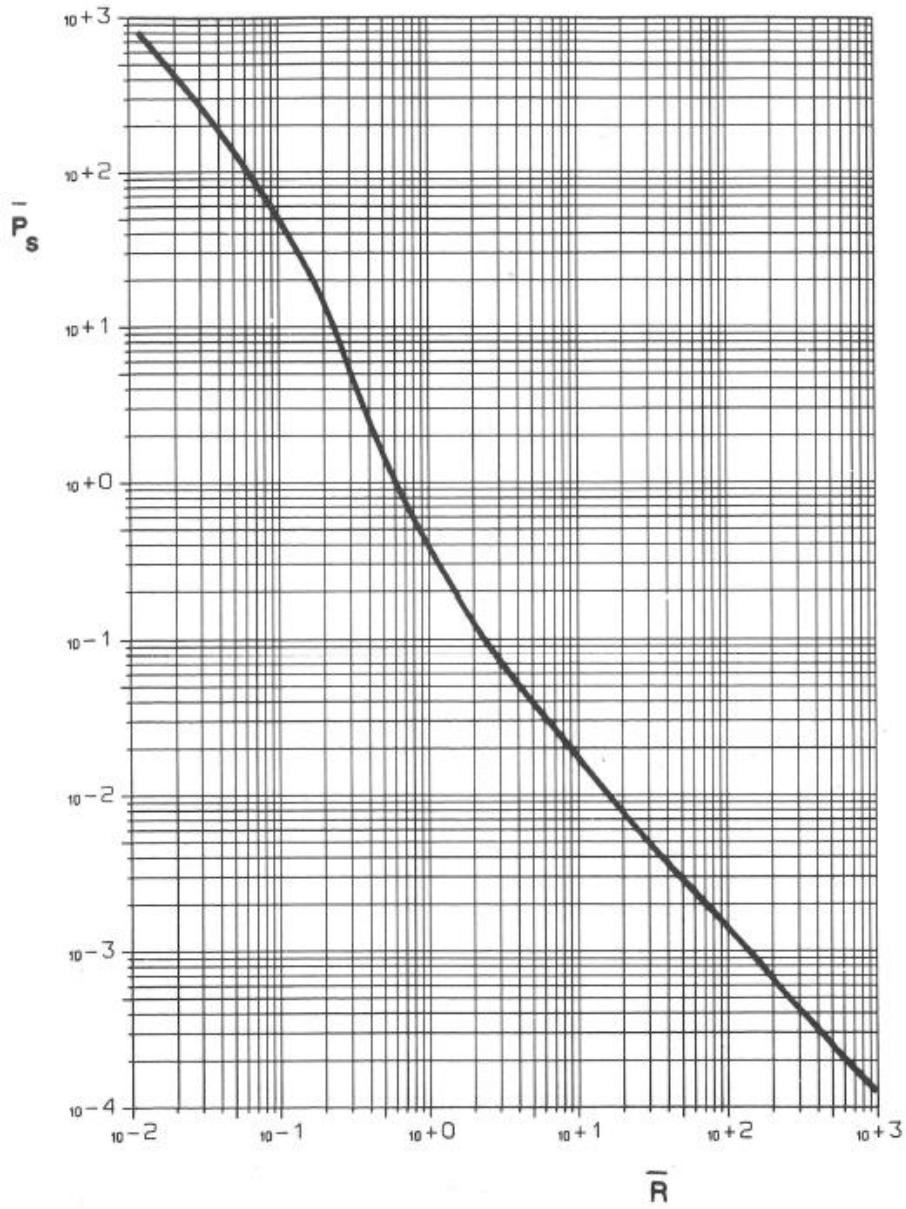


Figure A-2. Non-dimensional overpressure versus non-dimensional distance for broader range. (CCPS, 1994, p.208)

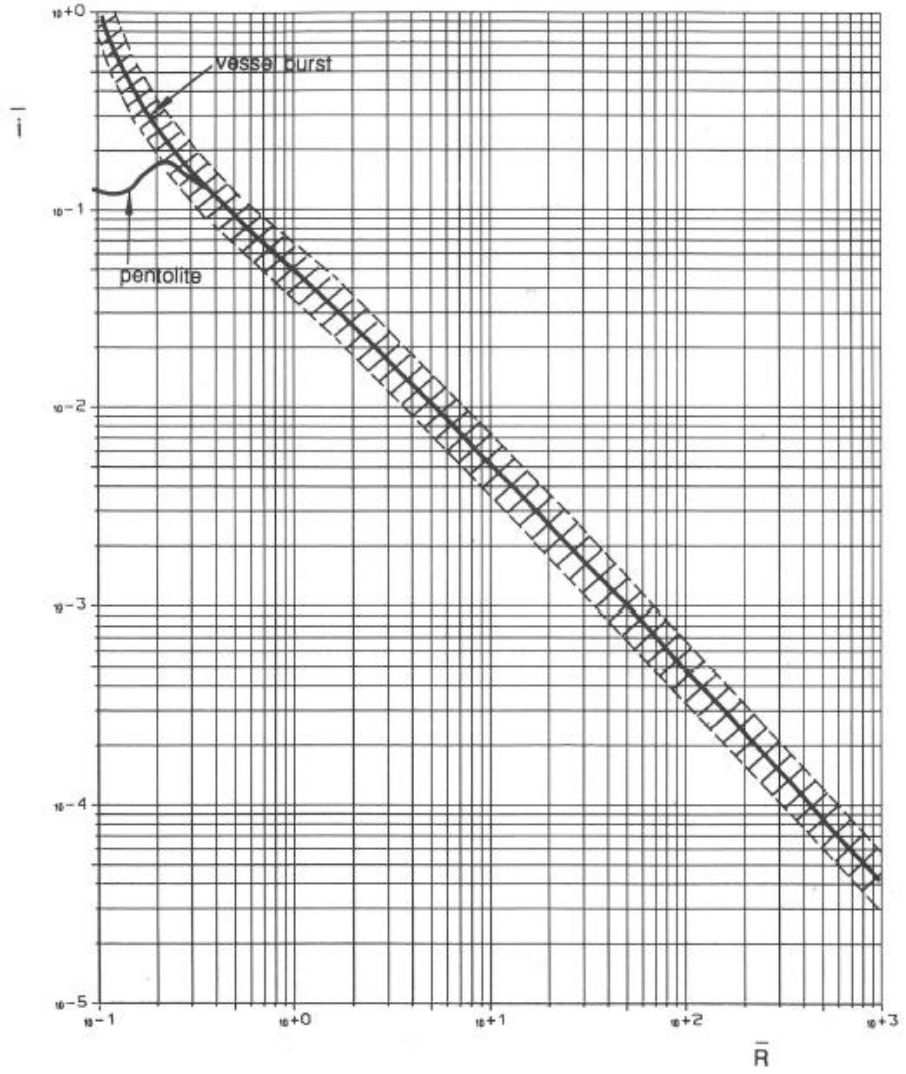


Figure A-3. Non-dimensional impulse versus non-dimensional distance for broader distance. (CCPS, 1994, p.210)

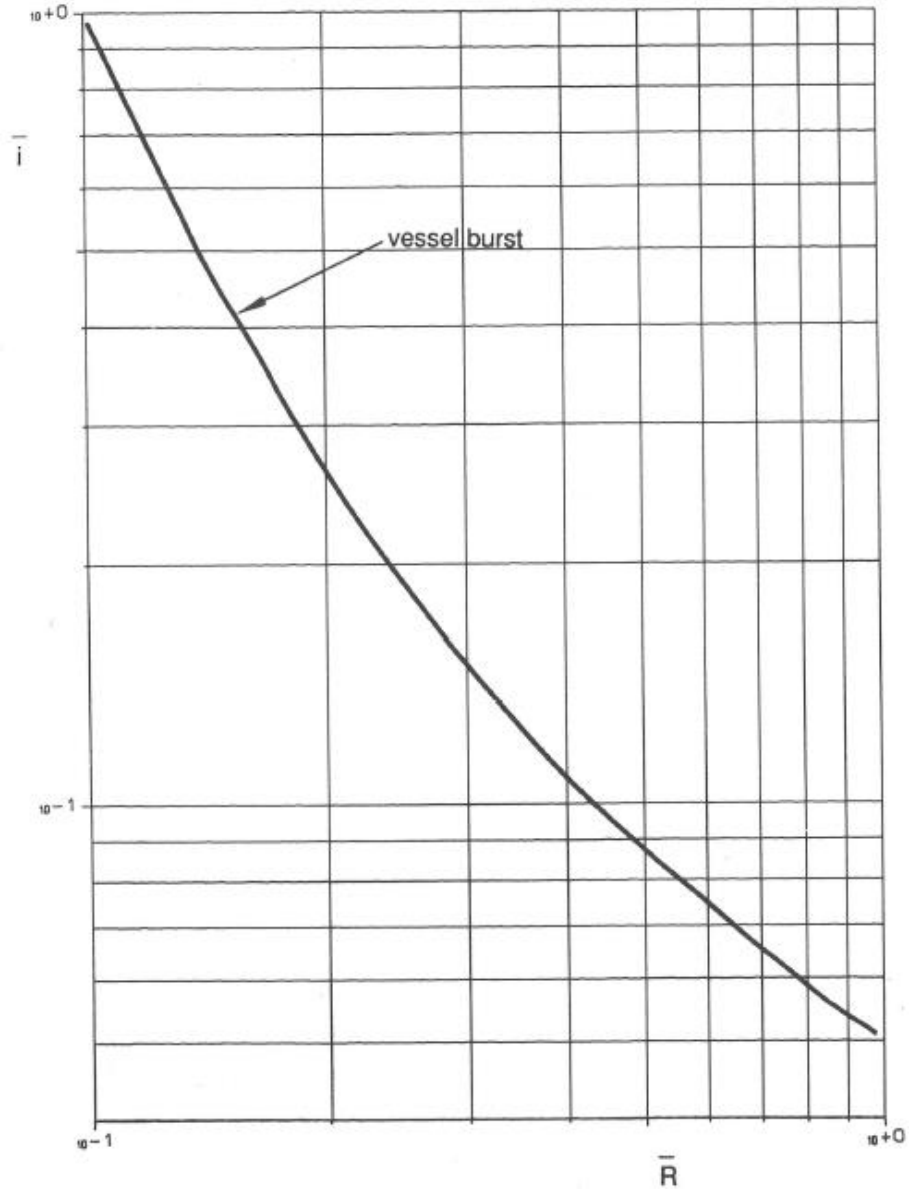


Figure A-4. Non-dimensional impulse versus non-dimensional distance for $\bar{R}$ from 0.1 to 1. (CCPS, 1994, p.211)

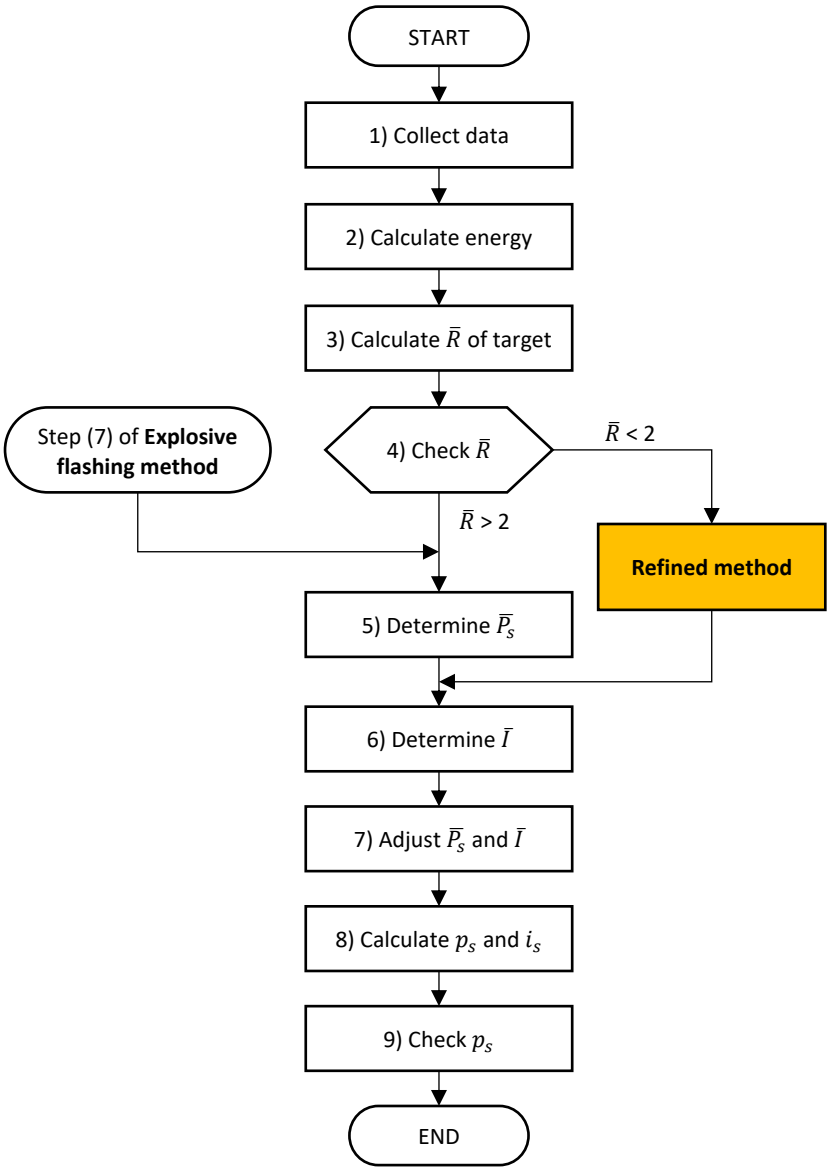


Figure A-5. Basic method. (CCPS, 1994)

## A.2 Refined Method

### Step 1: Collect additional data

Some additional data are required to calculate using refined method.

- Ratio of speed of sound in compressed gas to its speed in ambient air, $a_1/a_0$
- Ratio of specific heat of ambient air, $\gamma_0$ = 1.40.

For an ideal gas,

$$\left[\frac{a_1}{a_0}\right]^2 = \frac{\gamma_1 T_1 M_0}{\gamma_0 T_0 M_1} \quad \text{eq. A.5}$$

$T_0$ : Absolute temperature of ambient air [K]
$T_1$ : Absolute temperature of compressed gas [K]
$M_1$ : Molar mass of compressed gas [kg/kmol]
$M_0$ : Molar mass of ambient air = 29 kg/kmol
$\gamma_0$ : Specific heat ratio of ambient air [-]
$\gamma_1$ : Specific heat ratio of compressed gas [-]

**Step 2: Calculate the initial distance**

This refinement assumes that an explosion's shock wave will be completely symmetrical. Such a shape would result from the explosion of a hemispherical vessel placed directly on the ground. Therefore, a hemispherical vessel is used instead of the actual vessel for calculation purposes. Radius of the hemispherical vessel can be calculated using the following formula.

$$r_0 = \left[\frac{3V_1}{2\pi}\right]^{\frac{1}{3}} = 0.782 V_1^{\frac{1}{3}} \quad \text{eq. A.6}$$

$V_1$ : Volume of the actual vessel [$m^3$]

This is the starting distance on the overpressure versus distance curve. It must be transformed into the non-dimensional starting distance with:

$$\bar{R}_0 = r_0 \left[\frac{p_0}{E_{ex}}\right]^{\frac{1}{3}} \quad \text{eq. A.7}$$

**Step 3: Calculate the initial peak overpressure $\bar{P}_{so}$**

The initial peak overpressure will have lower value than the initial pressure inside the containment. The pressure decreases as it is moving away from the blast source. For this step, the formula given is complex and iteration process is required to obtain $\bar{P}_{so}$.

$$\frac{p_1}{p_2} = (\bar{P}_{so} + 1)\left[1 - \frac{(\gamma_1 - 1)\left(\frac{a_0}{a_1}\right)\bar{P}_{so}}{[2\gamma_0\{2\gamma_0 + (\gamma_0 + 1)\}\bar{P}_{so}]^{\frac{1}{2}}}\right]^{-\frac{2\gamma_1}{\gamma_1 - 1}} \quad \text{eq. A.8}$$

$p_1$ : Initial absolute pressure of compressed gas [Pa]
$p_0$ : Ambient pressure [Pa]
$\bar{P}_{so}$ : Non-dimensional peak shock overpressure directly after burst [-]

$$\bar{P}_{so} = \frac{p_{so}}{p_0} - 1$$

$p_{so}$ : Peak shock overpressure directly after burst [Pa]
$\gamma_0$ : Specific heat ratio of ambient air [-]
$\gamma_1$ : Specific heat ratio of compressed gas [-]
$a_0$ : Speed of sound in ambient air [m/s]
$a_1$ : Speed of sound in compressed gas [m/s]

**Step 4: Locate the starting point on Figure 6.21 (CCPS, 1994)**

From previous steps, $\bar{R}_0$ and $\bar{P}_{so}$ will be used to locate the starting point of the correct curve from several curves available on Figure 6.21 (CCPS, 1994). The curve will be used for the next step.

**Step 5: Determine $\bar{P}_s$**

The non-dimensional side-on overpressure $\bar{P}_s$ for respective $\bar{R}$ is determined using Figure 6.21 (CCPS, 1994). The curve which goes through the starting ($\bar{R}_0$,$\bar{P}_{so}$) should be used. The calculation continues to Step 6 of basic method.

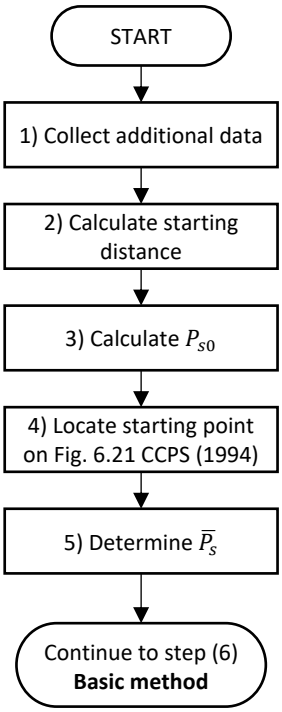


Figure A-6. Refined method to determine $\bar{P}_s$. (CCPS, 1994)

## A.3 Calculation Example for Simulation

Case: BG-1R

Known parameters:

Volume of containment = 5.7 $m^3$
Fuel = butane
Fill level = 77 %
Pressure at failure = 15.1 barg
Liquid temperature at failure = 95 °C
Vapour temperature at failure = 83 °C

Calculation of flash fraction

Based on the known parameters and refer to thermophysical data:

$H_v$ = 219580 J/kg
$C_p$ = 3272 J/(kg·K)
$T_c$ = 408 K
$T_b$ = 261.3 K
$T_0$ = 368 K

$$f = 1 - \exp\left[-2.63 \frac{C_p}{H_v}(T_c - T_b) \cdot \left(1 - \left(\frac{T_c - T_0}{T_c - T_b}\right)^{0.38}\right)\right]$$

$f$ = 0.8936

The total mass of liquid is 2000 kg; therefore, 1787.2 kg of liquid will be vaporized violently (flashing).

The pressure of pseudo-source region should be one-fifth of the rupturing pressure. The pressure, $P_{PS}$, is 3.02 barg. Gas density at rupturing temperature and pseudo-source pressure is 8.034 kg/m$^3$. Therefore,

$$V_{PS} = \frac{0.07f \cdot m_l}{\rho_{P,T}}$$

$$V_{PS} = \frac{0.07 \cdot 1787.2}{8.034}$$

$V_{PS}$ = 15.57 m$^3$

The volume of vapour space will be:

$$V_{vap} = (1 - FL) \cdot V$$

$V_{vap}$ = 1.3 m$^3$

We have to set those values to the grid. For vapour pressure, it is assumed that the shape of pressure is block and fully filled the control volumes. Therefore, the volume of vapour pressure becomes 2.4 m$^3$ assuming 0.2 m of core domain grid.

Based on Figure 6.31 (CCPS, 1994), the expansion energy of the liquid part per unit volume is 27.5 MJ/m$^3$ and the expansion energy of the vapour part per unit volume is 4 MJ/m$^3$. Those are based on the given temperature. Therefore, the total expansion energy of the liquid part contributing to blast waves generation is:

$$E_{ex,l} = 0.07 \cdot 2 \cdot 1 \cdot 27.5 \cdot 0.77 \cdot 5.7 = 16.90 \text{ MJ}$$

And the total expansion energy of the vapour part is:

$$E_{ex,v} = 2 \cdot 1 \cdot 4 \cdot 0.23 \cdot 5.7 = 10.49 \text{ MJ}$$

The total expansion energy is 27.39 MJ. Here, it is assumed that the fragment reduction factor is equal to 0, i.e. there is no contribution of energy related to the vessel fragmentation.

Assuming that the ambient pressure, $p_0$, is equal to 100 kPa, the non-dimensional distance for $r$ = 25 m is 3.85. Based on Figure 6.22 (CCPS, 1994), the non-dimensional blast overpressure will be 0.055 and the non-dimensional blast impulse will be 0.014. Respectively, the blast overpressure and impulse at $r$ = 25 m are 55 mbarg and 26.51 Pa·s.

*This page intentionally left blank*

# Appendix B

**Calculation for Radiation of Fireball (CCPS, 1994)**

Hymes (1983), as cited by CCPS (1994), suggested a specified point-source model for BLEVE. Radiation received by the receptor can be approached using the following formula.

$$q = \frac{2.2\tau_a R H_c m_f^{0.67}}{4\pi L^2}$$

$q$ : Radiation received by the receptor [W/m$^2$]
$\tau_a$ : Atmospheric transmissivity [-]
$H_c$ : Net heat of combustion per unit mass [J/kg]
$m_f$ : Mass of fuel in the fireball [kg]
$R$ : Radiative fraction of heat of combustion [-]
$L$ : Distance from fireball centre to receptor [m]

The value of $R$ is suggested to be 0.3 if the containment burst below relief valve pressure, and 0.4 otherwise.

In solid flame model, the radiation per unit time depends on view factor, emissive power per unit area, and atmospheric transmissivity. Mathematically, it can be written by:

$$q = FE\tau_a$$

$F$ : View factor [-]
$E$ : Emissive power per unit area [W/m$^2$]
$\tau_a$ : Atmospheric transmissivity [-]

Emissive power can be calculated using an approximation by Pape et.al. (1988), as cited by CCPS (1994). The approximation is based on 6.2 kg of fuel mass with 20 atm vapour pressure. For the conditions, emissive power can be approximated by:

$$E = 235P_v^{0.39}$$

$P_v$ : Vapour pressure [MPa]
$E$ : Emissive power per unit area [kW/m$^2$]

The equation is limited to vapour pressure at release time at or below 2 MPa.

View factor of a specific point on a plane surface can be calculated by:

$$F = \frac{r^2}{L^2}\cos\Theta \qquad \text{for} \quad \Theta \leq \frac{\pi}{2} - \Phi$$

$$F = \frac{1}{2} - \frac{1}{\pi}\sin^{-1}\left[\frac{(L^2 - r^2)^{\frac{1}{2}}}{L\sin\Theta}\right] + \frac{r^2}{\pi L^2}\cos\Theta\cos^{-1}\left[-\frac{(L^2 - r^2)^{\frac{1}{2}}}{r}\cos\Theta\right]$$
$$- \frac{1}{\pi L^2}(L^2 - r^2)^{\frac{1}{2}}(r^2 - L^2\cos^2\Theta)^{\frac{1}{2}} \qquad \text{for} \quad \Theta > \frac{\pi}{2} - \Phi$$

$r$ : Radius of fireball [m]

$L$ : Distance to centre of sphere [m]

$\Theta$ : Angle between normal to surface and connection point to centre of sphere [rad]

$2\Phi$ : View angle [rad]

# Appendix C

**Birk 01-4 – Blast Overpressure**

t = 0 ms, 10 ms, 20 ms, 30 ms

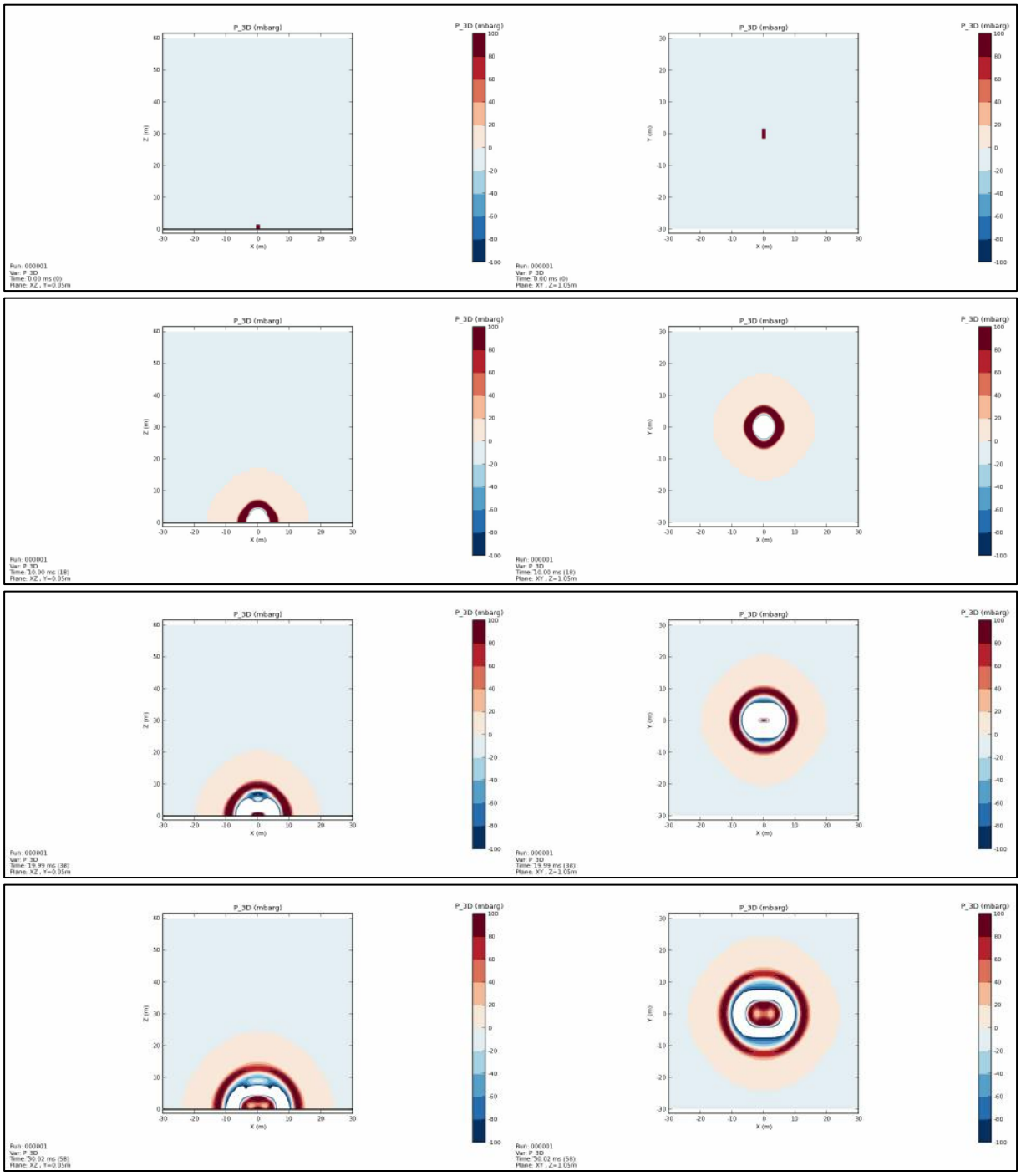

t = 40 ms, 50 ms, 60 ms, 70 ms, 80 ms

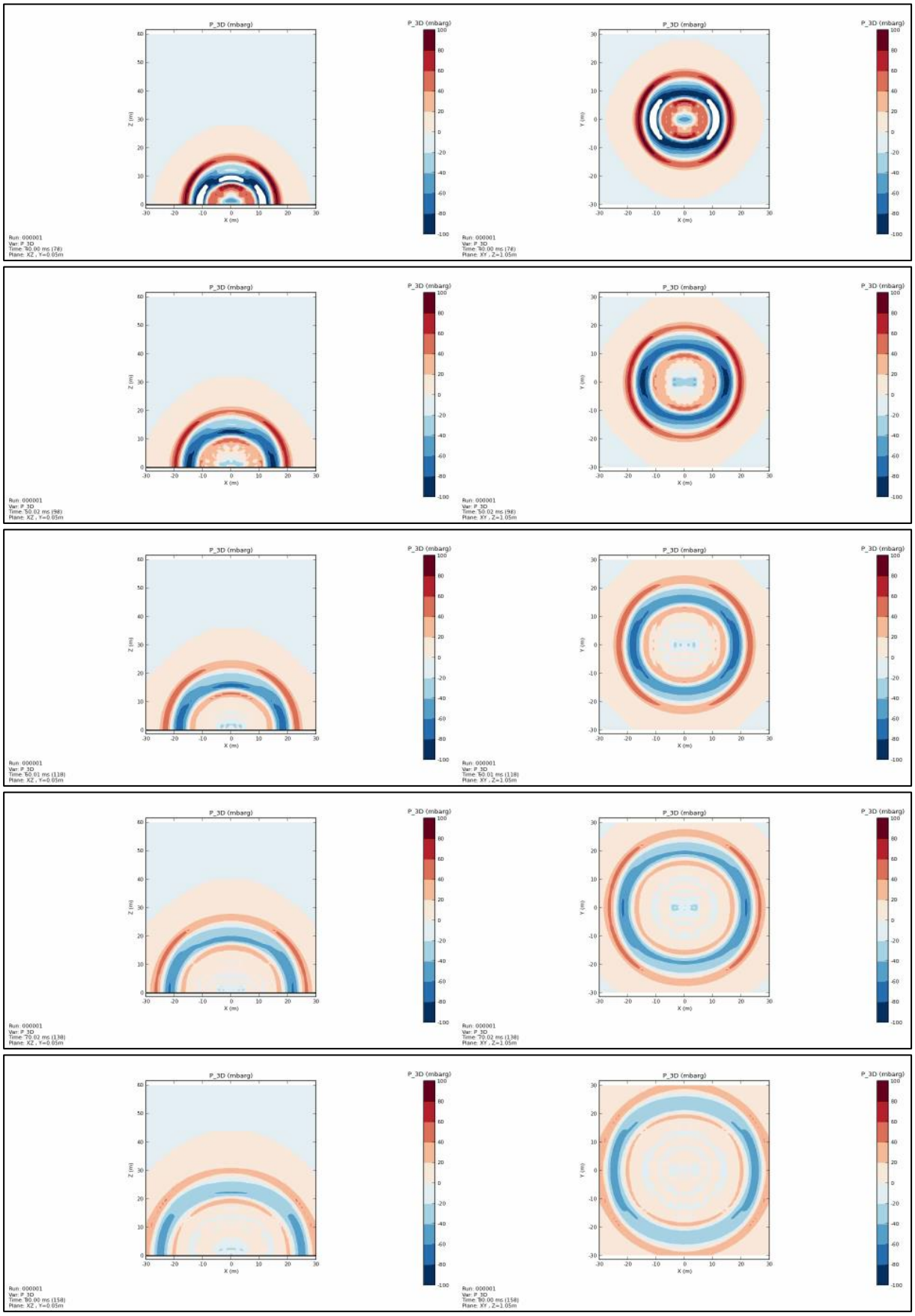

t = 90 ms, 100 ms, 110 ms, 120 ms, 130 ms

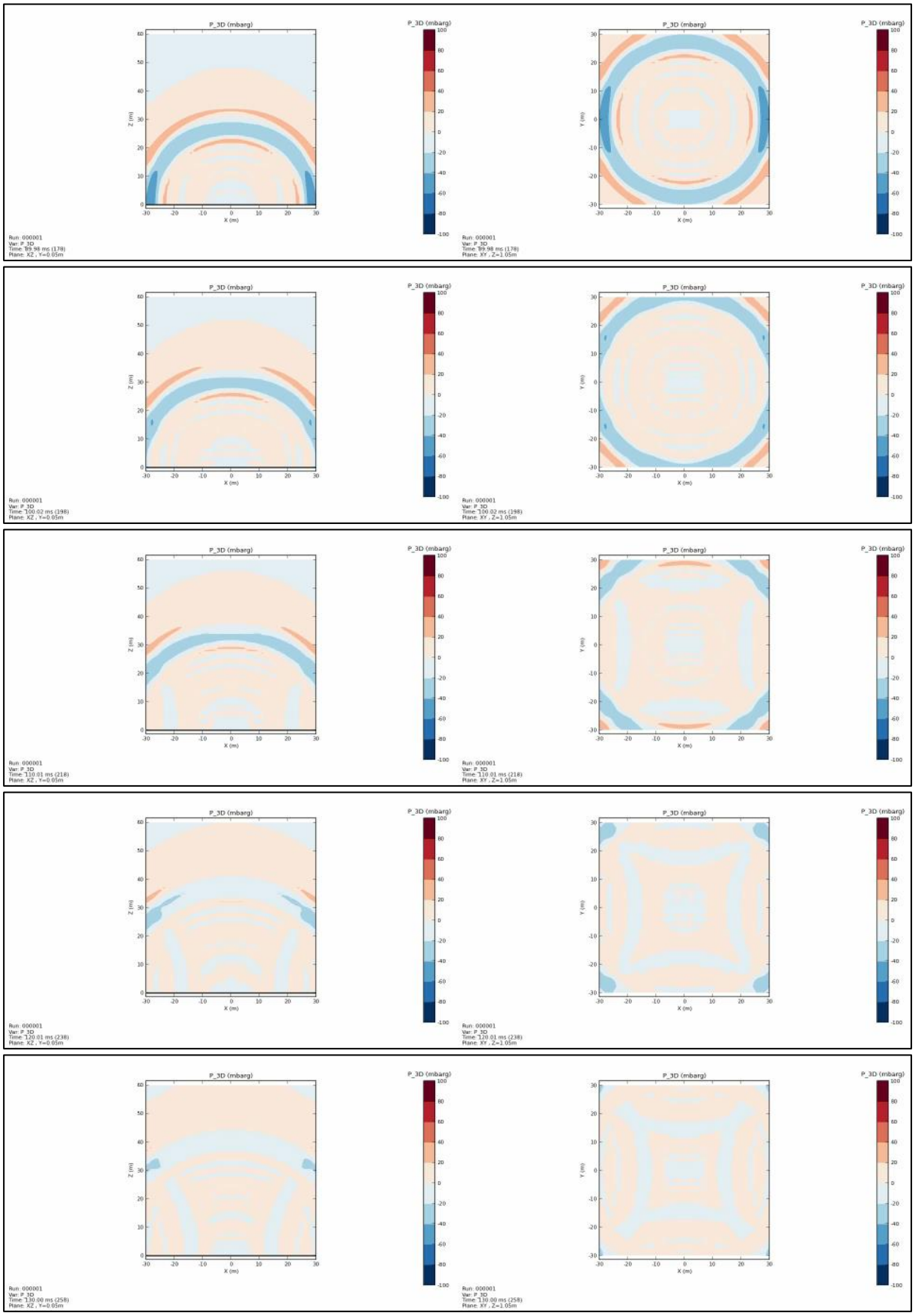

t = 140 ms, 150 ms

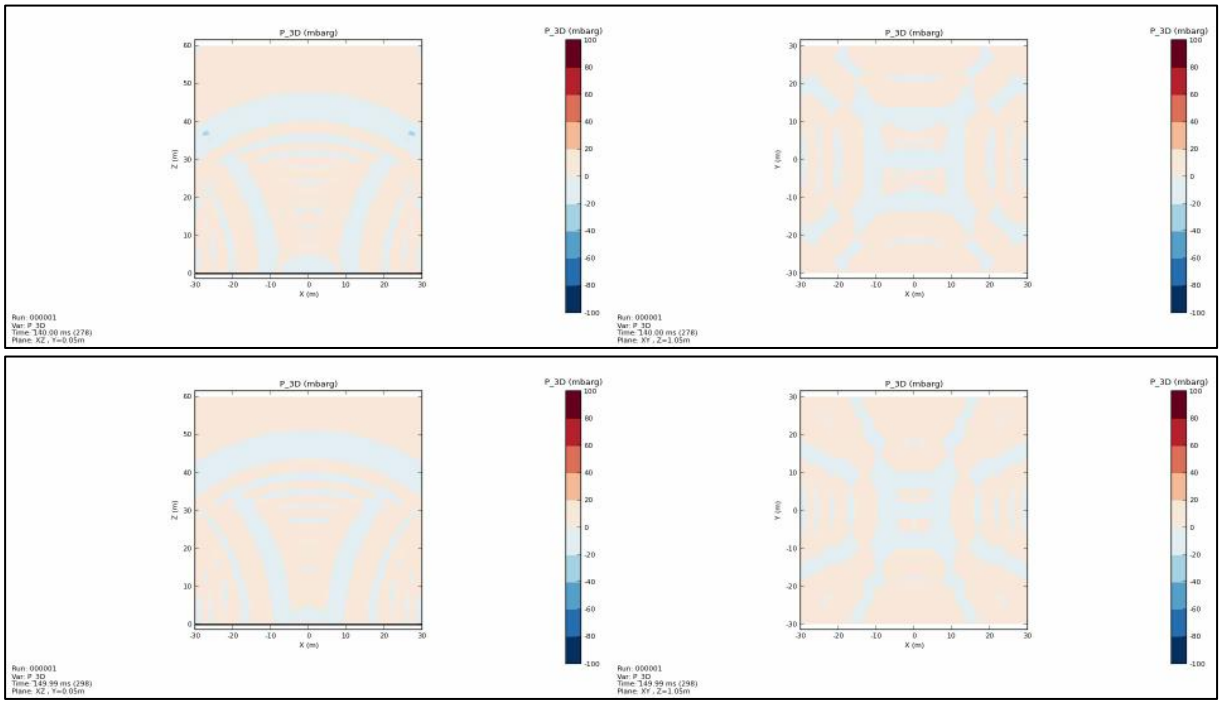

**Birk 01-4 – Fireball**

t = 0 ms, 55 ms, 100 ms, 200 ms, 400 ms

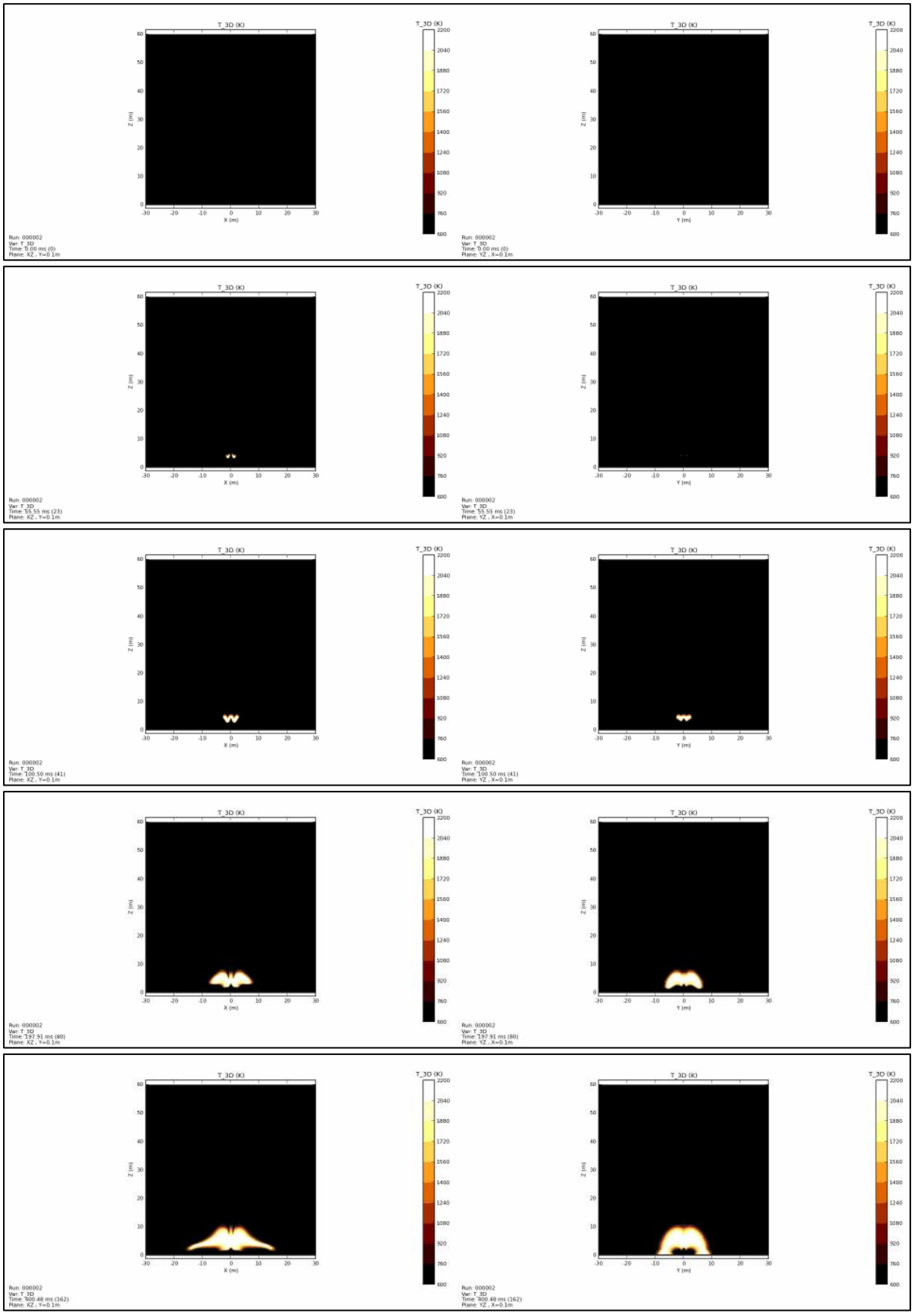

t = 800 ms, 1200 ms, 1400 ms, 1600 ms, 2000 ms, 2400 ms

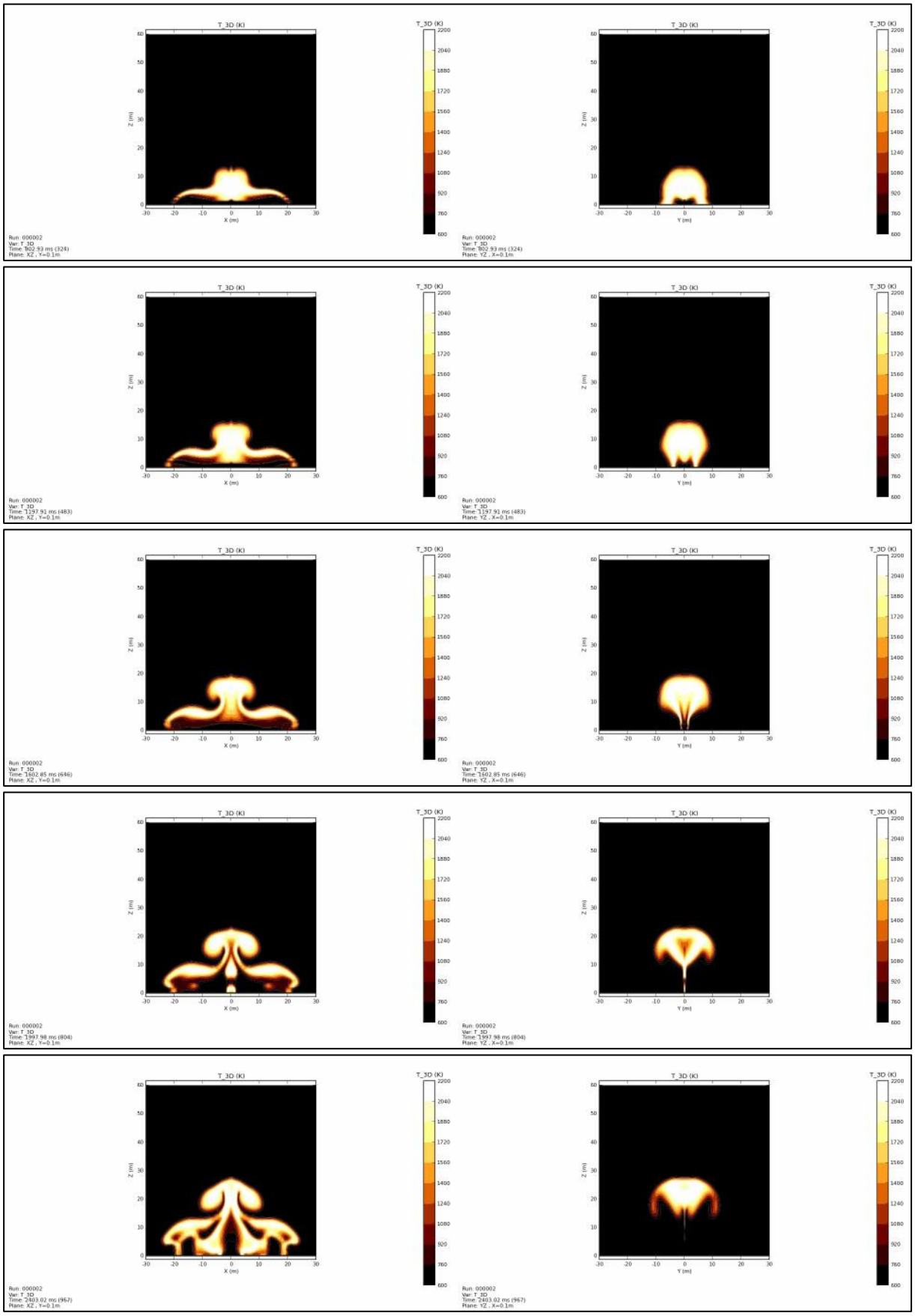

t = 2800 ms, 3200 ms, 3600 ms, 4000 ms, 4800 ms

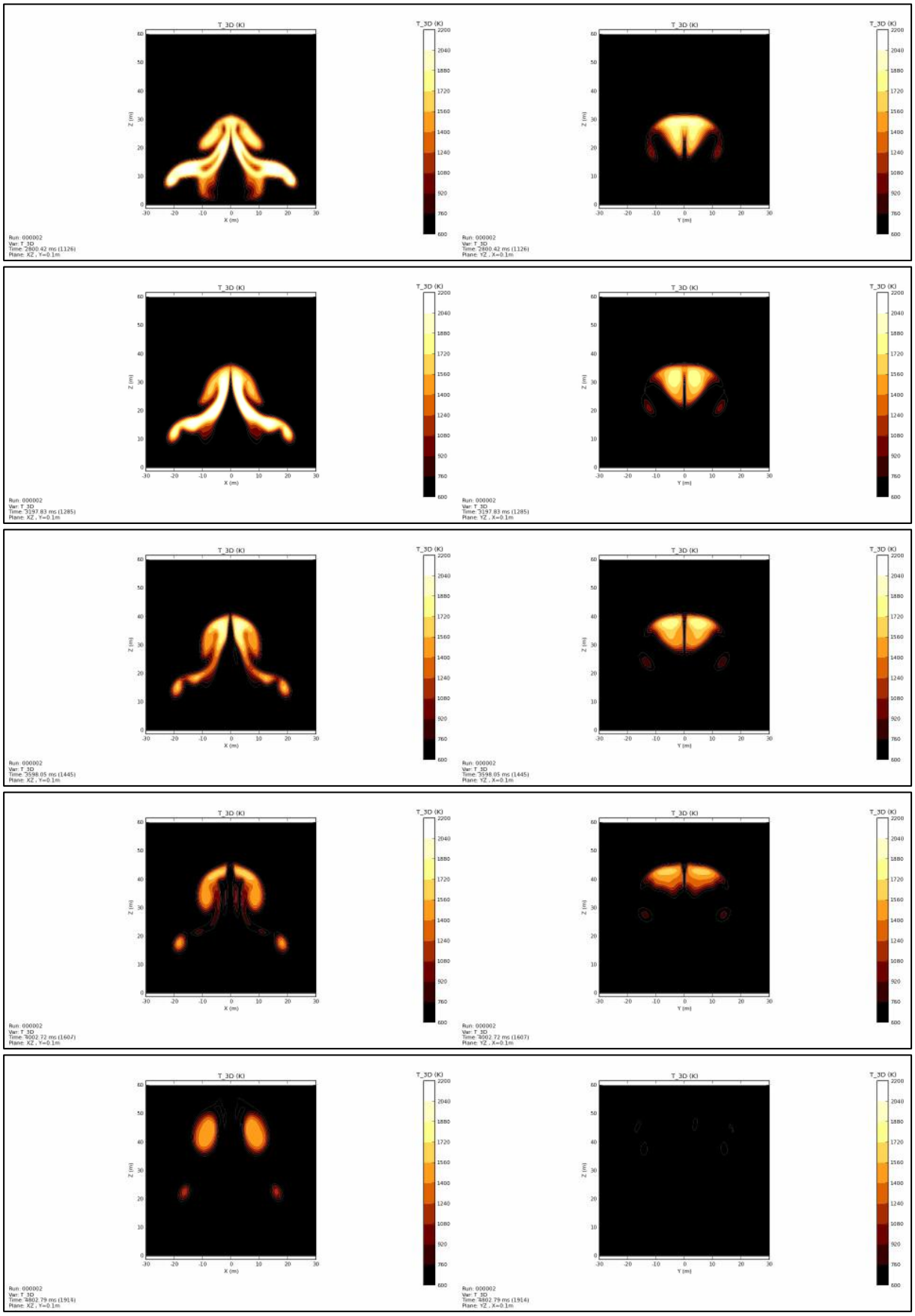

## Rogfast 2R – Blast Overpressure 1

t = 0 ms, 50 ms, 100 ms, 200 ms, 300 ms

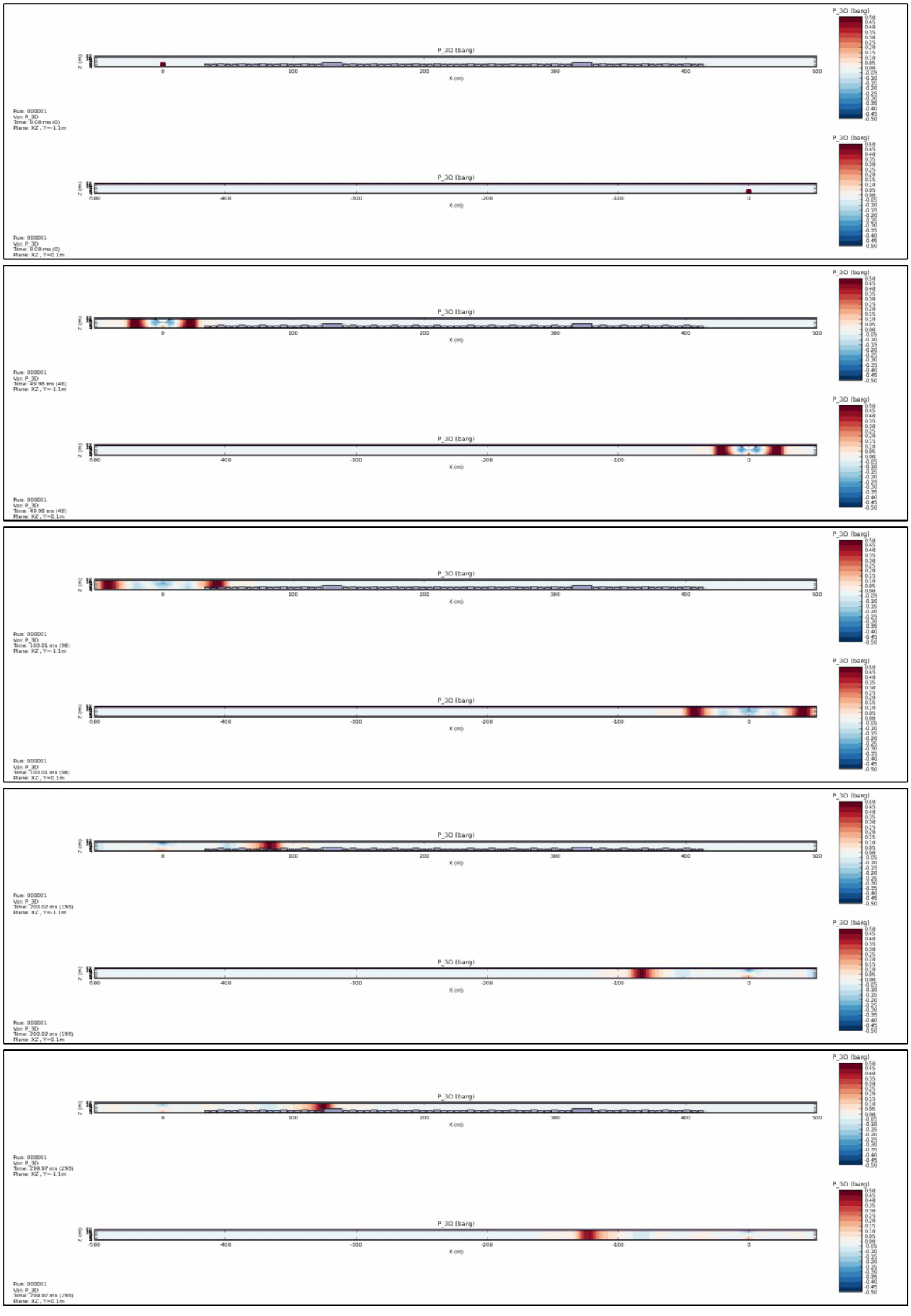

t = 400 ms, 500 ms, 600 ms, 700 ms, 800 ms

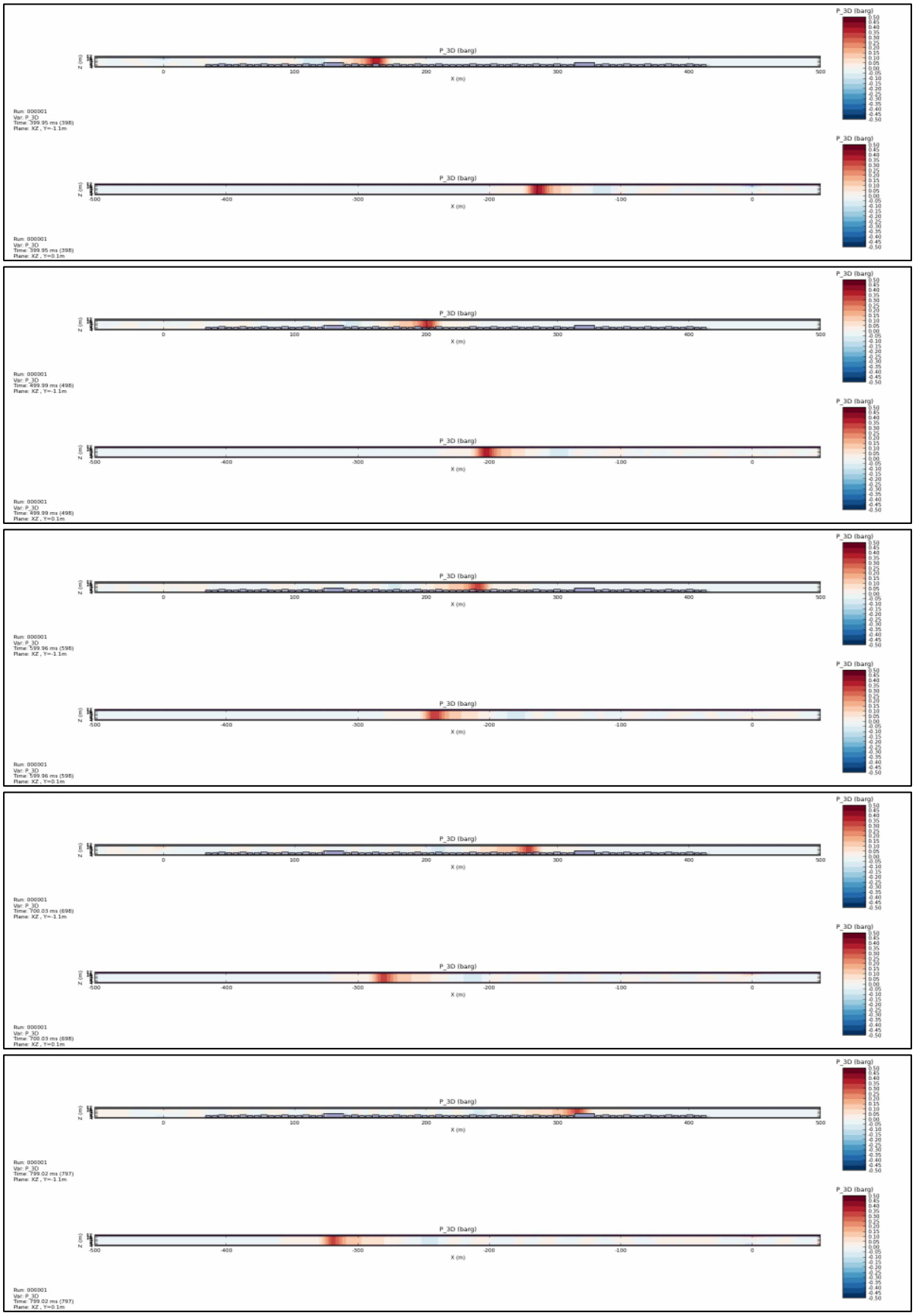

t = 900 ms, 1000 ms, 1100 ms, 1200 ms, 1400 ms

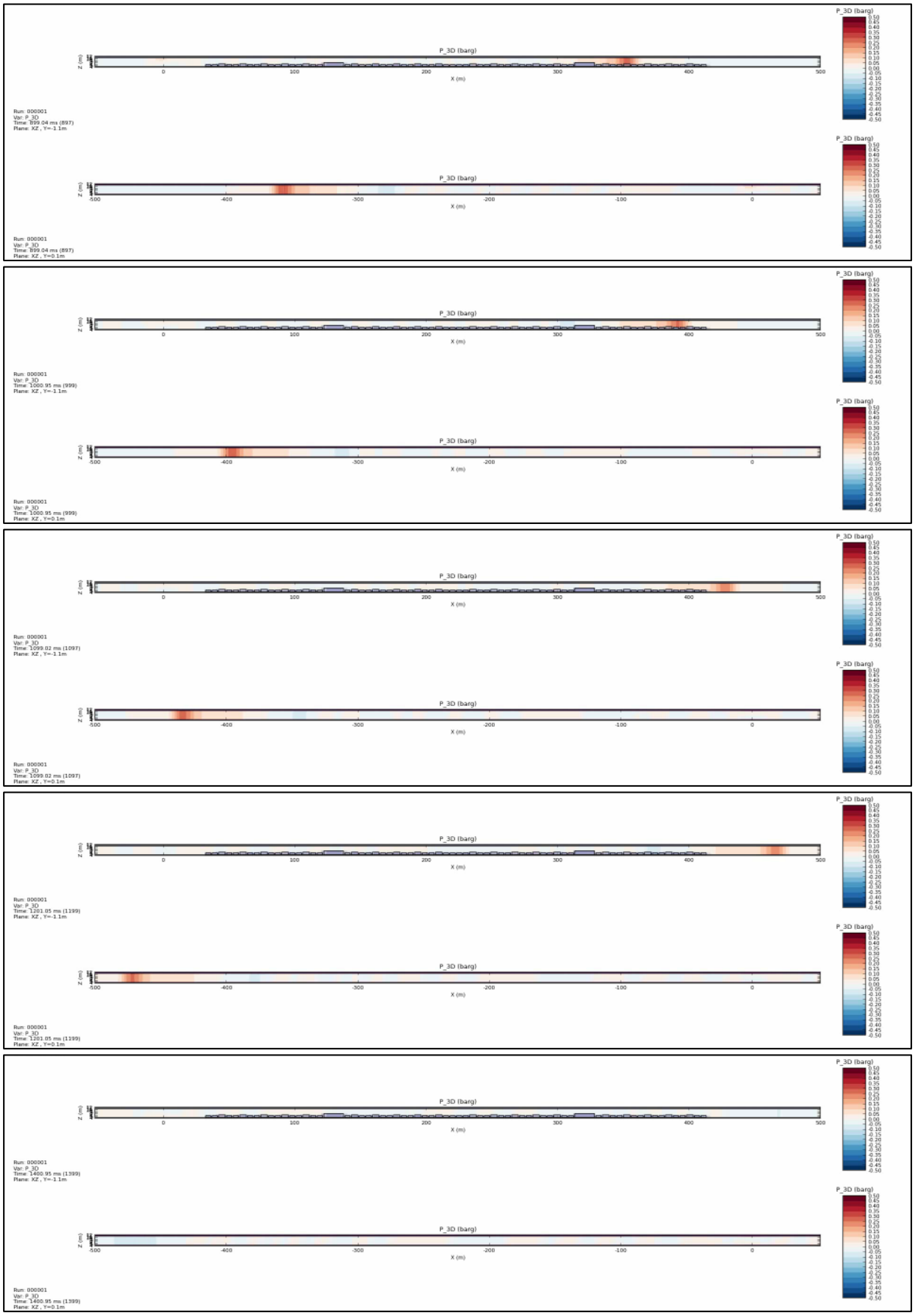

t = 1600 ms, 1800 ms, 2000 ms, 2200 ms, 2400 ms

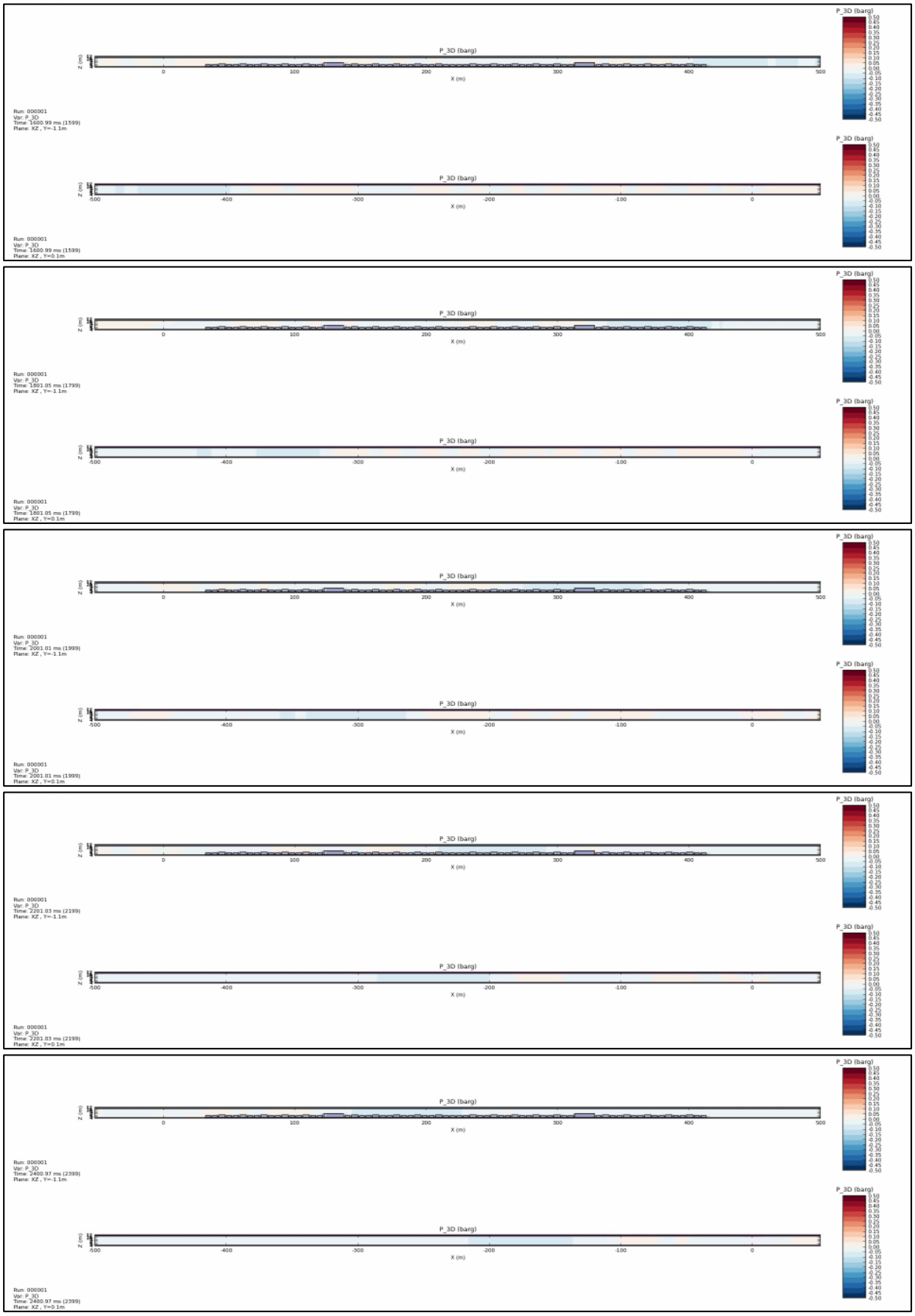

## Rogfast 2R – Fireball 1 (X-Y Plane)

t = 0 ms, 200 ms, 400 ms, 800 ms, 1200 ms, 1600 ms, 2000 ms

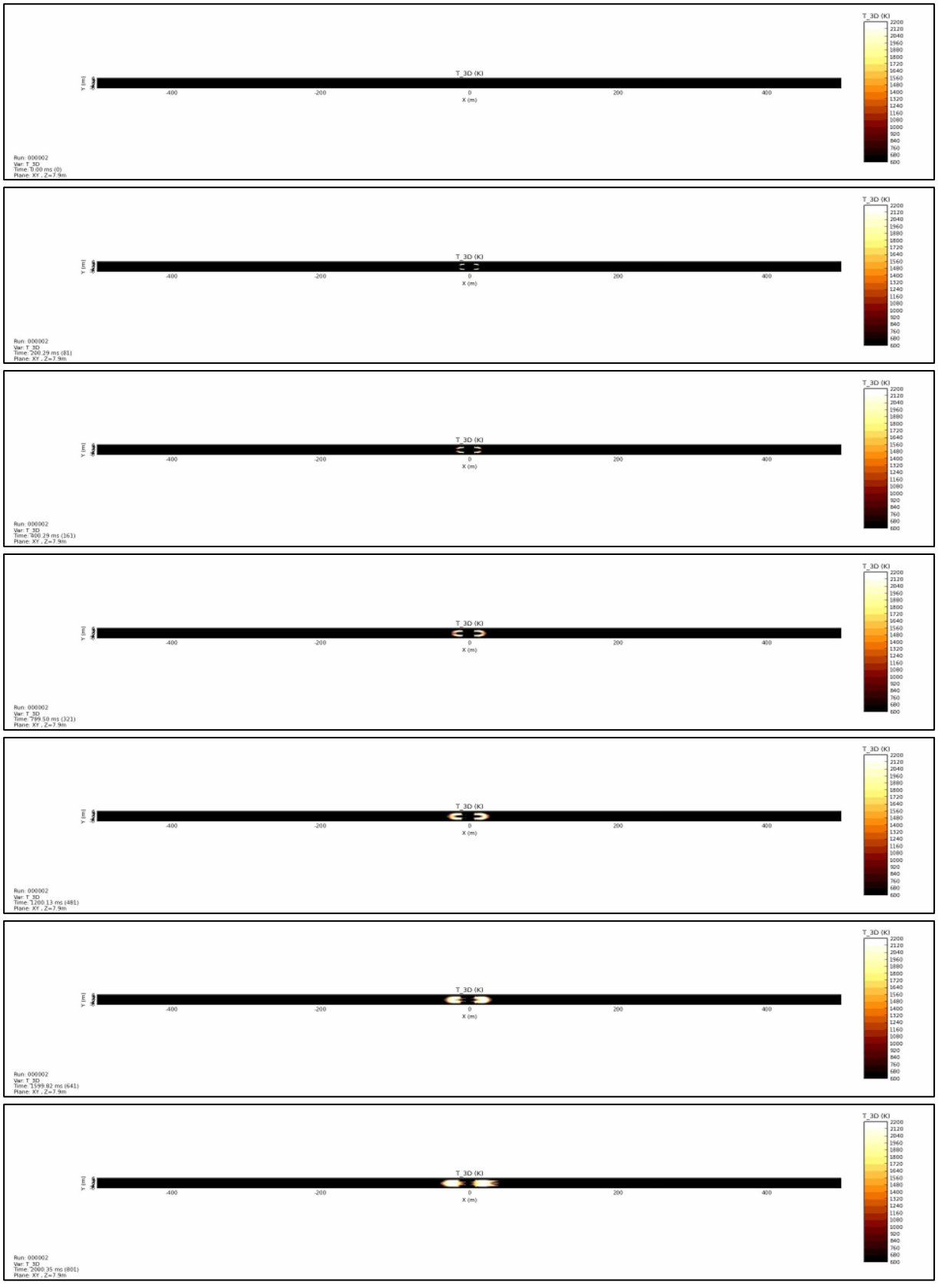

t = 2400 ms, 2800 ms, 3200 ms, 3600 ms, 4000 ms, 4800 ms, 5600 ms

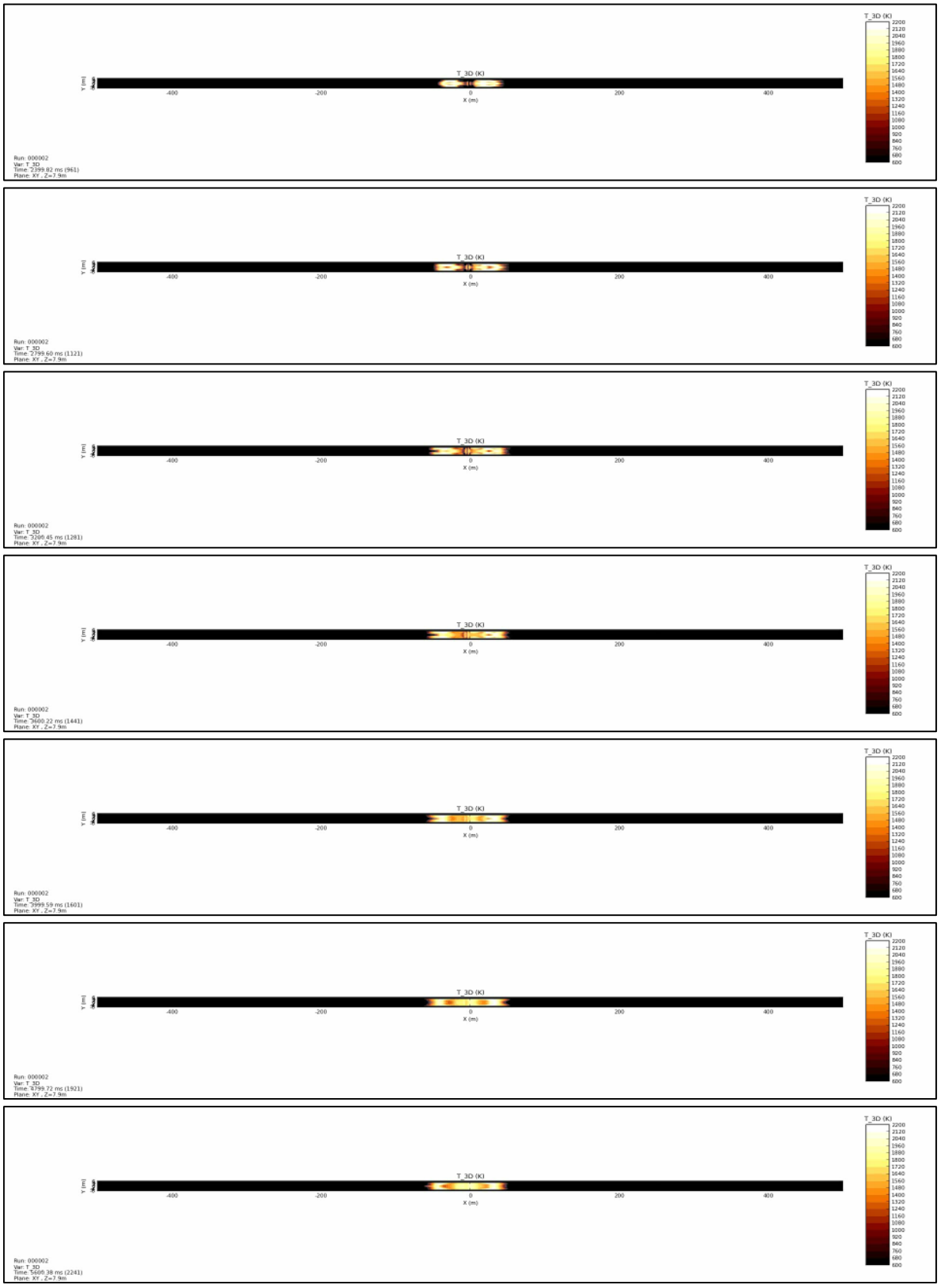

t = 6400 ms, 7200 ms, 8000 ms, 8800 ms, 9600 ms, 10000 ms, 11000 ms

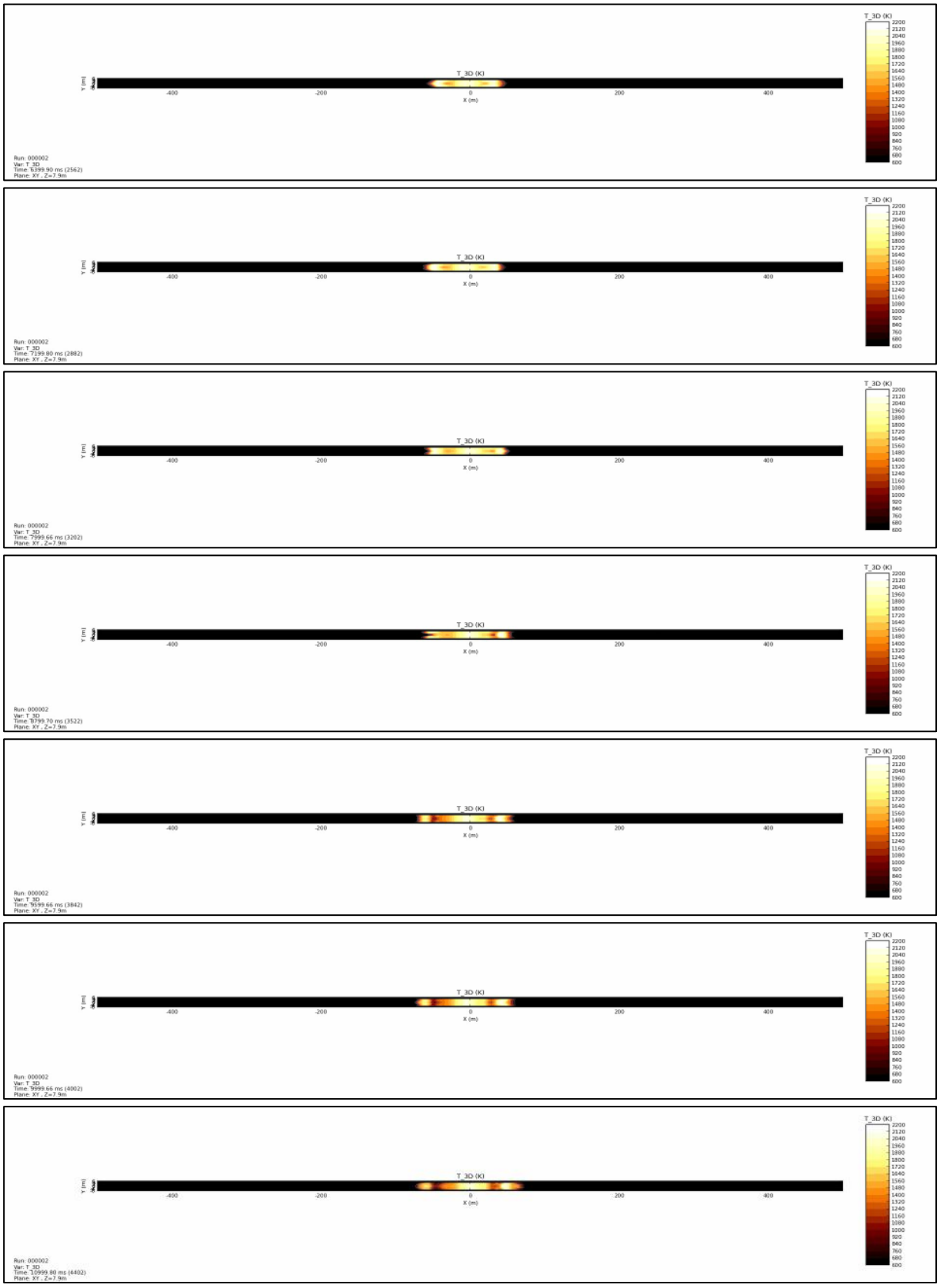

## Rogfast 2R – Fireball 2 (X-Z Plane)

t = 0 ms, 200 ms, 400 ms, 800 ms, 1200 ms, 1600 ms, 2000 ms

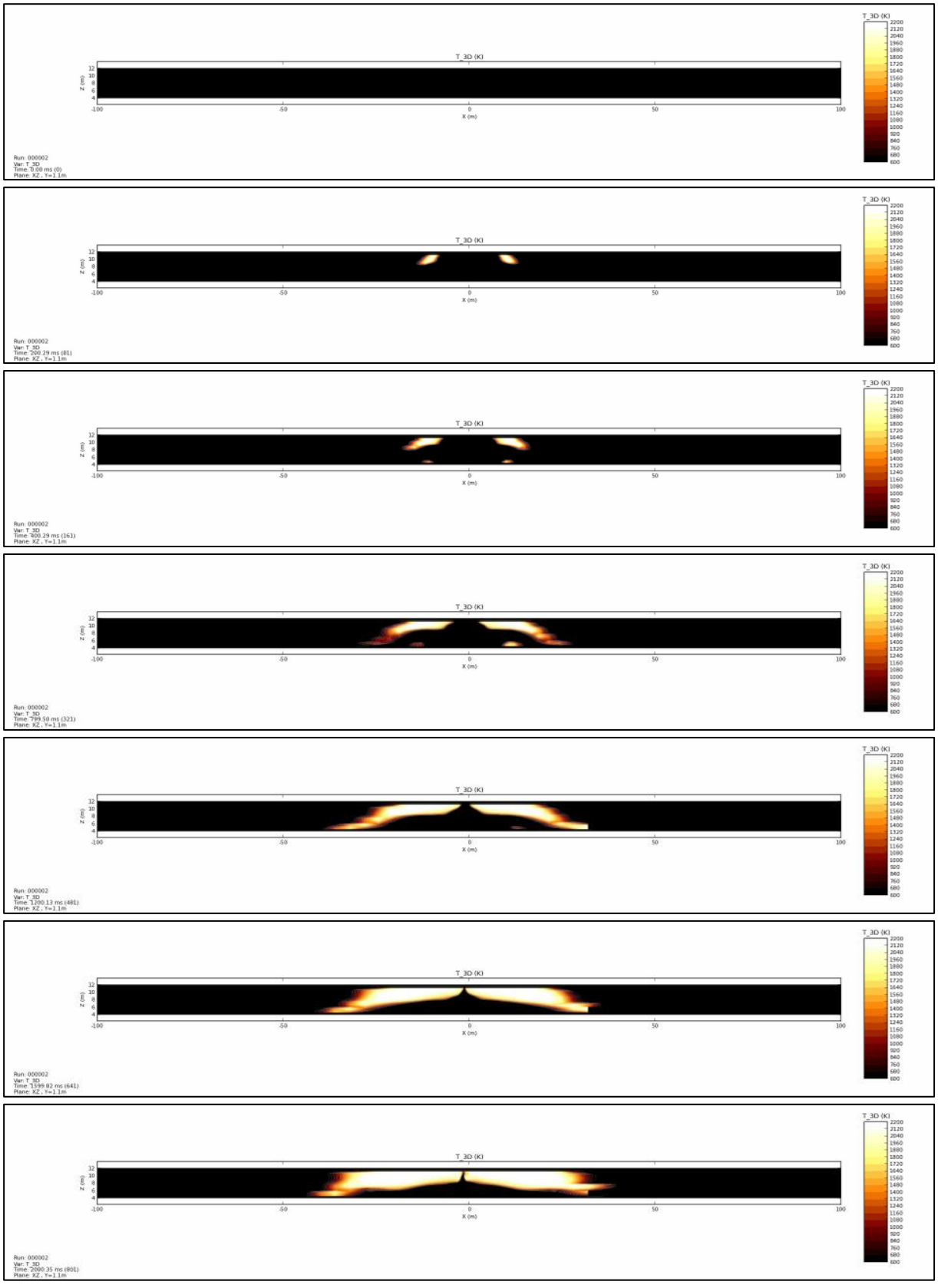

t = 2400 ms, 2800 ms, 3200 ms, 3600 ms, 4000 ms, 4400 ms, 4800 ms

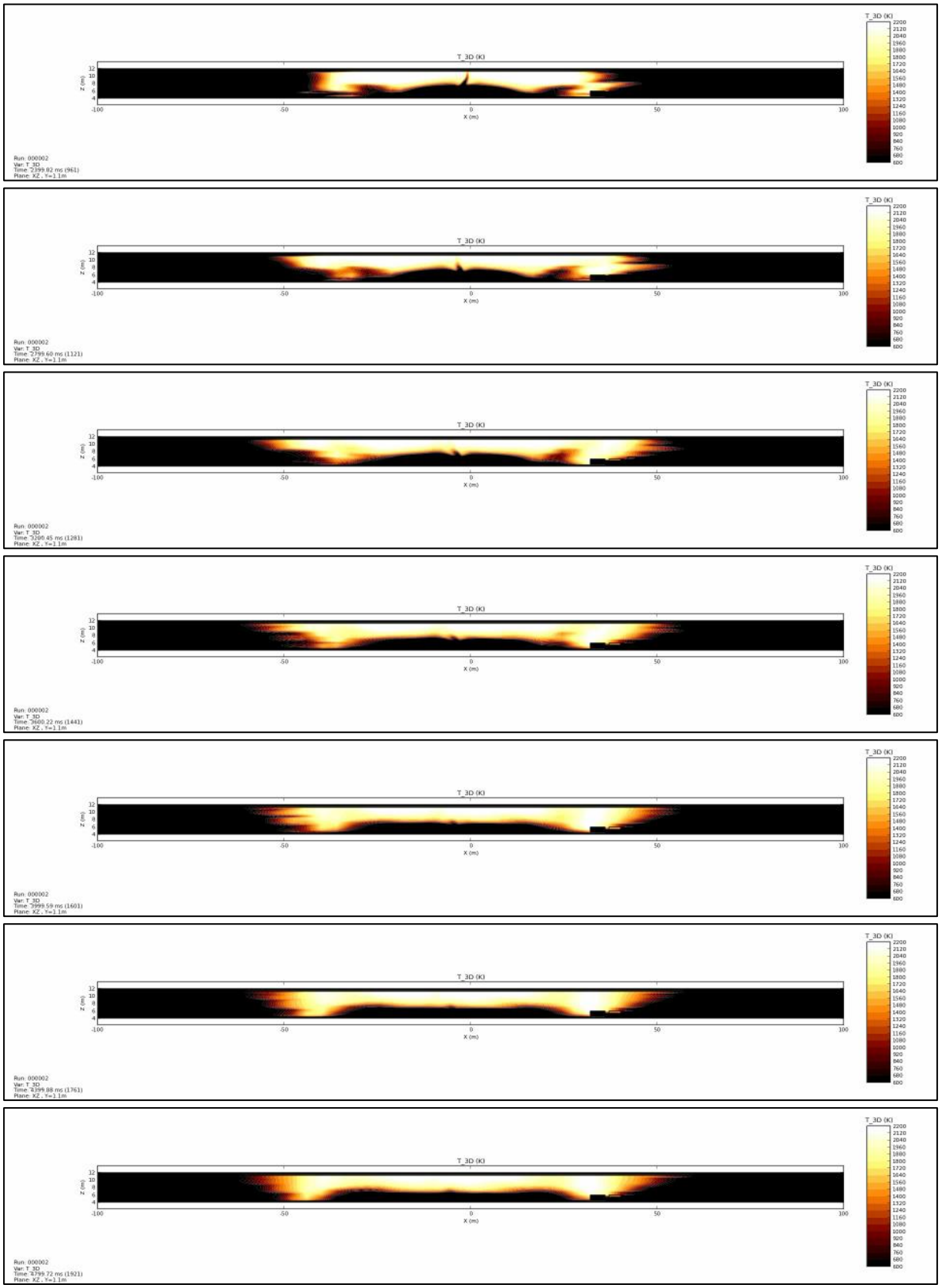

t = 5200 ms, 5600 ms, 6000 ms, 6400 ms, 7200 ms, 8000 ms, 8800 ms

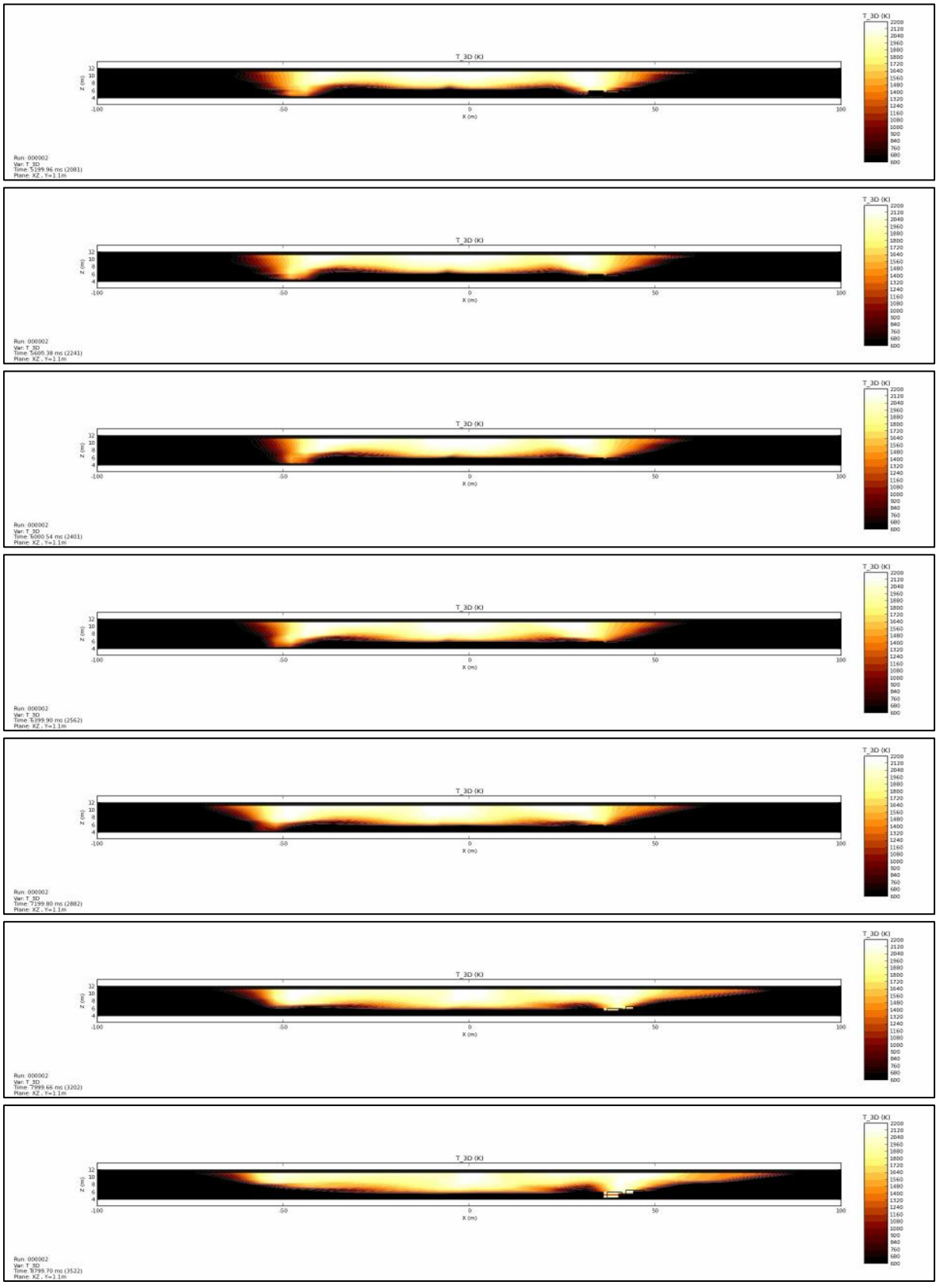

t = 9600 ms, 10000 ms, 11000 ms

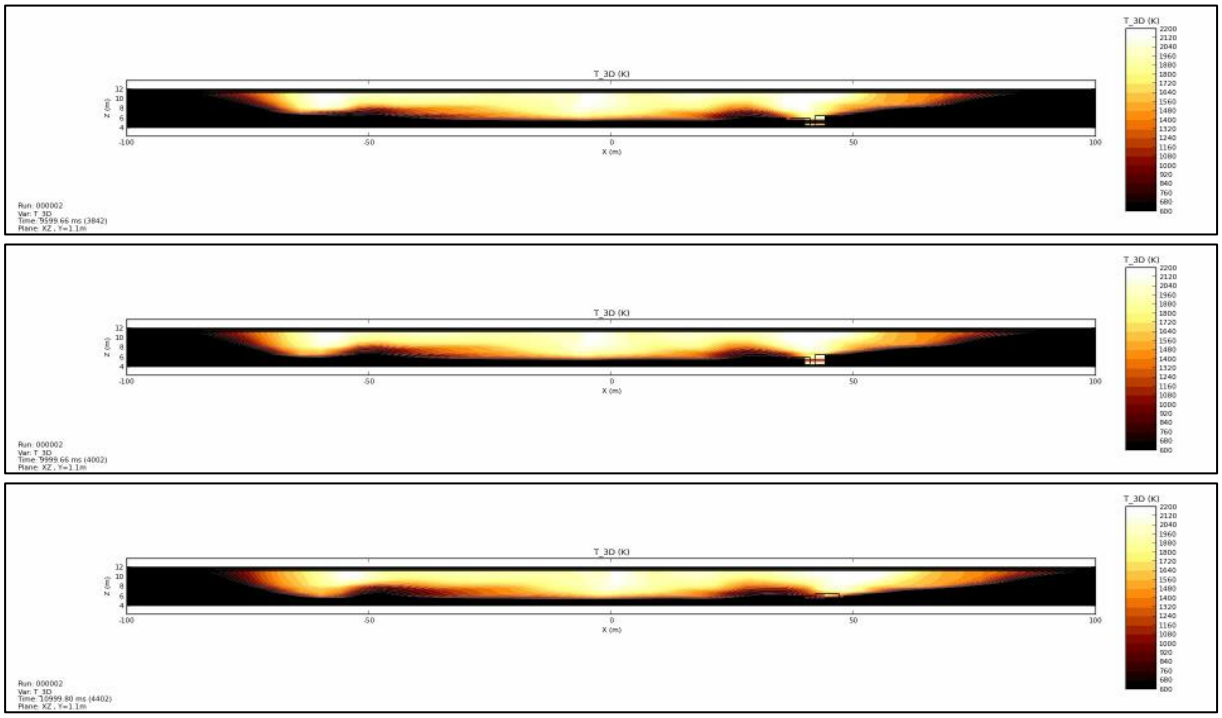

# Appendix D

## BG-1R – Blast Overpressure

### Distance: 10 m

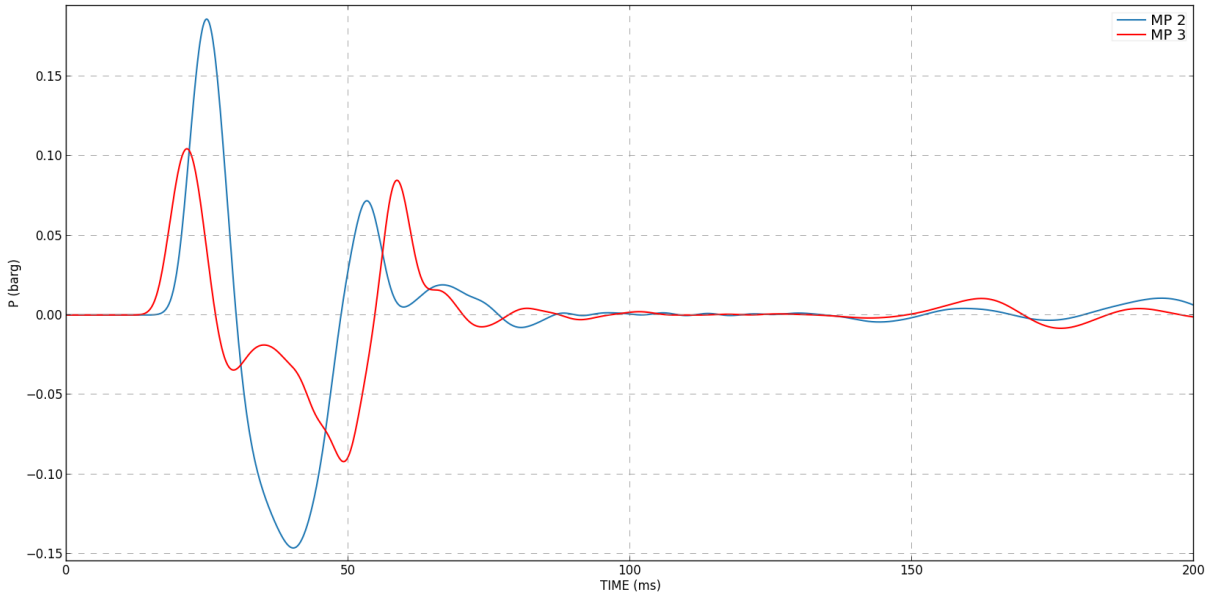


### Distance: 25 m

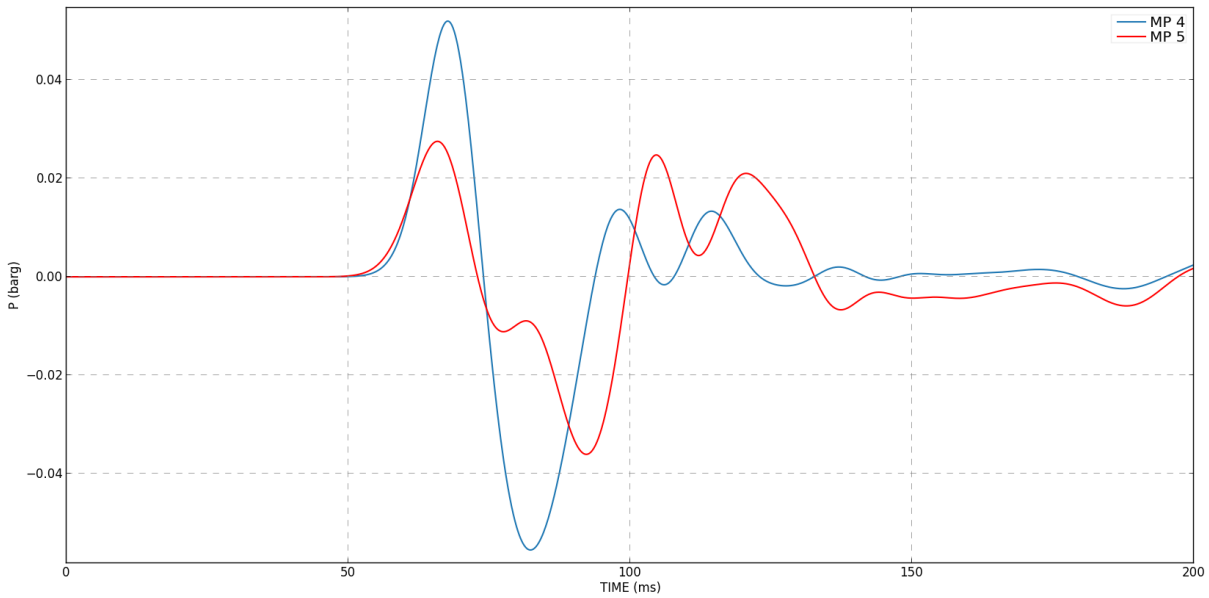

## BG-1R – Impulse

### Distance: 10 m

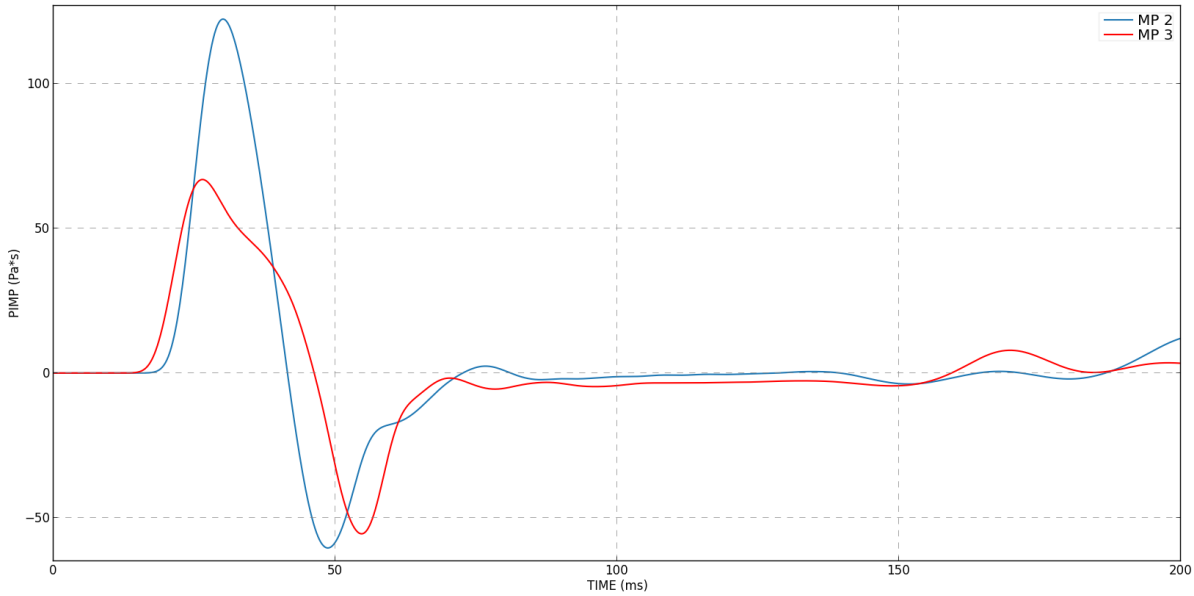


### Distance: 25 m

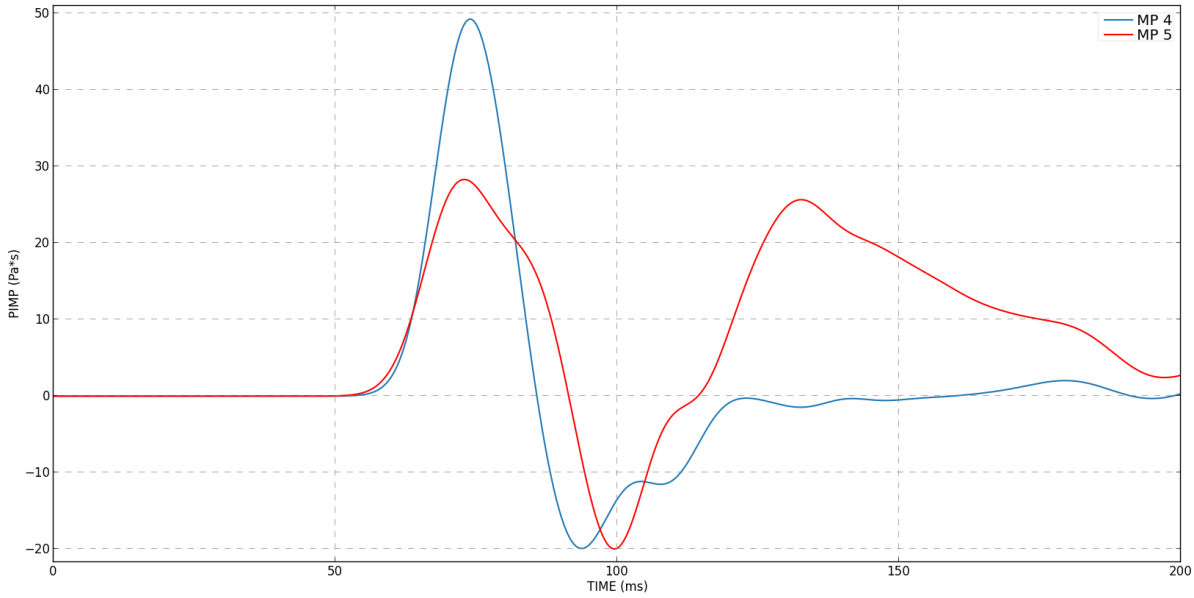

## BG-2 – Blast Overpressure

### Distance: 10 m

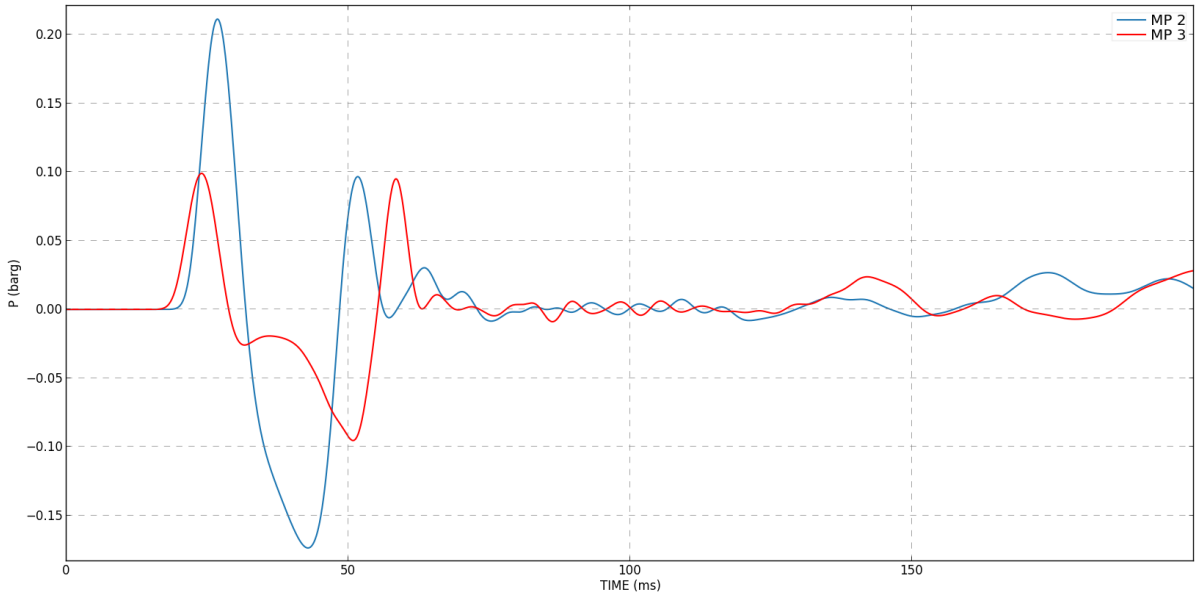


### Distance: 25 m

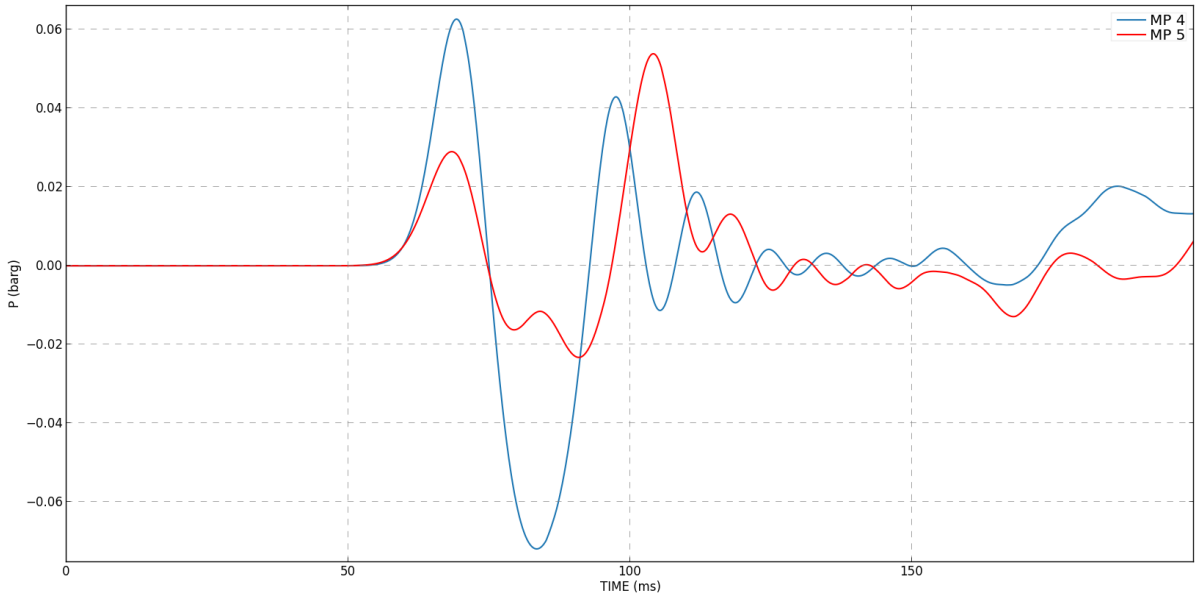

## BG-2 – Impulse

### Distance: 10 m

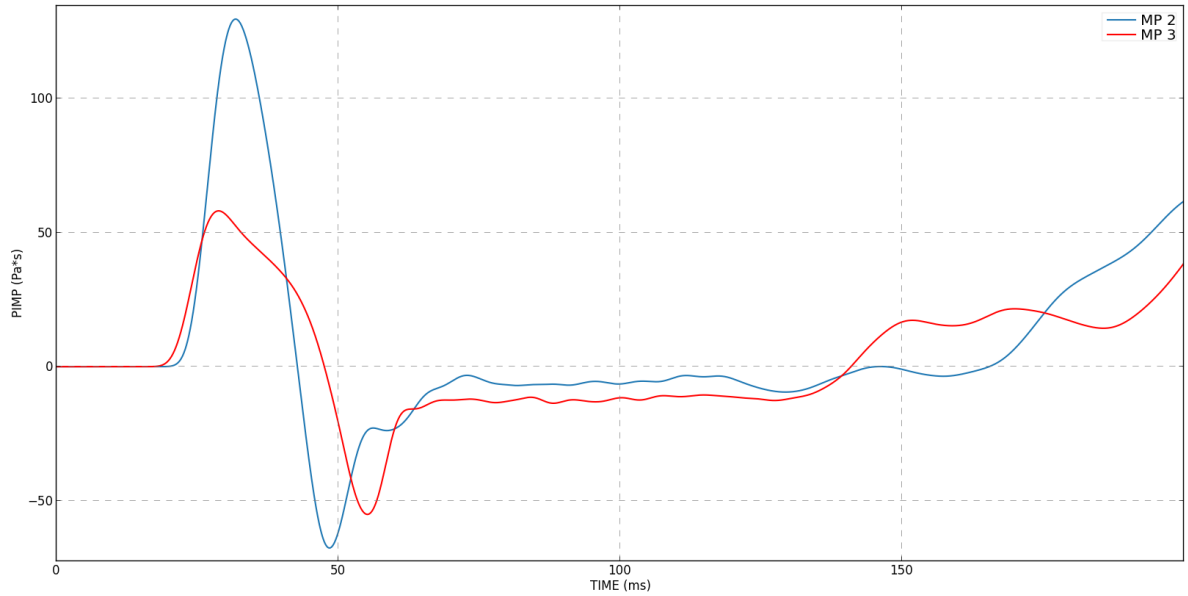


### Distance: 25 m

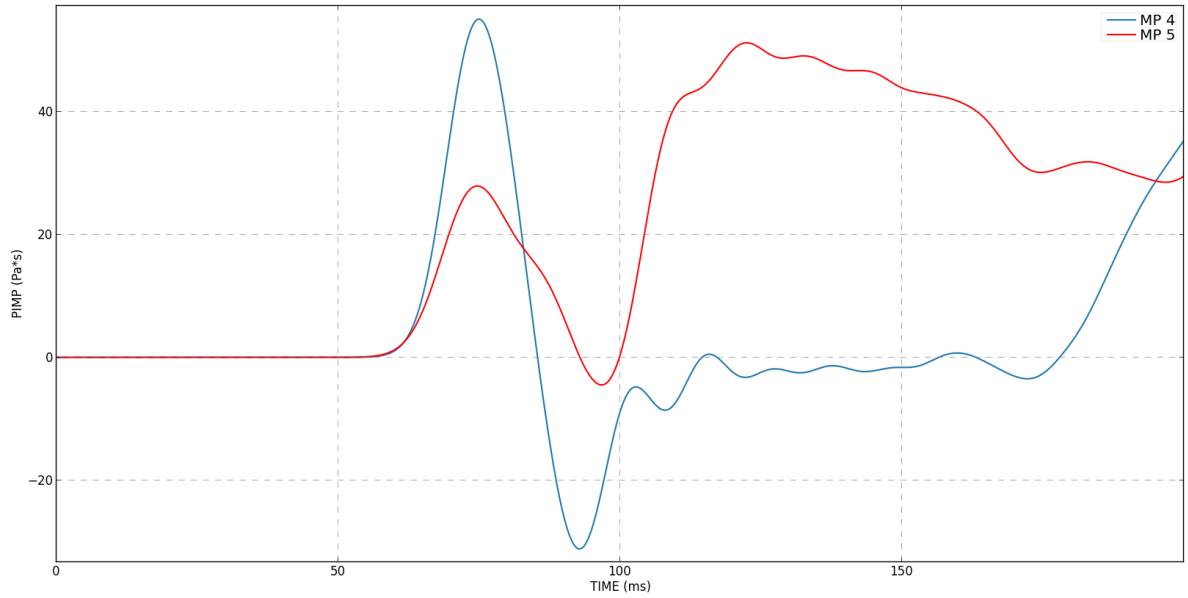

## BG-3 – Blast Overpressure

### Distance: 10 m

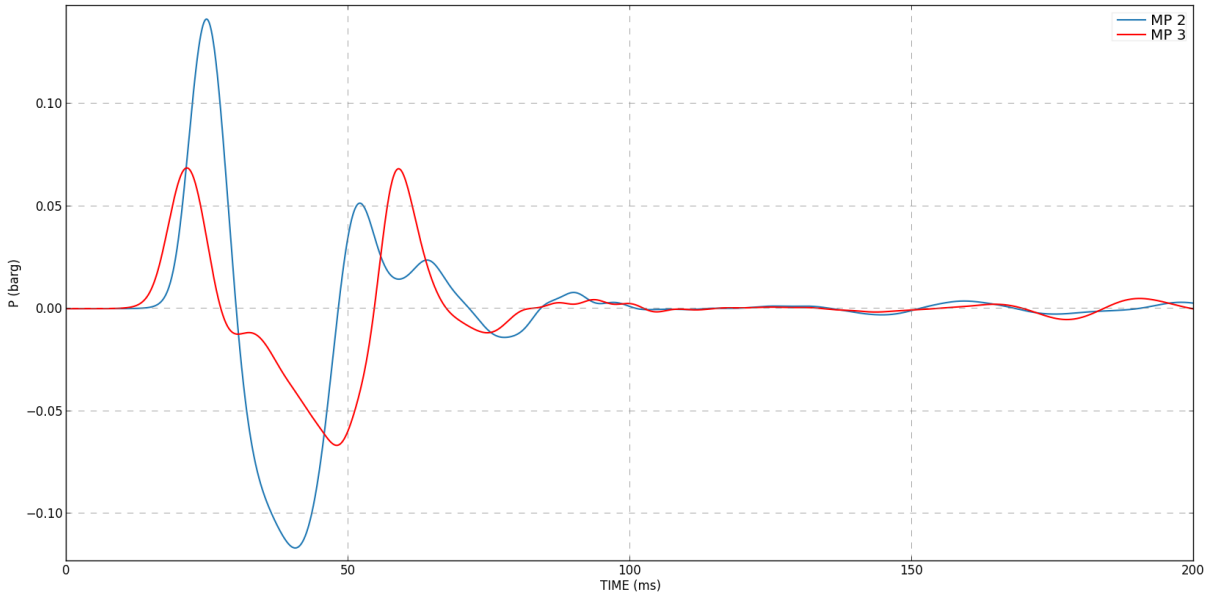


### Distance: 25 m

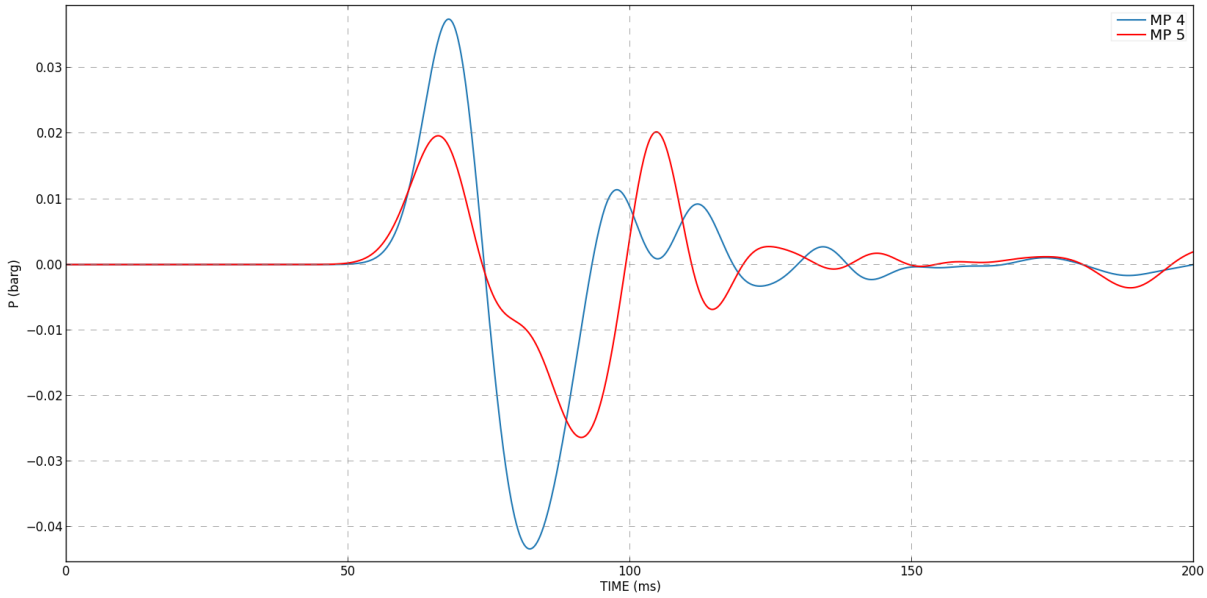

## BG-3 – Impulse

### Distance: 10 m

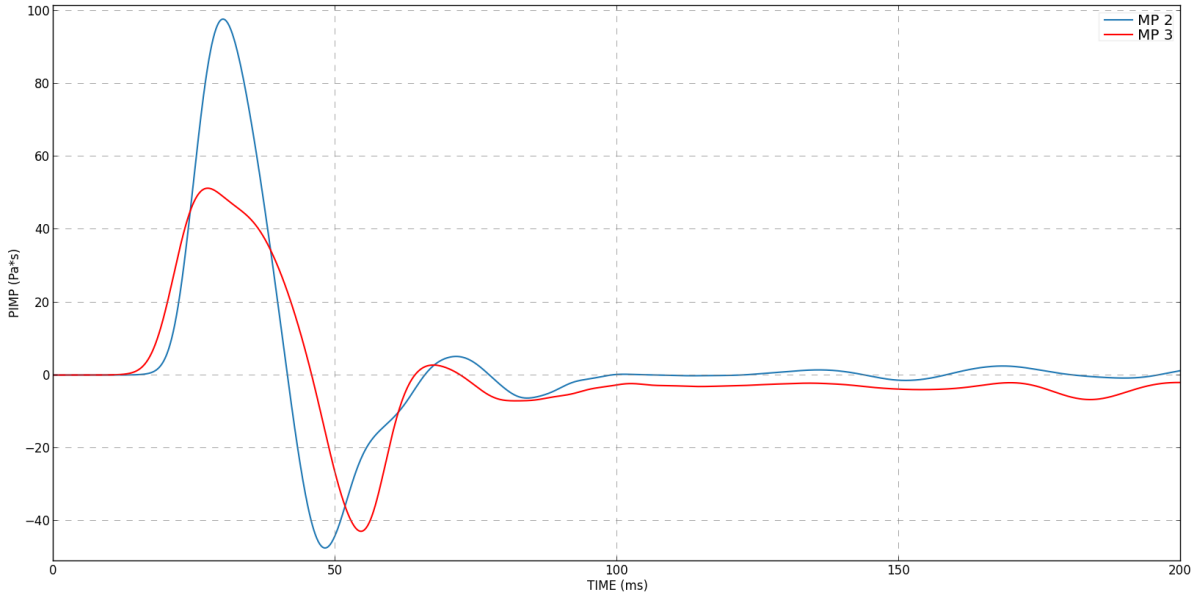


### Distance: 25 m

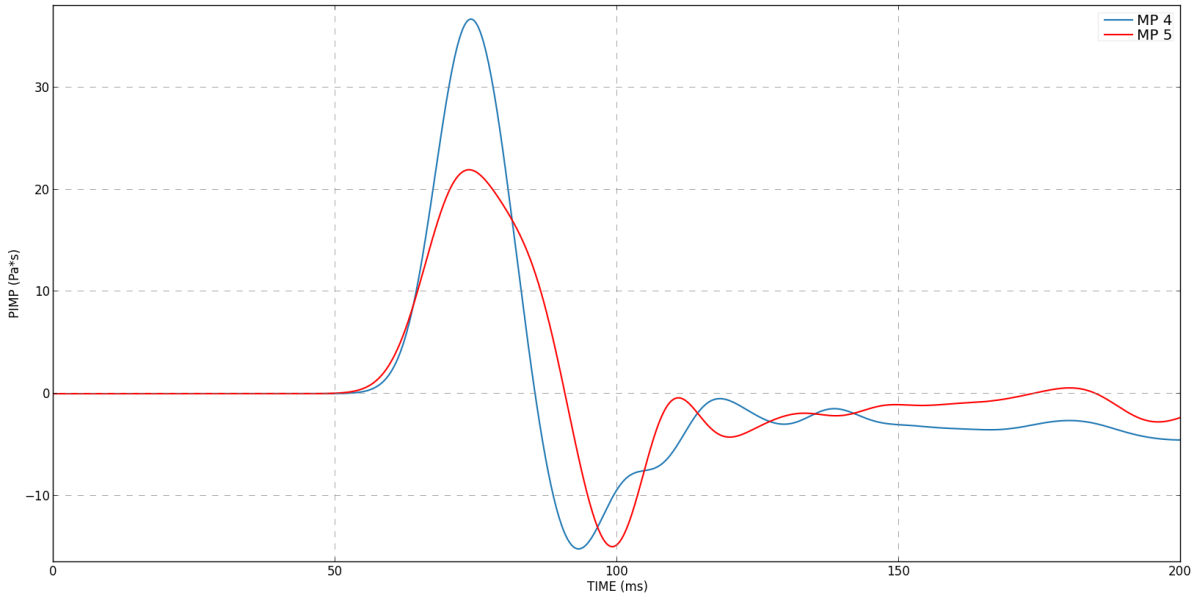

## BG-4 – Blast Overpressure

### Distance: 10 m

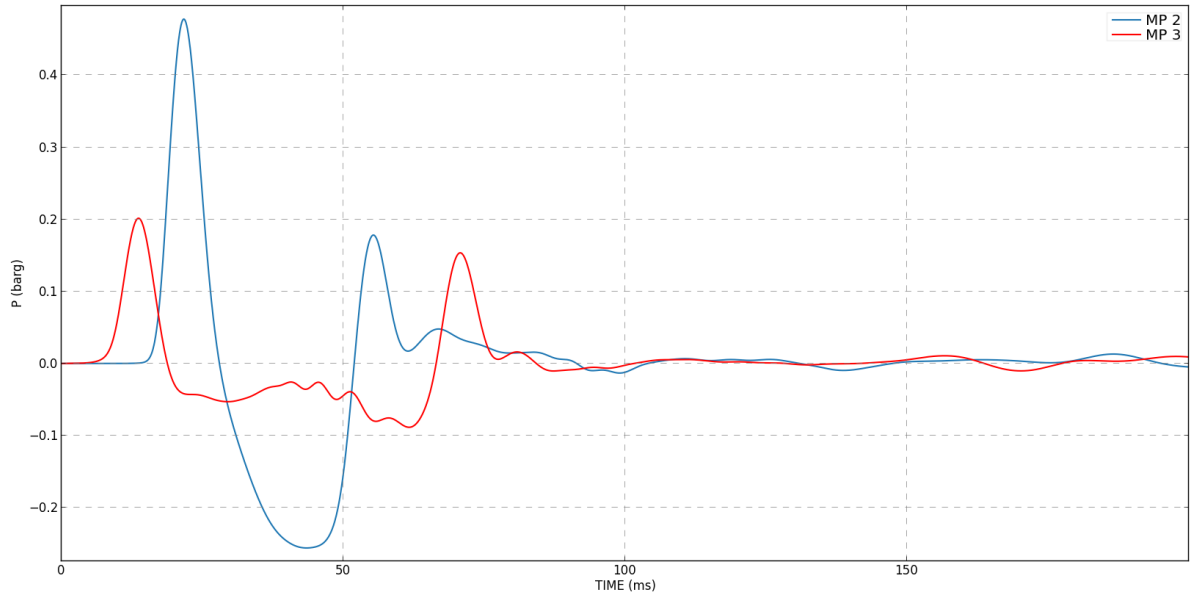


### Distance: 25 m

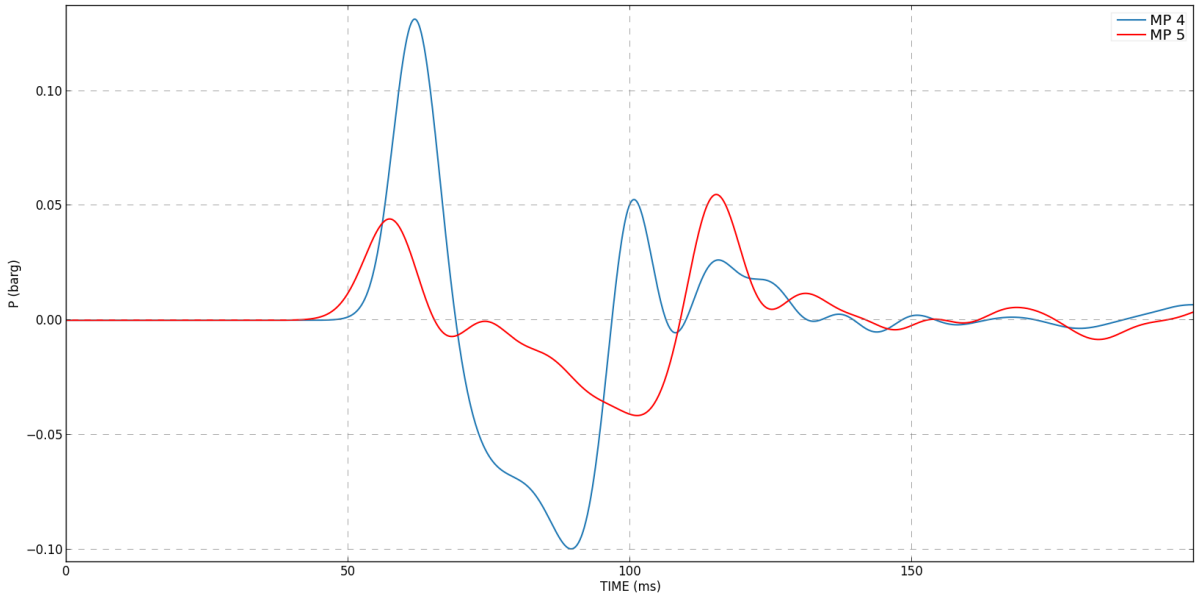

## BG-4 – Impulse

### Distance: 10 m

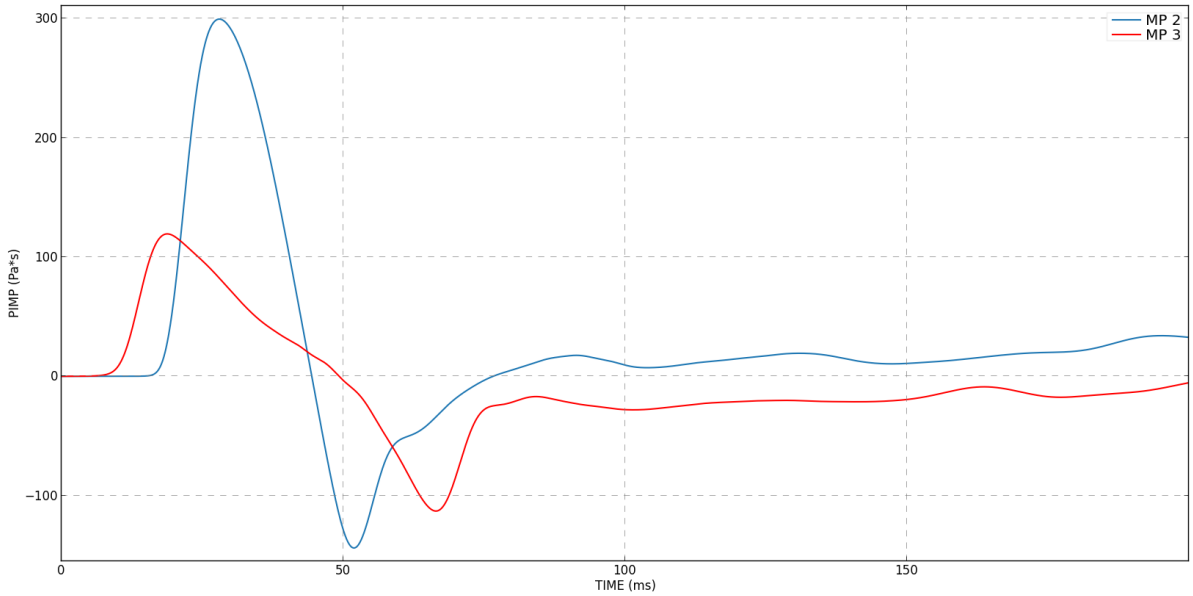


### Distance: 25 m

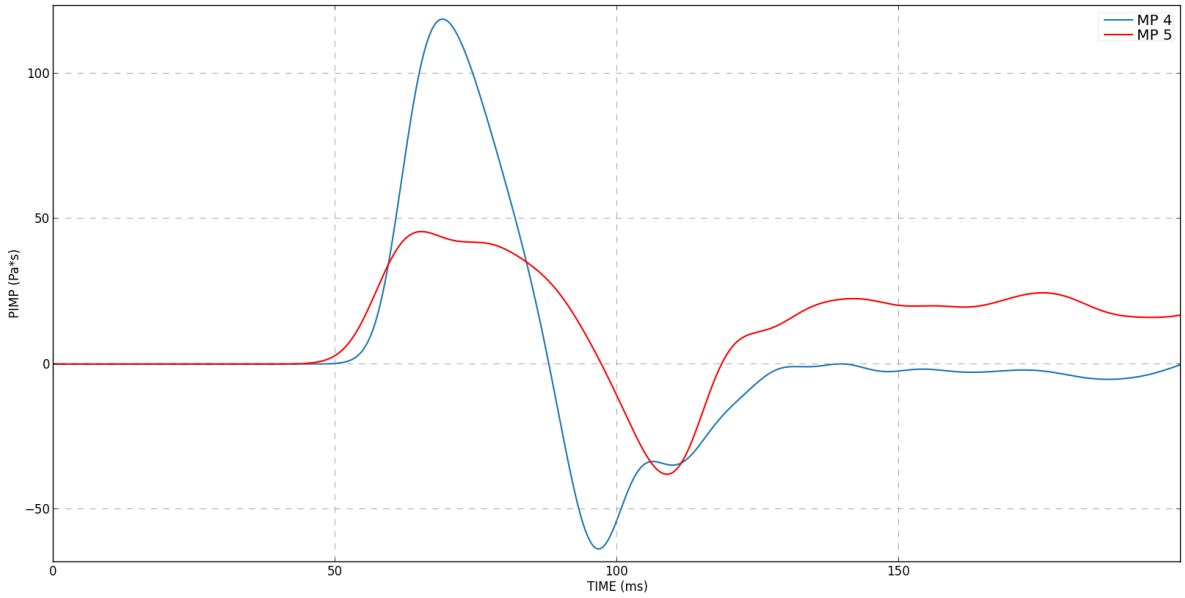

## BG-5 – Blast Overpressure

### Distance: 10 m

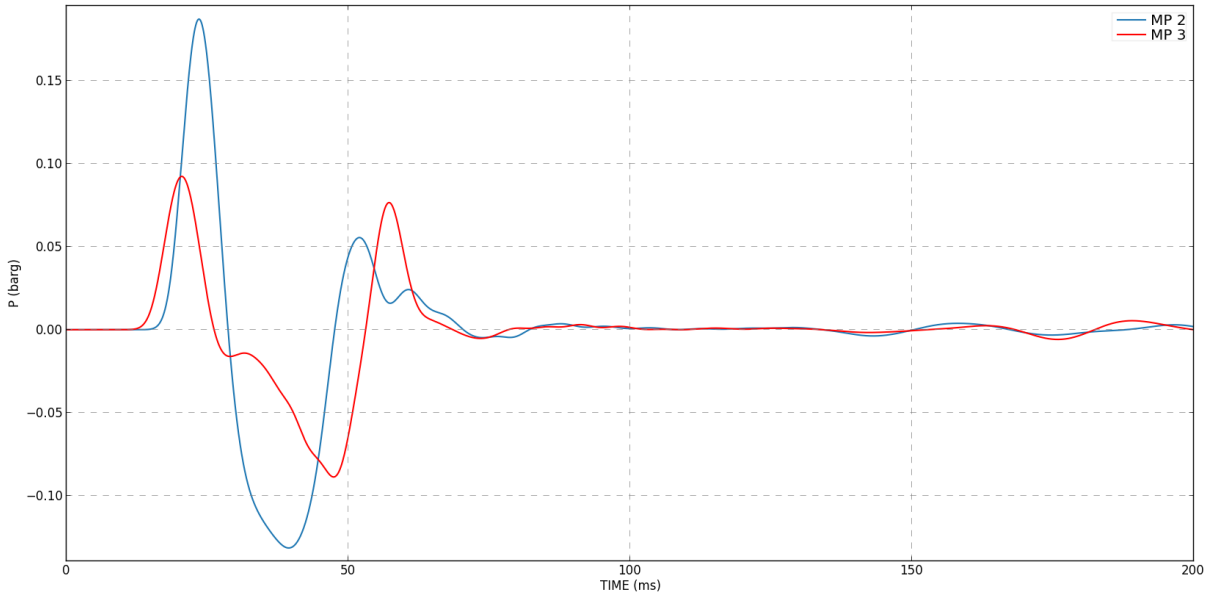


### Distance: 25 m

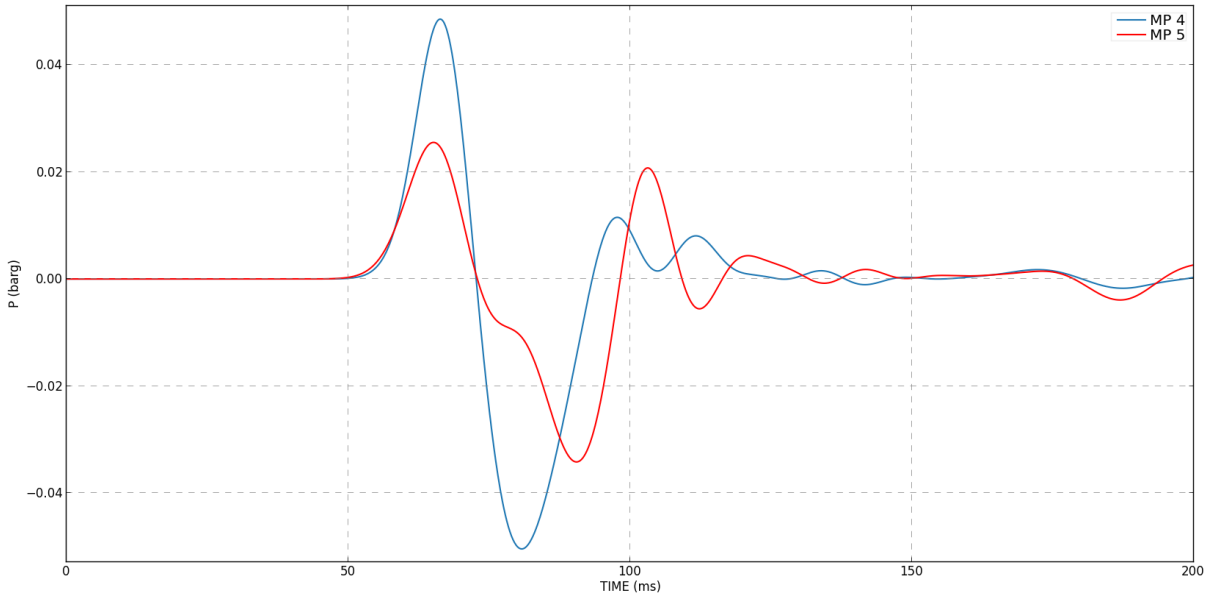

## BG-5 – Impulse

### Distance: 10 m

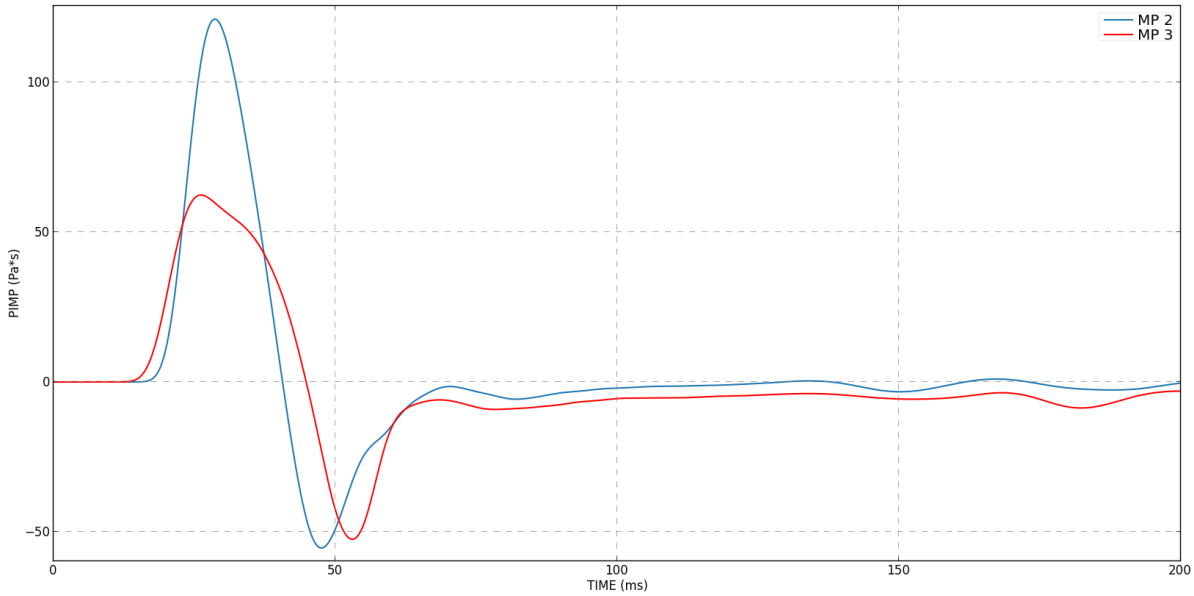


### Distance: 25 m

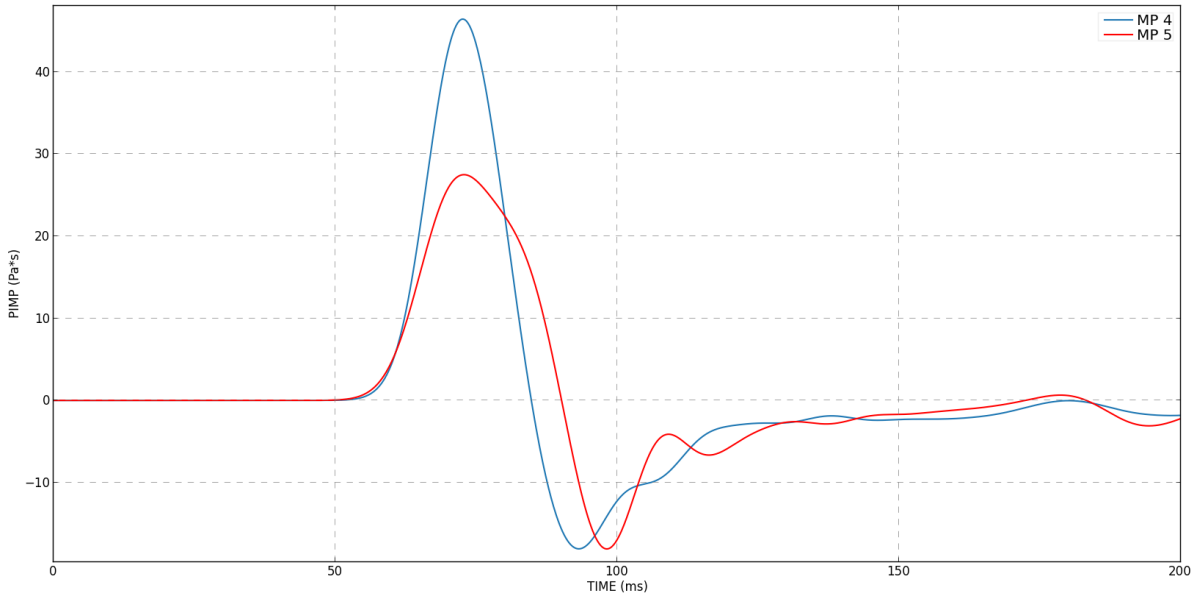

## Birk 01-4 – Blast Overpressure

### Distance: 10 m

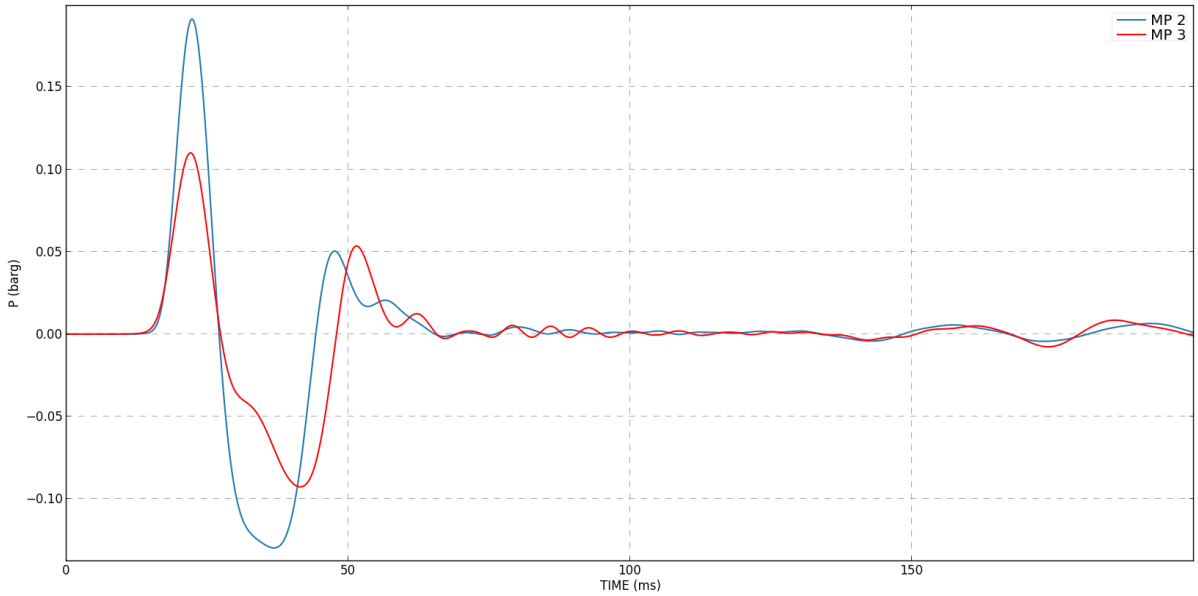


### Distance: 25 m

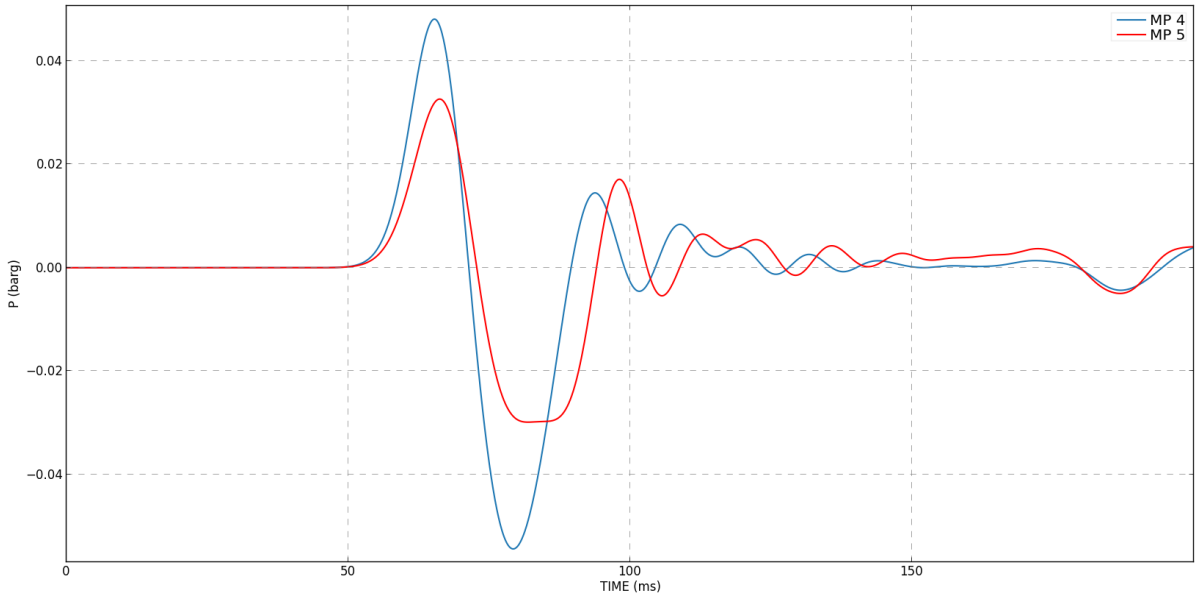

## Birk 01-4 – Impulse

### Distance: 10 m

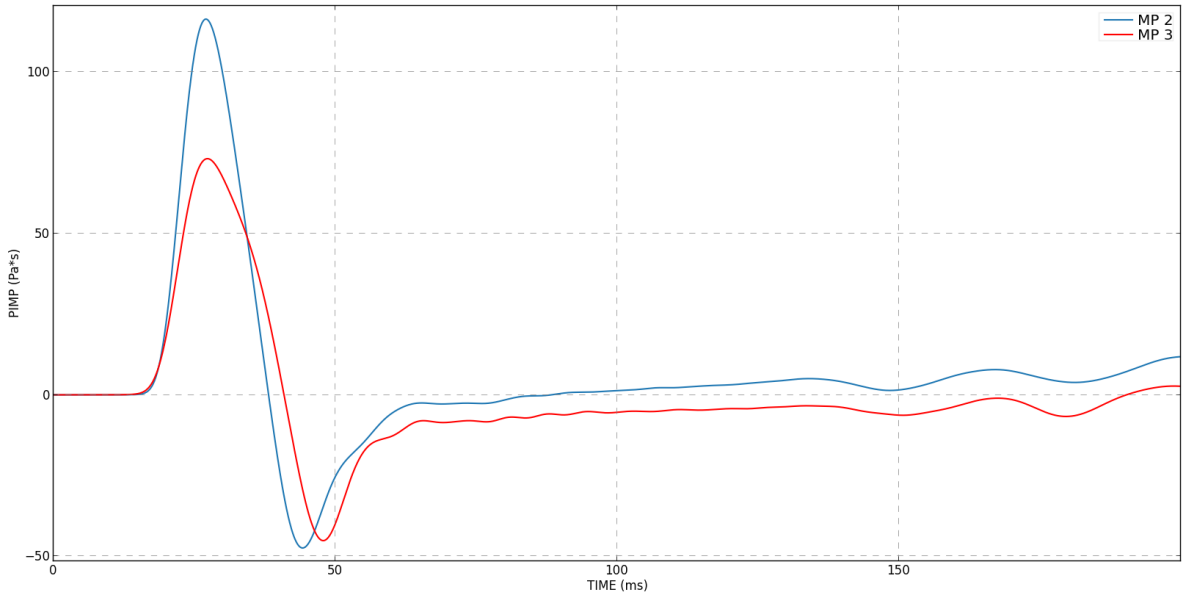


### Distance: 25 m

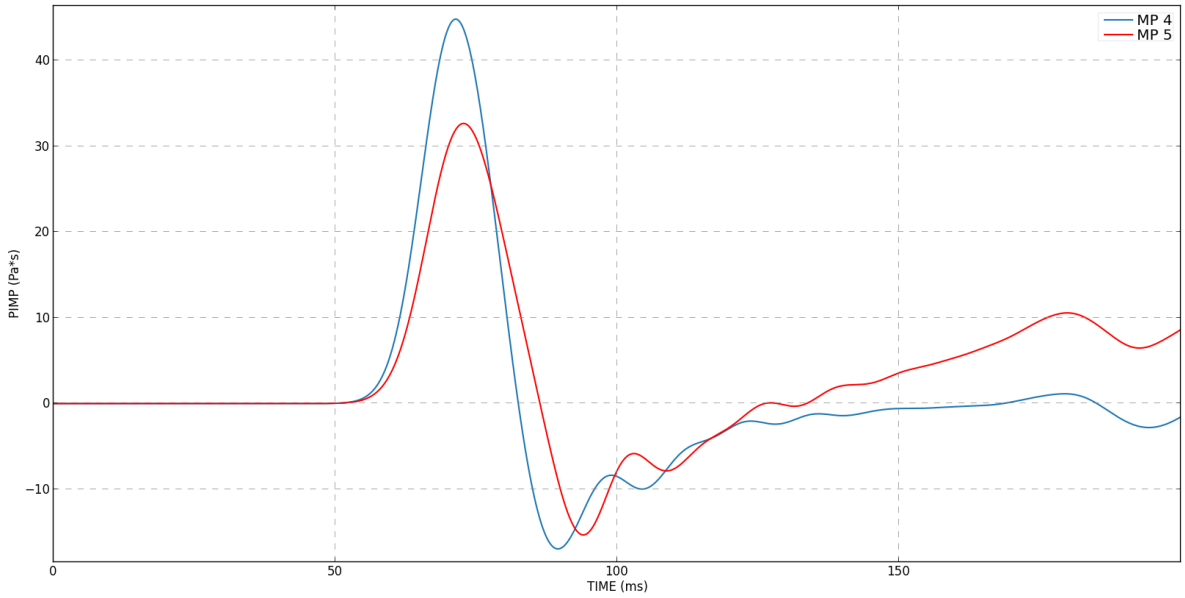

## Birk 02-4 – Blast Overpressure

### Distance: 10 m

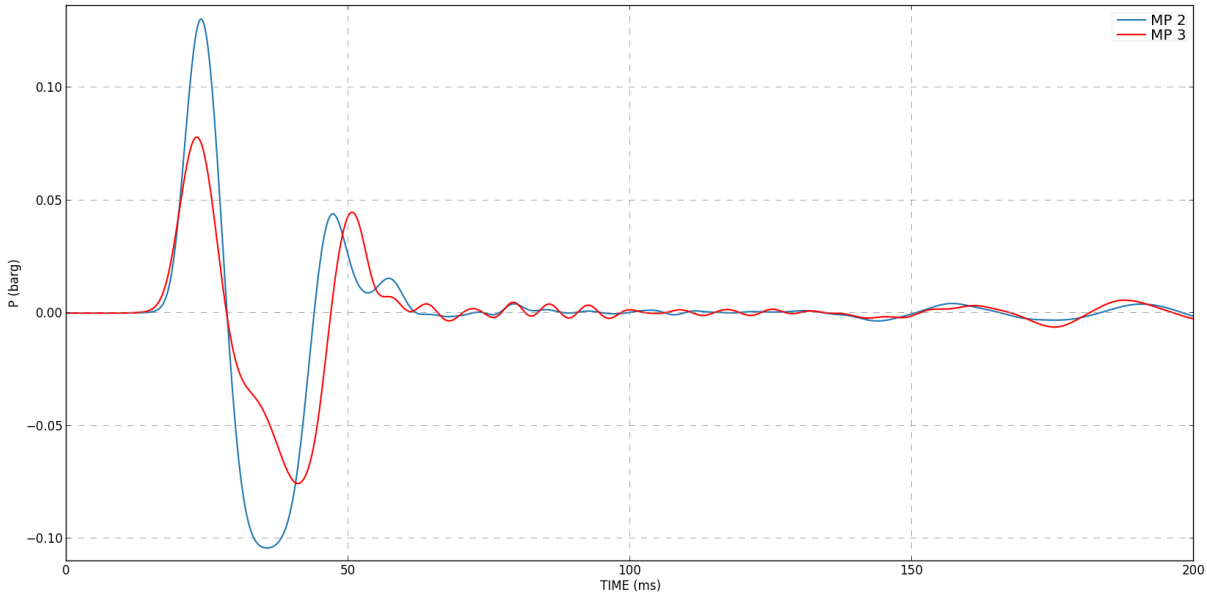


### Distance: 25 m

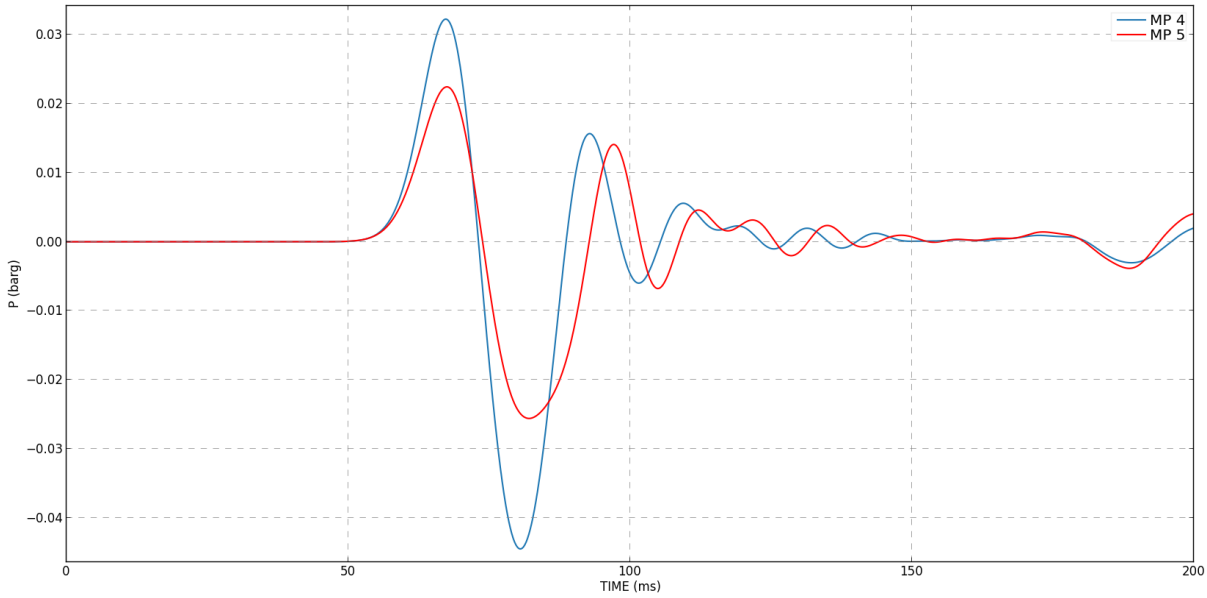

## Birk 02-4 – Impulse

### Distance: 10 m

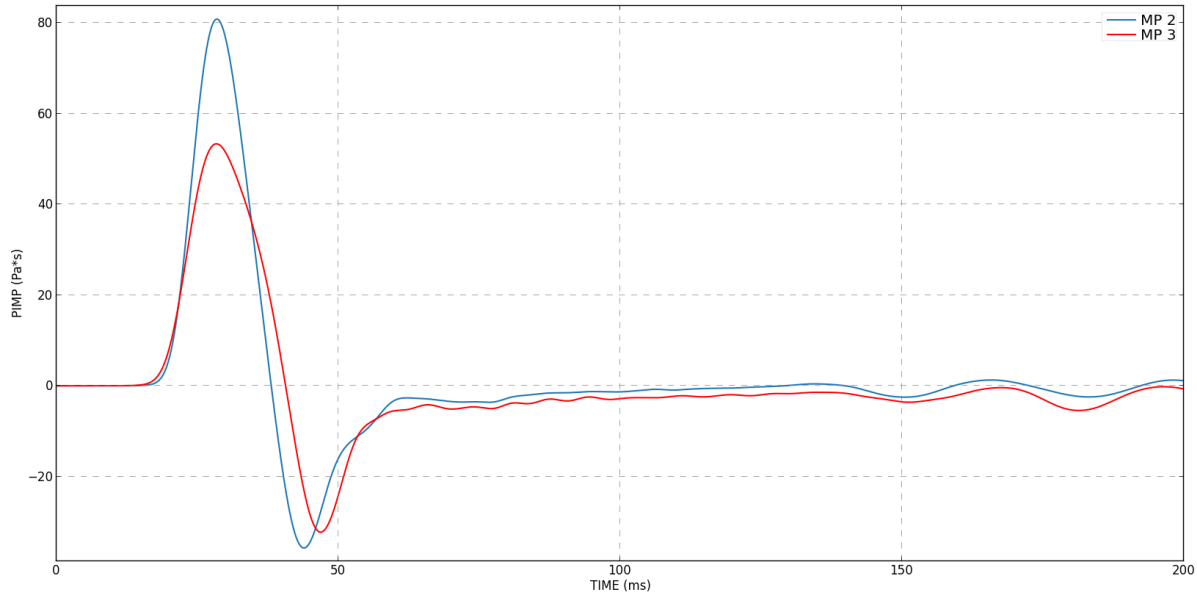


### Distance: 25 m

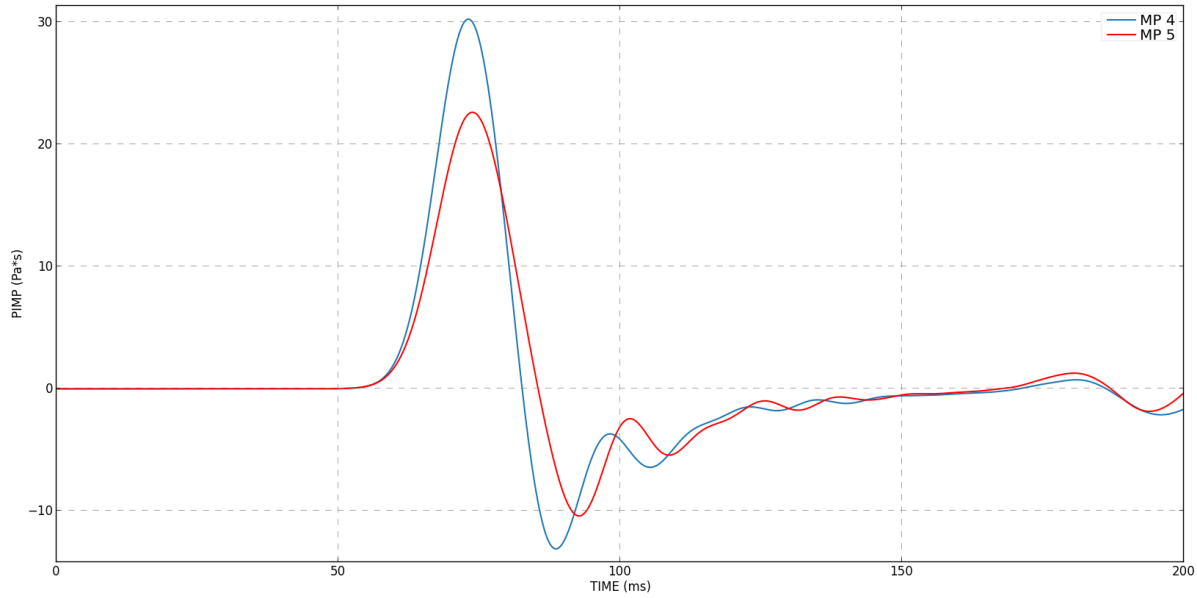

## Rogfast 1 – Blast Overpressure

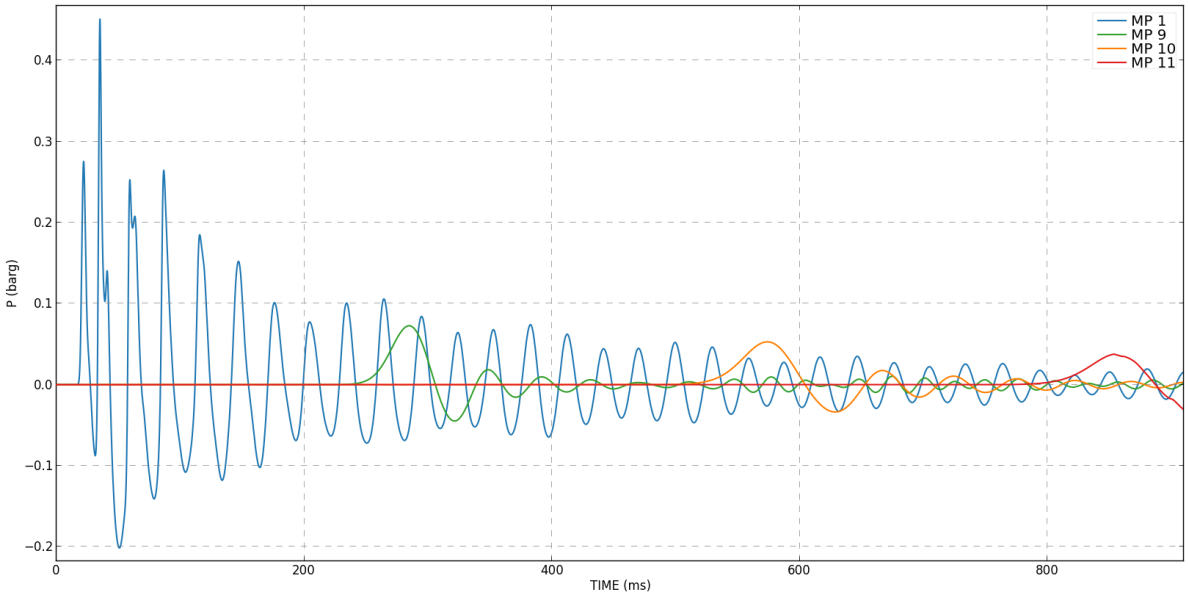


## Rogfast 1 – Impulse

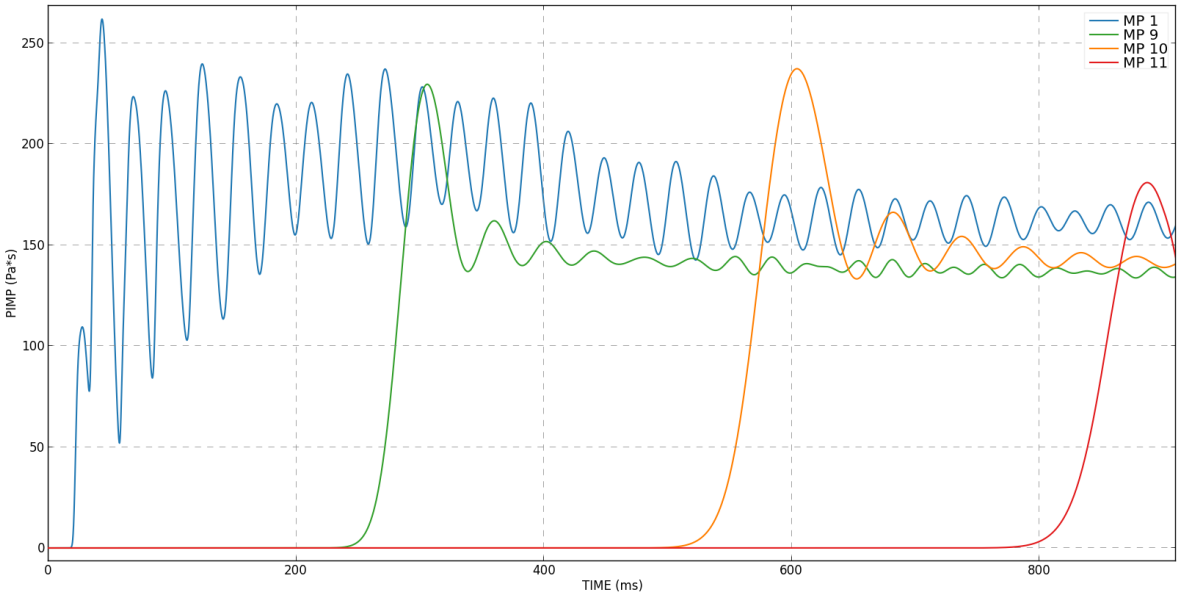

## Rogfast 2R – Blast Overpressure

### Congested

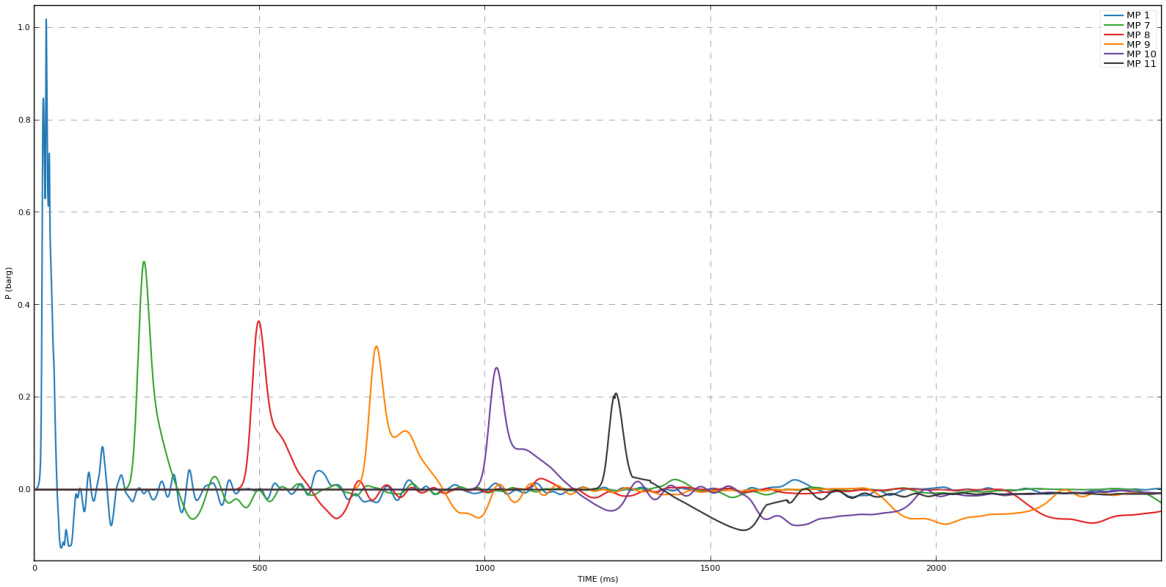


### Uncongested

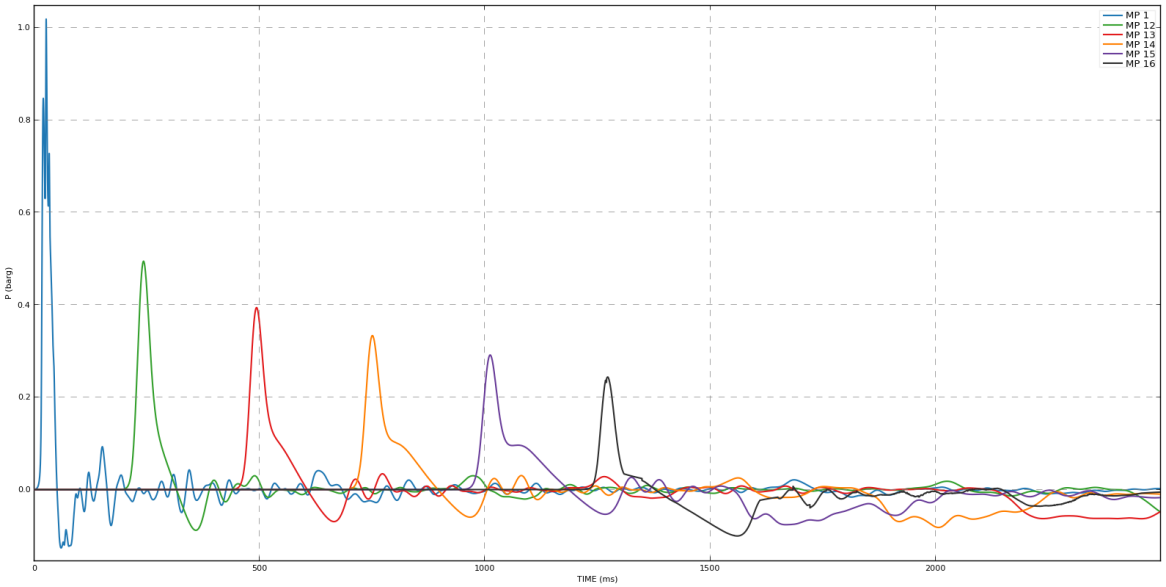

## Rogfast 2R – Impulse

### Congested

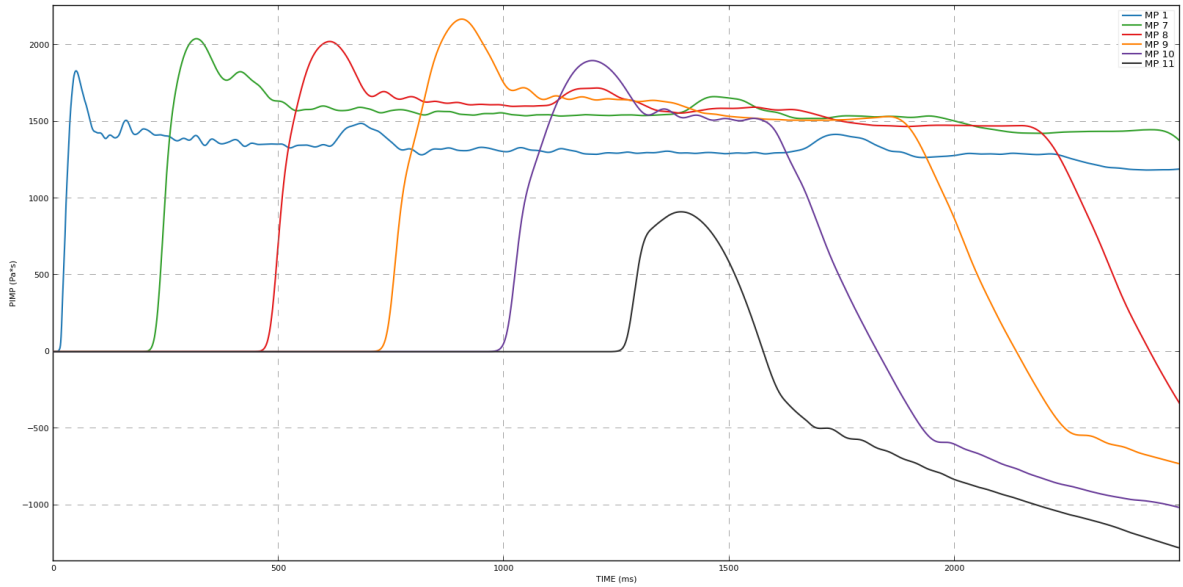


### Uncongested